# WELLBORE HEAT LOSS CALCULATION DURING STEAM INJECTION IN ONSHORE & OFFSHORE ENVIRONMENTS

A THESIS SUBMITTED TO THE DEPARTMENT OF
ENERGY RESOURCES ENGINEERING
OF STANFORD UNIVERSITY
IN PARTIAL FULFILLMENT OF THE REQUIREMENTS FOR
THE DEGREE OF MASTER OF SCIENCE

Selçuk Fidan

September 2011

I certify that I have read this thesis and that in my opinion it is fully adequate, in scope and in quality, as partial fulfillment of the degree of Master of Science in Energy Resources Engineering.

Prof. Anthony R. Kovscek
(Principal Adviser)

I certify that I have read this thesis and that in my opinion it is fully adequate, in scope and in quality, as partial fulfillment of the degree of Master of Science in Energy Resources Engineering.

Dr. Louis Castanier

# Abstract

In the oil industry, the problem of wellbore heat loss during hot fluid injection is classical. Even today the topic is important for practical application of steam injection. Most thermal reservoir simulators today do not yet take into account heat losses and pressure drops along the wellbore. Neglecting these items may be acceptable for shallow reservoirs. For deeper injection wells and injection wells in offshore environments, however, wellbore heat loss is often significant.

Accurate predictions of heat loss, temperature distributions and pressure profile are essential for modeling steam injection wells. The main goal of this study is to investigate heat losses along the wellbore during steam injection in both onshore and offshore environments. Steam quality, steam temperature, steam pressure, and heat loss values with and without insulation are calculated. In the literature, it is shown that the Fontanilla and Aziz model [20] yields results in good agreement with field data. The Fontanilla and Aziz approach is used in this study, with an improvement in the application of two-phase flow correlations and the determination of several input parameters.

The equations describing mass and heat flow are solved in discretized well-bore framework. Steam properties are incorporated directly. Several two-phase flow correlations for injection tubing, are used and results are compared. The calculated steam temperature and steam pressure agree well with the field data using the Beggs and Brill model [13, 14]. Six insulation materials are examined: 1) black aerogel, 2) white

aerogel, 3) fiberglass, 4) carbon fiber, 5) thermolastic insulation and 6) calcium silicate. Aerogel insulations present the opportunity to create a superinsulated tubing that overcomes many limitations of current steam injectors. A Matlab Graphical User Interface ($GUI$) is developed, that enables other users to change the input parameters and visualize the results without going into the details of the calculations.

To our knowledge, no one has predicted the result of non-condensible gas addition on steam injectors. In this work, a novel approach is introduced for adding non-condensible gas to steam to increase the injection pressure without increasing the steam temperature. Additional partial pressure is obtained by adding $N_2$ to the system. Steam quality, steam temperature, steam pressure, and heat loss calculation are conducted for steam injection with non-condensible gas ($N_2$). Compared with the case of just steam injection, the steam temperature values are smaller, so are the amounts of heat loss.

# Acknowledgments

First and foremost, I would like to express my sincere gratitude to my adviser Prof. Anthony R. Kovscek for his time, support, guidance and his unbelievable patience. Without his support I would not be able to finish this work, Thank you Tony!

My thanks also go to Dr. Louis Castanier with whom I had helpful discussions in the early and late stage of this project. I would also like to thank to visiting Prof. Jan Dirk Jensen to teach us "Design and analysis of production systems for oil and gas reservoirs" to understand multiphase flow concept better. My special thanks go to Prof. Khalid Aziz to provide one of his Master students Fontanilla's thesis. I would like to thank both to Turkish National Petroleum Cooperation (T.P.A.O) and SUPRI-A Affiliates for their support. It was one of the biggest dream I had since second year of undergraduate to come to Stanford and study there. It came true, this success was not only one person' success it was the success of the several people in my life and I will briefly talk about those people here. My mother is the highest priority person in my life not only she raised us with devoting her entire life to her children but also lack of opportunity she had not to allowed to get educated, she dedicated herself to her children to get all of them (4 sons) educated and she achieved this, thank you 'Anne' (means mom in Turkish). My adviser in Turkey Prof. Dr. Mustafa Onur who has great impact on my life in terms of his knowledge, support and trust on me. He is a unique person both in Academic world and personal world. He always gave his students courage to excel their skills and motivated them to work

hard, because of him I am here, many thanks to him. My adviser Dr. Mehmet Parlar at Schlumberger during my internship last summer, he gave me an opportunity to work with him and learn from his experiences, many thanks to him and as well as my supervisor Dr. Rajesh Chanpura. Now my friends ; Elnur Aliyev, Amar Alshehri, Mehrdad Honarkhah, Rustem Zaydullin, Alireza Iranshahr, Obi Isebor: I enjoyed studying with you guys during my stay at Stanford.

It was my fortune to be one of the member of the such a great team SUPRI-A that I have learned a lot and found my women of dreams and got married. My wife, Wenjuan Lin, is the softest part of my heart and inspiration of my life, and more. She always supported me, not only several days I stayed at school she never became angry, but also she showed her love to me every seconds of our life. Because of her love, I enable to finish this work! Thank you, CANIM! And my little baby daughter Su Lin Fidan who brought fun, joy, and energy to our life, thank you little angel;).

# IF

If you can keep your head when all about you
Are losing theirs and blaming it on you;
If you can trust yourself when all men doubt you,
But make allowance for their doubting too;
If you can wait and not be tired by waiting,
Or, being lied about, don't deal in lies,
Or, being hated, don't give way to hating,
And yet don't look too good, nor talk too wise;

If you can dream - and not make dreams your master;
If you can think - and not make thoughts your aim;
If you can meet with triumph and disaster
And treat those two imposters just the same;
If you can bear to hear the truth you've spoken
Twisted by knaves to make a trap for fools,
Or watch the things you gave your life to broken,
And stoop and build 'em up with wornout tools;

If you can make one heap of all your winnings
And risk it on one turn of pitch-and-toss,
And lose, and start again at your beginnings
And never breath a word about your loss;
If you can force your heart and nerve and sinew
To serve your turn long after they are gone,
And so hold on when there is nothing in you
Except the Will which says to them: "Hold on";

If you can talk with crowds and keep your virtue,
Or walk with kings - nor lose the common touch;
If neither foes nor loving friends can hurt you;
If all men count with you, but none too much;
If you can fill the unforgiving minute
With sixty seconds' worth of distance run -
Yours is the Earth and everything that's in it,
And - which is more - you'll be a Man my son!

*-Rudyard Kipling*

Dedicated to my father *Hüsnü Fidan* (R.I.P)

# Contents

# List of Tables

# List of Figures

# Chapter 1

# Introduction

Increasing oil prices have helped raise investment in EOR applications during the last two decades. Steam injection is the thermal method that add heat to the reservoir to expand the oil in-place, reduce oil viscosity, provide drive energy and thereby improve the displacement efficiency of injected fluid [44] . Crude-oil viscosity is inversely proportional to temperature. When the temperature increases, viscosity decreases. Less viscous oil results in greater mobility. Prats[41] indicated that the effect of steam injection on recovery is significantly greater as compared to hot-water injection. It is because steam carries more enthalpy per unit mass. The displacement of fluids by steam is self stabilizing movement of the crude oil to the production well. Lake[30] emphasized that thermal methods especially steam injection and steam soak, are easily the most successful enhanced oil recovery processes. Steam injection is applied to viscous oil reservoirs in order to reduce oil viscosity and increase production. Many applications of steam injection have been done with success in the onshore environment, but only one example exists in the literature for offshore fields. It was the "Emeraude Vapeur" pilot test that had great technical success [9].

Many investigators have studied heat transfer to the surrounding formation while

hot fluid injection travels downward along the wellbore. Ramey [42] was the pioneer and his model is used by most researchers as a starting point. Ramey assumed that flow is steady state, non-compressible, and single phase. He solved energy and momentum balance equations analytically to get approximate pressure and temperature distributions. He neglected kinetic energy, frictional loss, and assumed that the overall heat transfer coefficient does not change with depth. In 1967, Willhite [49] proposed a well known overall heat transfer coefficient calculation that has been widely used in the oil industry since. In 1969, Earlougher [17] considered steam and casing conditions with respect to depth. He used the Hagedorn and Brown model [22] for two-phase flow calculation and assumed that there is no slippage between the phases for steam injection. He actually assumed that the gas and liquid phase flow at the same speed. Several years later Pacheco and Farouq Ali [38] presented a comprehensive mathematical model of steam injection without taking into account slip and the multiphase flow regime concept. Early in the 1980s, Farouq Ali [18] solved this issue and proposed a comprehensive wellbore steam flow model. He took into account the slip concept and flow regime of the flow and concluded that considering the slip and the flow regime is important for calculating pressure drop and steam quality during the downward steam injection.

Heat loss and pressure drop calculation for steam injection in offshore environments are not reported in the literature. The objective of this study is to calculate the heat losses, pressure losses, temperature losses, and steam quality changes along the wellbore during steam injection in both onshore and offshore environments. For the onshore cases, pressure drops and quality changes along the wellbore are calculated by coupling non-linear equations and solving them simultaneously. Several two-phase correlations in the literature are used. Offshore cases take into account the thermophysical properties of sea water to get the correct radiation and convection heat transfer coefficients. For all calculations, we start with a base case following

similar procedures as shown by Fontanilla[20], then extend our work by applying several more updated two-phase correlations. The results obtained using different two-phase flow correlations are compared. Sensitivity analysis using different insulation materials are also conducted to investigate the effect of insulation materials on downhole steam properties. As another step forward, we conduct calculation of heat transfer, pressure drops and steam quality change along the wellbore during injection of steam with an additive of non-condensable gas, such as $N_2$. This is the first time that this kind of calculation is described in the open literature. A novel approach is proposed to solve this problem.

Figure 1.1 shows the schematic view of the our calculation for both onshore and offshore environments. In order to calculate heat losses from the offshore environments you must consider surface lines, sea level to sea floor and sea floor to the reservoir. Surface lines does not contribute heat losses with comparing sea level and sea floor to reservoir, however, insulating small amount of length gives much efficiency on steam quality.

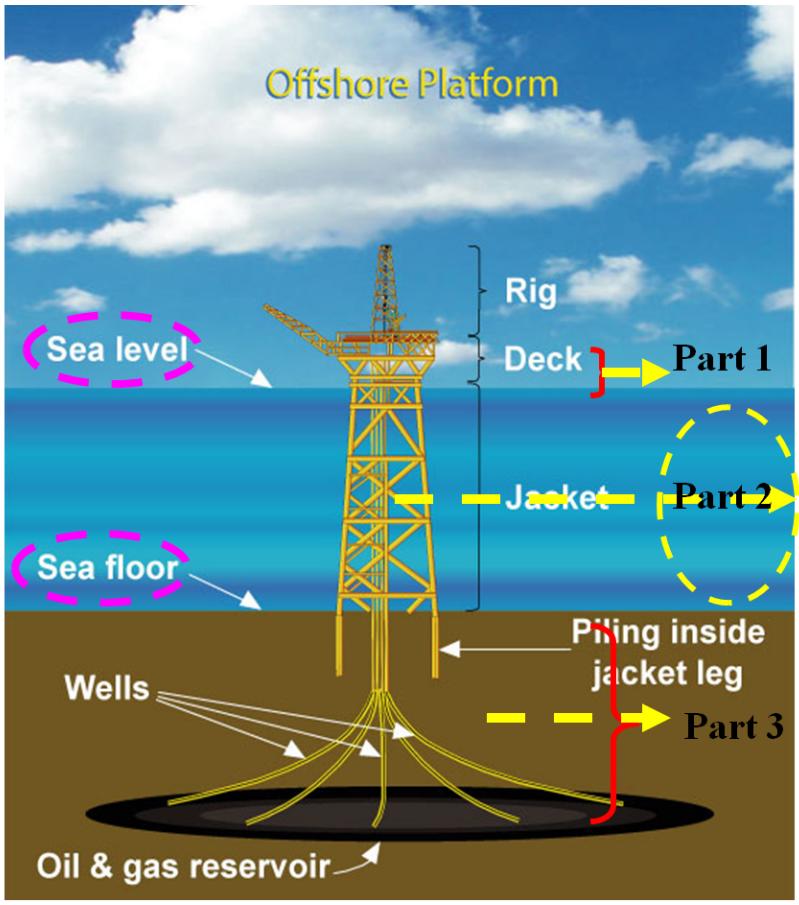


Figure 1.1: Schematic view of the objective of our calculations, (retrieved from [2]).

## 1.1 Thesis Outline

In Chapter 2, we review two cases of heat flow from wells for offshore fields. One case had great success in terms of producing more oil resulting from steam injection, the other case used vacuum insulating tubing (VIT) to reduce heat losses and failed. Then, we review a summary of three basic heat transfer mechanisms and their combinations that are the backbone of our study. In addition, the wellbore heat transmission concept is reviewed starting from Ramey's [42] classical paper.

In Chapter 3, we discuss model formulation that we used in our calculations.

Starting with heat transfer calculation in three parts: surface lines, sea, and sea floor to reservoir based on both Prats's [41] and Willhite's [49] algorithm. Besides the analogy for offshore, we also provide a robust solution that takes into account thermo physical properties of seawater in order to calculate important parameters [36] for heat-loss calculations. Continue with steam properties calculation, we present and discuss most of the two-phase correlations that can be applied for downward steam injection operations. Several of correlations are explained in detail. For other correlations, references are provided.

In Chapter 4, the problem of steam with non-condensable gas ($N_2$) is considered. The $N_2$ gives additional pressure into our steam and helps to reduce heat loss. Once $N_2$ is injected into the system, it causes a decrease in steam pressure and so steam temperature. In order to achieve this purpose, we calculated steam and non-condensible gas properties for insulated and non-insulated tubing in both onshore and offshore environments.

Chapter 5, is the one of the exciting parts of this thesis because we developed a Graphical User Interface (GUI) for our calculations and gave the basics of the program input and output that is used in our calculations. This program allows a user to choose several correlations to be applied such as insulated or uninsulated tubing. With this program a user can study the role of several parameters and see the effects of those parameter on the system.

Chapter 6 discusses the results obtained in preceding chapters and compares them in terms of using different insulation materials and steam properties. We validated our program with field data from the literature [11] and obtained good agreement with field data and also with Fontanilla's approach [19]. We augment Fontanilla's approach as well.

A summary of our findings and suggestions for future work are presented in Chapter 7.

# Chapter 2

# Literature Review

We review two examples from the literature for offshore cases of wellbore heat losses. The first is Emeraude Vapeur[9] and subsequently the Marlin failure and redesign [16, 43, 48] are discussed. This chapter continues with heat transfer mechanism and with heat transfer discussions.

## 2.1 Emeraude Vapeur : A Steam Pilot in an Offshore Environment

The Emeraude field is located offshore Zaire (Congo), Figure 2.1 a, on the West African coast. Water depth is 65 m. The depth of reservoirs is shallow (200-500 m) and they consist of silt layers alternating with thin fractured limestone beds. These very heterogeneous reservoirs are significantly depleted and oil is viscous (0.1 Pa s (100 cp)) at reservoir conditions. A steam drive pilot test was decided in order to estimate a recovery rate and an oil-steam ratio on two independent reservoirs in 1980.

The adverse environmental conditions required original solutions: tilted conductor pipes, a tilted rig, and adapted pumping units on one platform because of reservoir

shallowness and steam production equipment on a second platform because of the distance to the shore. The Emeraude field is estimated to contain 1 billion barrels of viscous original oil in place (OOIP). After 14 years of production (1972-1986), only 170 million barrels had been recovered, about 3% of OOIP, and the reservoir was severely pressure depleted. To produce the remaining reserves by primary recovery in 15-20 years, several additional platforms would be needed, and the final recovery would still be only 5-10% OOIP [9]. Various EOR methods were considered to meet the challenge

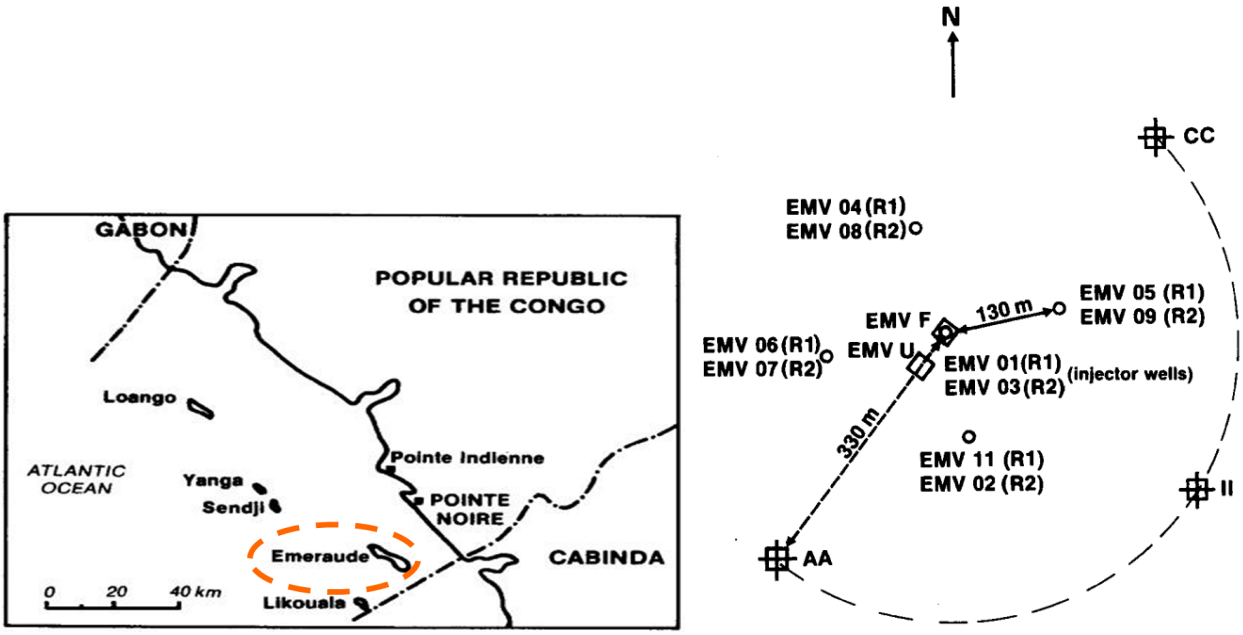


(a) Emeraude field location. (b) Emeraude five spot.

Figure 2.1: Emeraude field location and five spot[9].

of this large amount of oil associated with this poor recovery rate. Water injection was implemented in 1972 in a five-spot pattern, assuming that imbibition would be active. The results were disappointing, with water breaking through to producers almost immediately. In-situ combustion tests under laboratory conditions showed that most of the oil would be burned in the fracture network. Promising results, however, were obtained from steam-injection tests under laboratory conditions. The

experimental work of Willman et al.[15] shows that both steam and hot-water drives may improve oil mobility by reducing viscosity and also may reduce residual oil at high temperatures.

A steam-flood in Figure 2.1 b shows the five spot steam injection implemented to.

- prove the technological feasibility of such a project in adverse conditions (drilling with a tilted rig, drilling through and cementing depleted and fractured zones, pumping tilted wells, and producing steam from seawater) and

- evaluate reservoir responses to steam injection, steam injectivity, steam breakthrough time, recovery rate, and OSR (oil steam ratio).

The Emeraude steam drive pilot provided original solutions to recover a larger amount of OOIP than could be recovered by primary production despite difficult conditions. Technological problems were solved during the pilot design. One of the first developments was obtained interms of getting sufficient well spacing by using a tilt rig for drilling. A second success of development was that depleted and fractured zones were adequately drilled and completed. A third was that pumping units were adapted to tilted wells and electronically regulated. Lastly, facilities for steam production from seawater were located on a platform because of the long distance to shore.

In addition to these technological solutions, some reservoir engineering conclusions were obtained. For instance, steam can be injected at a sufficient rate in reservoirs R1 and R2. A final conclusion was that steam improves the oil production rate in heterogeneous reservoirs. Significant response by Well EMV07 in reservoir R2 (oil rate increased four-fold) and other wells, located on adjacent platforms were noted.

## 2.2 Marlin Failure Analysis and Redesign

In this section, three papers are reviewed related to this subject and including basic information about **V**acuum **I**nsulated **T**ubing (**VIT**). Bradford et al. [16] describe the Marlin failure and give several possible failure modes. They try to reduce them by making analysis and physical evidence. Ellis et al. [43] apply the failure analysis from the first paper to the remaining Marlin wells and focuses on the **VIT** redesign process. Gosch et al. [48] addresses focusing on the value of combined VIT and fiber/software monitoring system as a means of both controlling and observing well thermal behavior.

VIT provides a solution for heat loss in steam injection in Arctic and offshore environments. VIT is a tubular apparatus conveying steam or other hot fluids ($> 400^oF$) to the formation through an inner tubular that is surrounded by an outer tubular [6]. The annular space between the inner and the outer tubular is under vacuum. The annulus is usually filled with a better material for absorbing hydrogen formed by corrosion of the outer tubular and gases such as nitrogen, carbon monoxide, and hydrogen released from the inner tubular at elevated temperatures [6].

The Marlin field is located in the Gulf of Mexico, Viosca Knoll Blocks 871/915, and was originally intended to be produced from a tension-log platform by means of five predrilled dry-tree penetrations. Right after production began, a minor tubing leak occurred, and after that casing pressure jumped to shut in tubing pressure. It was the first alert of a major tubing failure. Analysis of the failure came up with several critical issues including

- excessive helical buckling of the production tubing,
- hydrate formation and dissolution,
- trapped annulus pressure leading to casing collapse, and

- improper tubulars and wellhead movement

After the fishing operation and ultrasonic caliper, they concluded that deformation of Well A-2's tubing was the result of collapse of production tieback. They still do not know whether it was because of the production tieback collapsed alone or as a result of collapse of the intermediate casing is unknown [16].

Although Marlin wells predrilled up to the completion stage limited mitigation options, well design concepts were developed and screened using agreed-upon risk-acceptance criteria for health, safety, and environment (**HSE**). They chose VIT based on the economic analysis and risk profile associated with each option. Using VIT, they had significant thermal isolation due to the low conductivity or low convecting annular fluids [43]. They did several experimental studies on VIT and found out three important facts. The overall thermal properties of the unaltered VIT were not adequate for Marlin requirements due to the fact that heat loss at coupling dominates the performance of a VIT joint. Second, a combination of thermal coatings and insulated inserts provides adequate additional insulation at the couplings. Last, several materials were tested in the annulus to reduce heat loss and $N_2$ is the most effective barrier to heat loss.

In the third paper of the Marlin failure redesign [48], they have tested VIT performance with developed software to see the production annulus temperature profile in real time. This real-time monitoring gave them better control of the well such as when a low safety factor is calculated, a well is shut in automatically. VIT design itself has lots of design considerations and challenges. They tried to understand whether the VIT was a good choice or not based on the both experimental and numerical results [48]. They sum up their work in several with giving results. Design of VIT introduces a number of considerations not present in a design using conventional tubing. Another important conclusion was natural convection can significantly affect the ability of VIT to isolate tubing temperatures from the annulus. Additionally, it

was remarked that regional heating can add a temperature increase to outer annuli that is not anticipated in a single well analysis. Both the thermal performance of the VIT and its mechanical integrity require special consideration. These results lead the authors to suggest that each well has to studied and treated individually.

## 2.3 Heat Transmission Mechanisms and Discussion from Authors

### 2.3.1 Heat Transmission Mechanisms

In this section we review the heat transfer mechanisms during steam injection operations. Including conduction, convection, and radiation and a combination of two or more in our calculations.

#### 2.3.1.1 Heat Transfer by Conduction

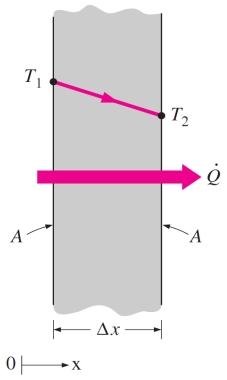


Figure 2.2: Schematic view of conduction (after [8]).

Heat conduction also called diffusion is the transfer of energy from the more energetic particles of a substance to the adjacent, less energetic ones as a result of interaction between particles.

$$\dot{Q}_{cond} = kA\frac{T_1 - T_2}{\Delta x} = -kA\frac{\Delta T}{\Delta x} \quad (2.1)$$

where k is the thermal conductivity of the material (Fig. 2.2). In the limiting case $\Delta x \rightarrow 0$ the equation above reduces to the differential form that is

called **Fourier's law** of heat conduction after J. Fourier and becomes [8, 35].

$$\dot{Q}_{cond} = -kA\frac{dT}{dx} \tag{2.2}$$

#### 2.3.1.2 Heat Transfer by Convection

One mode of convection heat transfer is between a solid surface and the adjacent liquid or gas that is in motion. Convection is called forced convection if the fluid is forced to flow over the surface by external means such as fan, pump, or the wind. In contrast, convection is called natural (or free) convection if the fluid motion caused by buoyancy forces that are induced by density differences due to the variation of temperature in the fluid (Fig. 2.3). The rate of convection heat transfer is expressed by **Newton's law** of cooling as [8, 35]

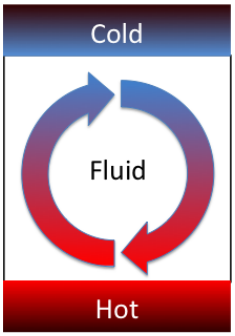


Figure 2.3: Heat transfer from a hot surface to air by convection (retrieved from [1]).

$$\dot{Q}_{conv} = -hA_s(T_s - T_\infty) \tag{2.3}$$

#### 2.3.1.3 Heat Transfer by Radiation

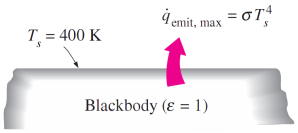


Figure 2.4: Representation of heat transfer by radiation(after [8]).

Radiation is the energy emitted by matter in the form of electromagnetic waves as a result of changes in the electronic configurations of the atoms or molecules. The radiation that can be emitted from a surface at an absolute temperature $T_s$ (in K or R) is given by the **Stefan – Boltzman** law as [8, 35]

$$\dot{Q}_{emit,max} = \sigma A_s T_s^4 \tag{2.4}$$

### 2.3.2 Heat Transmission Discussion from Authors

In the literature many investigators have worked on the thermodynamic properties of the hot fluid movement through wells in onshore fields for both production and injection. One of the well-known papers for wellbore heat transmission is by Ramey[42]. Most of the publications follow upon his approach. He provided an approximate analytical solution for wellbore heat transmission. In his paper, Ramey [42] made several assumptions. He assumed that fluid is non-compressible and flow is single phase with constant thermal and physical properties along the wellbore. He considered that heat flows radially away the wellbore and the overall heat treansfer coefficient is independent of depth. He did not take into account frictional pressure loss and kinetic energy effect in his calculation.

Squier et al. [47] solved differential equations describing fluid temperature along the wellbore, using a complete analytical method. They used hot water as injection fluid.

Satter [45] presented a method that improved Ramey's [42] model by making the overall heat transfer coefficient dependent on depth-step method for calculating heat loss and steam quality for saturated steam as a function of depth. Since Satter assumed that there is no change in pressure with depth, he assumed, in effect that the temperature of the injected saturated steam remains constant, and that only the quality varies with depth.

One year after Satter's [45] paper, Holst and Flock [25] added the friction loss and kinetic energy effects on Ramey's [42] and Satter's [45] models, in order to calculate the heat loss and quality distribution versus depth for saturated steam injection operations. They neglected, however, the static pressure change.

In 1966, Leutwyler [31] gave a comprehensive treatment of casing temperature behavior. Hans and Huitt [26] also developed a graphical solution for wet steam

injection operations. In their model, they calculate wellbore heat loss, steam condensation rate, and casing temperature.

One year later, Willhite [49] proposed his well known method for estimation of over-all heat transfer coefficient that is applied in our calculation as well.

Two of the pioneers in the prediction of heat loss and pressure drop in the wellbore were Pacheco and Farouq Ali [38]. They formulated a mathematical model that consisted of two coupled nonlinear differential equations that were solved iteratively in terms of pressure and quality of steam. They assumed single phase flow, which is not valid, and later on Farouq Ali [18] solved this problem by taking into account slip between the fluids and the flow regime. He used several correlations and stated that importance of applying two-phase flow concept and flow regime.

Wu and Pruess [50] presented a new analytical for wellbore heat transmission without Ramey's assumptions. Their approach was assuming non-homogeneous formations as layered formation with different physical properties.

All the development both technological and understanding of the problem have been done so far helped to understand heat transfer mechanism and solve the problem with taking into account considerations from the authors.

# Chapter 3

# Model Formulation

This chapter presents the methodology for heat-loss calculations and pressure drop estimation in injection tubing.

## 3.1 Heat Loss Calculations

We have adapted Fontanilla's [19] assumptions for the solution of offshore and onshore injectors. These assumptions follow:

1. Heat transfer in and around the wellbore takes place under pseudo steady state conditions. Conduction is pseudo steady state when the change in temperature with respect to time at any given point in the wellbore remains constant. This would mean that the heat rate through the wellbore components is the same at any given time. This can be seen in the derivation of the equation to evaluate the overall heat transfer coefficient $U_{to}$. The heat transfer into the earth occurs under unsteady-state condition.

2. The heat diffusivity and the conductivity of the formation is constant.

3. The tubing hangs symmetrically inside the casing.

As steam travels downward in the wellbore, it loses energy to the surrounding formation. This heat loss may result in condensation with consequent reduction in steam quality and enthalpy.

Heat losses through pipes, whether surface lines or wells, usually are estimated at steady-state conditions in oilfield operations. The procedures for estimating heat losses may appear laborious. The calculation procedures of both Prats [41] and Willhite [49] are discussed here. For offshore heat losses calculations an analogy between electrical circuits and heat resistance is made.

One of the classic papers about over-all heat transfer coefficient was published by Willhite [49]. He presented his widely used method that is incorporated in most simulators for hot fluid injection and hot water. Here in our study, we will give the equations for both surface lines and wellbores based on the methods discussed. For comprehensive calculation procedure we refer to read Appendix A. In addition, we provide the equations for insulated and noninsulated cases and also for offshore heat loss calculations. In Table 3.1, we have provided thermal conductivity of the different insulation material based on the values from the thesis of Marques[34].

Table 3.1: Thermal Conductivity of the materials

| **Insulation Materials** | **W/(m*K)** | $(BTU/(ft-hr-^o\,\mathbf{F}))$ |
|---|---|---|
| **Black Aerogel** | 0.012 | 0.0069 |
| **White Aerogel** | 0.014 | 0.0081 |
| **Fiberglass** | 0.028 | 0.0162 |
| **Carbon Fiber** | 0.036 | 0.0208 |
| **Thermolastic Insulation** | 0.041 | 0.0237 |
| **Calcium Silicate** | 0.069 | 0.0400 |

### 3.1.1 Heat Loss from Surface Lines

#### 3.1.1.1 With/without Insulation

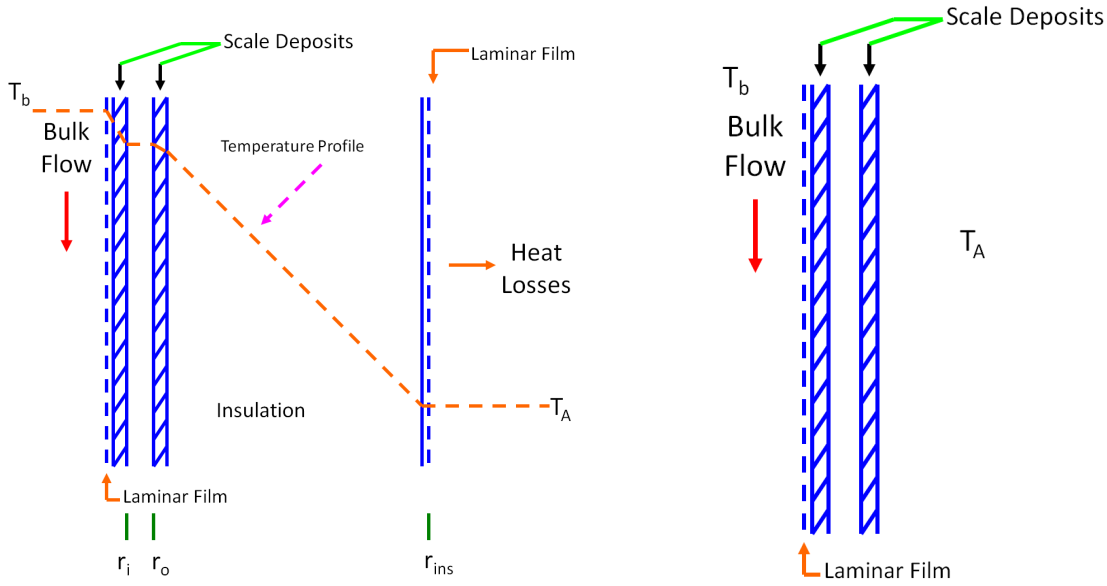


(a) Surface pipe with insulation.

(b) Surface pipe without insulation.

Figure 3.1: Schematic representation of resistance to heat transfer with or without temperature profile.

In Figure 3.1 a. we have a representative resistance to heat transfer and a temperature profile. Prats [41] stated that even though heat losses from surface lines in hot fluid injection operations may be a small fraction of the total heat injected, it is generally worthwhile to use insulation to reduce heat losses to save both money and fuel. That savings can be significant will be demonstrated by means of steam injection examples.

The basic equation used to calculate heat losses per unit length of pipe, $\dot{Q}_{ls}$, is

$$\dot{Q}_{ls} = \frac{T_b - T_A}{R_h} \tag{3.1}$$

where $R_h$ is represented as $R_h = \frac{1}{2\pi r U}$, $U$ is the overall coefficient of heat transfer, and

r is an arbitrary radius that usually coincides with the radius of one of the surfaces for which the heat loss is being determined. Here, $R_h$ is the specific thermal resistance (thermal resistance per unit length of pipe) and is given in units of $(BTU/(ft-hr-^o$ F$))^{-1}$, $T_b$ is the bulk temperature of the fluid in the pipe in degrees Fahrenheit, $T_A$ is the ambient temperature of the atmosphere in degrees Fahrenheit, and $\dot{Q}_{ls}$ is the rate of heat loss per unit length of pipe in $BTU/(ft-hr)$. Rates of heat loss during transient periods can be several times greater than at steady state. Transient effects generally are neglected in calculations of heat losses from thermal lines, because the transient phase is often of short duration (of the order of less than a day). For a pipe covered with insulation, the specific thermal resistance of heat loss is given as

$$R_h = \frac{1}{2\pi}\left[\frac{1}{h_f r_i} + \frac{1}{h_{pi} r_i} + \frac{1}{\lambda_p} ln\frac{r_o}{r_i} + \frac{1}{h_{po} r_o} + \frac{1}{\lambda_{ins}} ln\frac{r_{ins}}{r_o} + \frac{1}{h_{fc} r_{ins}}\right] \tag{3.2}$$

Here $h_f$ is the film coefficient of heat transfer between the fluid inside the pipe and the pipe wall, $h_{pi}$ is the coefficient of heat transfer across any deposits of scale or dirt at the inside wall of the pipe, $h_{po}$ is the coefficient of heat transfer across the contact between pipe and insulation, $h_{fc}$ is the coefficient of heat transfer due to forced convection (air currents) at the outer surface of the insulation, $r_i$ is the inner radius of the pipe,$r_o$ is the outer radius of the pipe and essentially the inner radius of the insulation, $r_{ins}$ is the external radius of the insulation, and $\lambda_p$ and $\lambda_{ins}$ are the thermal conductivities of the pipe and insulation. Coefficients of heat transfer are expressed in $(BTU/(sqft - hr -^o$ F$))$ , radii in feet, and thermal conductivities in $(BTU/(ft - hr -^o$ F$))$. Because the temperature on the surface of most insulated lines is low, radiation is usually insignificant and is not included in Eq.3.2 above. The physical significance of each of the six terms in the right side of Eq.3.2 is illustrated in Figure 3.1. Each of the six terms is proportional to a thermal resistance in the system affecting heat losses. Adjacent to the inner surface of the pipe is a low-velocity

fluid film (1). Because of its low velocity, this film has heat transfer characteristics different from those of the flowing bulk fluid and accounts for the introduction of the film coefficient of heat transfer $h_f$. Note that the resistance to heat flow across this film decreases as the value of the coefficient of heat transfer increases. Scale or dirt deposits at the inside (2) and outside (4) pipe walls lead to coefficients of heat transfer $h_{pi}$ and $h_{po}$, respectively. Heat transfer through the pipe wall (3) and the insulation (5) is by conduction. A low velocity fluid film at the exterior surface of the insulation (6), which affects heat losses to the atmosphere by forced convection, leads to the coefficient of heat transfer $h_{fc}$. It should be pointed out that adding more insulation does not necessarily reduce the rate of heat losses further.

### 3.1.2 Heat Loss from Sea Level to Sea Floor

#### 3.1.2.1 With/without Insulation

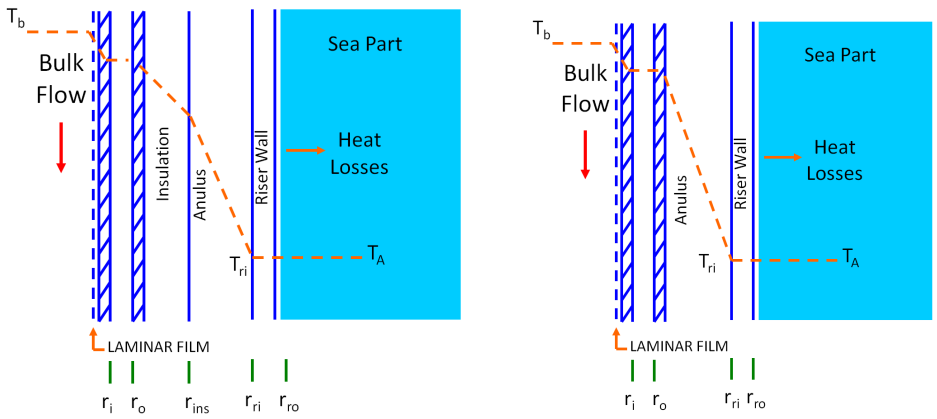


(a) Sea Part with insulation.

(b) Sea Part without insulation.

Figure 3.2: Schematic representation of resistance to heat transfer with temperature profile.

For the sea level heat loss calculation, we have made several assumptions taking Figure 3.4 as reference:

1. heat transfer is steady because the specified thermal conditions at the boundaries do not change with time,
2. heat transfer is one dimensional due to thermal symmetry about the midpoint,
3. thermal conductivity is constant,
4. sea temperature does not change along the wellbore

$$R_{total} = R_{conv,1} + R_{cycl,1} + R_{cycl,2} + R_{cycl,3} + R_{conv,2} \tag{3.3}$$

$$R_{total} = \frac{1}{h_1 A_1} + \frac{1}{2\pi L k_1} ln\frac{r_2}{r_1} + \frac{1}{2\pi L k_2} ln\frac{r_3}{r_2} + \frac{1}{2\pi L k_3} ln\frac{r_4}{r_3} + \frac{1}{h_2 A_4} \tag{3.4}$$

In order to calculate heat losses from offshore wells we have to find $T_{ins}$ and $U_{to}$ and also sea water parameters such as thermal diffusivity, thermal conductivity, density, specific heat at the given salinity and temperature of the sea.

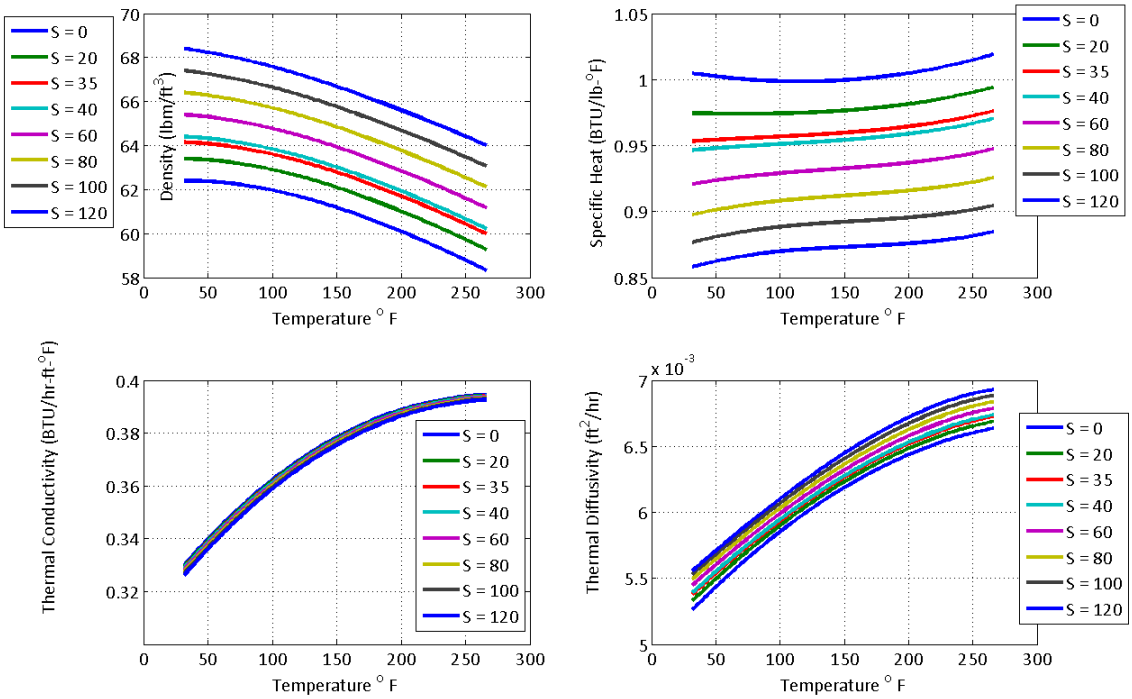


Figure 3.3: Sea water properties change with temperature and salinity[36].

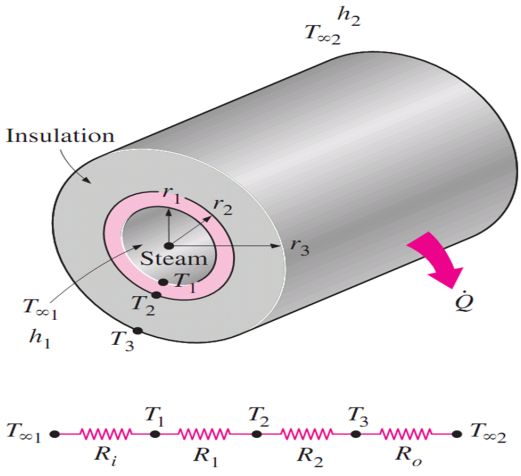


Figure 3.4: Schematic representation of the wellbore.

### 3.1.3 Heat Loss from Sea Floor to Reservoir

#### 3.1.3.1 With/without Insulation

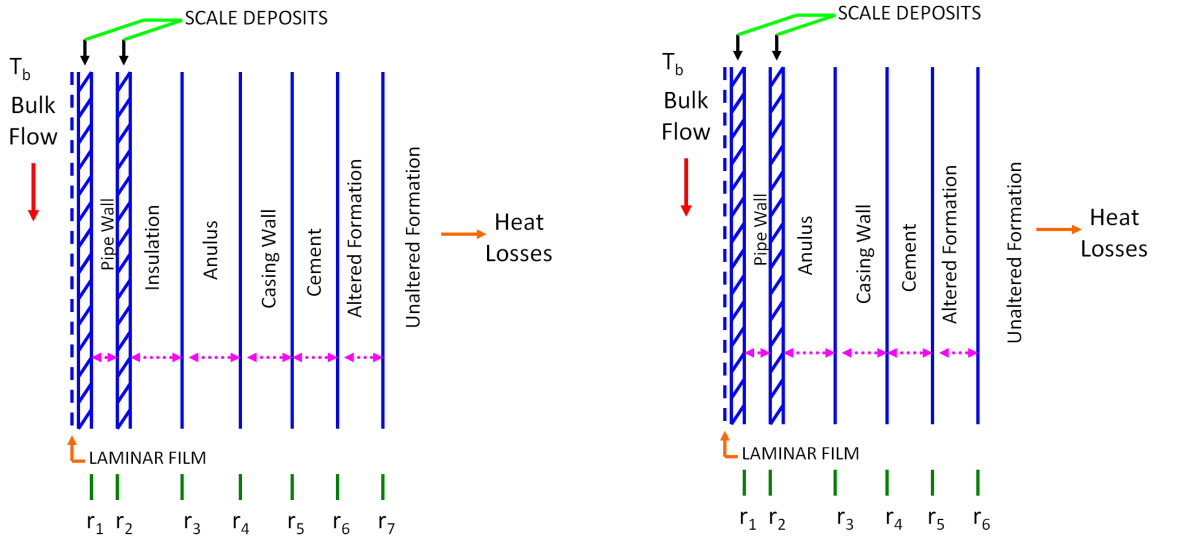


(a) Sea Floor to Reservoir with insulation.

(b) Sea Floor to Reservoir without insulation.

Figure 3.5: Schematic representation of resistance to heat transfer sea floor to reservoir.

Heat losses from wells never reach a steady state. They attain, as pointed out by Ramey [42] and Willhite [49], a quasisteady state in which the rate of heat loss is a monotonically decreasing function of time. This function of time, is discussed later in more detail. It is a measure of how fast the earth conducts heat away from the well. Heat losses from the well to the earth are characterized by Eq. 3.1, where in this case the ambient temperature is the geothermal temperature and, thus, a function of depth. In this case, of course, the specific thermal resistance is time dependent, reflecting the variable effective thermal resistance of the earth. A representation of the typical elements offering resistance to heat losses from the wellbore is given in Fig 3.5. For the insulated tubing held concentrically within the casing shown in this

figure, the heat resistance elements are combined to obtain the overall coefficient of heat loss:

$$R_h = \frac{1}{2\pi}\left[\frac{1}{h_f r_i} + \frac{1}{h_{pi} r_i} + \frac{1}{\lambda_p} ln\frac{r_o}{r_i} + \frac{1}{h_{po} r_o} + \frac{1}{\lambda_{ins}} ln\frac{r_{ins}}{r_o} + \frac{1}{h_{\varsigma,an} r_{ins}} + \frac{1}{\lambda_p} ln\frac{r_{co}}{r_{ci}} + \frac{1}{\lambda_{cem}} ln\frac{r_w}{r_{co}} + \frac{1}{\lambda_{Ea}} ln\frac{r_{Ea}}{r_w} + \frac{f(t_D)}{\lambda_E}\right] \tag{3.5}$$

The first five terms have been discussed in the preceding section for heat loss from surface lines. The last five terms represent, in order of appearance, the resistance to radiation and convection in the annulus, the resistance of casing, the resistance of the cement, the resistance of an altered zone (resulting from drying due to high temperatures) in the earth, and the variable resistance of the earth.

Different well designs lead to different expressions for determining the overall thermal resistance $R_h$. In Eq, $h_{\varsigma,an}$ is the radiation and convection coefficient of heat transfer for the annulus, $r_{ci}$ and $r_{co}$ are the inner and outer casing radii, $r_w$ is the wellbore radius, $r_{Ea}$ is the radius of the altered zone in the earth near the wellbore, $\lambda_{cem}$ is the thermal conductivity of the cement, $\lambda_{Ea}$ and $\lambda_E$ are the thermal conductivities of the altered and unaltered earth, and $f(t_D)$ is the time function that reflects the thermal resistance of the earth. Coefficients of the heat transfer are expressed in $(BTU/(sqft - hr - ^o\mathrm{F}))$, radii in feet, and thermal conductivities in $(BTU/(ft - hr - ^o\mathrm{F}))$. The function $f(t_D)$ is dimensionless, and the dimensionless time is discussed later. The function $f(t_D)$ and the radiation-convection coefficient of heat transfer in the annulus, $h_{\varsigma,an}$, are the only additional terms requiring discussion. The function $f(t_D)$ has been discussed by a number of authors, here only the Ramey[42] and Willhite[49] representation is going to be discussed. $f(t_D)$ is represented in terms of dimensionless time:

$$t_D = \frac{\alpha_E t}{r_w^2} \tag{3.6}$$

if there is an altered zone,

$$t_D = \frac{\alpha_E t}{r_{Ea}^2} \tag{3.7}$$

here $\alpha_E$ is the thermal diffusivity of the earth in square feet per hour, and t is the time from start of heating in hours. For values of $t_D \leq 100$ and is then Ramey [42] gives calculation:

$$f(t_D) \simeq \frac{1}{2} * (lnt_D) + 0.403 \tag{3.8}$$

for $t_D \leq 100$. For values of of $t_D \leq 100$, Willhite [49] has published Table 3.2. This Table 3.2 is used to interpolate the value for finding $f(t_D)$.

Table 3.2: Time Function $f(t_D)$ for the boundary condition model [49].

| $t_D$ | **100** | **50** | **20** | **10** | **5.0** | **2.0** | **1.0** | **0.5** | **0.2** | **0.1** | **0.05** | **0.02** | **0.01** | **0.0** |
|---|---|---|---|---|---|---|---|---|---|---|---|---|---|---|
| 0.1 | 0.313 | 0.313 | 0.314 | 0.316 | 0.318 | 0.323 | 0.330 | 0.345 | 0.373 | 0.396 | 0.417 | 0.433 | 0.438 | 0.445 |
| 0.2 | 0.423 | 0.423 | 0.424 | 0.427 | 0.430 | 0.439 | 0.452 | 0.473 | 0.511 | 0.538 | 0.568 | 0.572 | 0.578 | 0.588 |
| 0.5 | 0.616 | 0.617 | 0.619 | 0.623 | 0.629 | 0.644 | 0.666 | 0.698 | 0.745 | 0.772 | 0.790 | 0.802 | 0.806 | 0.811 |
| 1.0 | 0.802 | 0.803 | 0.806 | 0.811 | 0.820 | 0.842 | 0.872 | 0.910 | 0.958 | 0.984 | 1.000 | 1.010 | 1.010 | 1.020 |
| 2.0 | 1.020 | 1.020 | 1.030 | 1.040 | 1.050 | 1.080 | 1.110 | 1.150 | 1.200 | 1.220 | 1.240 | 1.240 | 1.240 | 1.250 |
| 5.0 | 1.360 | 1.370 | 1.370 | 1.380 | 1.400 | 1.440 | 1.480 | 1.520 | 1.560 | 1.570 | 1.580 | 1.590 | 1.590 | 1.590 |
| 10.0 | 1.650 | 1.660 | 1.660 | 1.670 | 1.690 | 1.730 | 1.770 | 1.810 | 1.840 | 1.860 | 1.860 | 1.870 | 1.870 | 1.880 |
| 20.0 | 1.960 | 1.970 | 1.970 | 1.990 | 2.000 | 2.050 | 2.090 | 2.120 | 2.150 | 2.160 | 2.160 | 2.170 | 2.170 | 2.170 |
| 50.0 | 2.390 | 2.390 | 2.400 | 2.420 | 2.440 | 2.480 | 2.510 | 2.540 | 2.560 | 2.570 | 2.570 | 2.570 | 2.580 | 2.580 |
| 100.0 | 2.730 | 2.730 | 2.740 | 2.750 | 2.770 | 2.810 | 2.840 | 2.860 | 2.880 | 2.890 | 2.890 | 2.890 | 2.890 | 2.900 |

## 3.2 Steam Phase behavior calculations

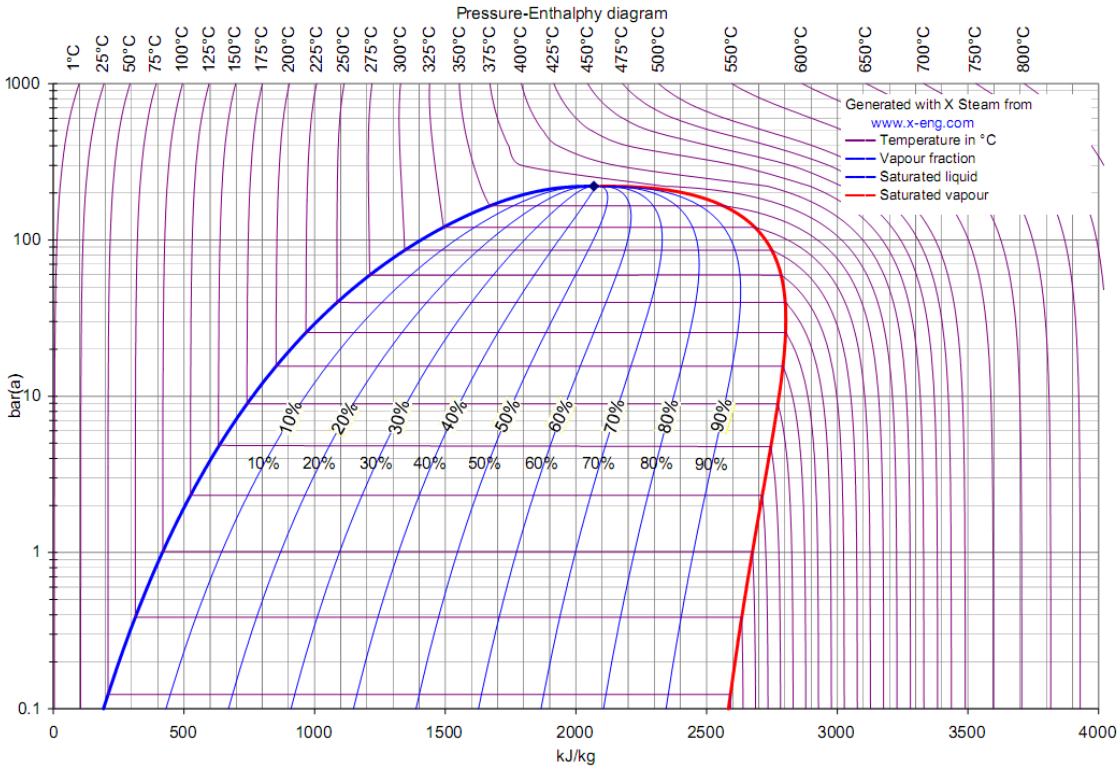


Figure 3.6: Pressure-enthalpy diagram (retrieved from [24]).

The steam properties such as density of the saturated steam and density of the saturated liquid are calculated directly using IAPWS IF97[24]. Based on the function from[24], our pressure versus enthalpy diagram looks like Figure 3.6. Steam quality changes with depth. The appropriate ordinary differential equations are described in Appendix A. To solve this differential equation in each interval of the well, a fourth order Runge-Kutta method is used with Matlab "ode45" function.

## 3.3 Two Phase Flow Correlations

Unlike single-phase flow, two-phase flow behavior is more complex than for single-phase flow. The phases tend to separate because of differences in density. Shear stresses at the pipe wall are different for each phase because of their different densities and viscosities. The main difference between gas and liquid phase is they do not travel at the same speed in the pipe. For downward flow, liquid always flows faster than the gas or vapor phase. We give information about the two phase correlations that are applied in our calculations for vertical downward flow with insulated and uninsulated tubing for both an onshore and offshore environments. The two-phase flow correlations we used in our calculations are modified Beggs and Brill, Aziz, Govier and Fogarasi, Drift Flux model, and Hasan and Kabir correlations. Besides, we also addressed flow regimes for vertical flow. We provide flow regimes in two phase vertical flow in Figure 3.7.

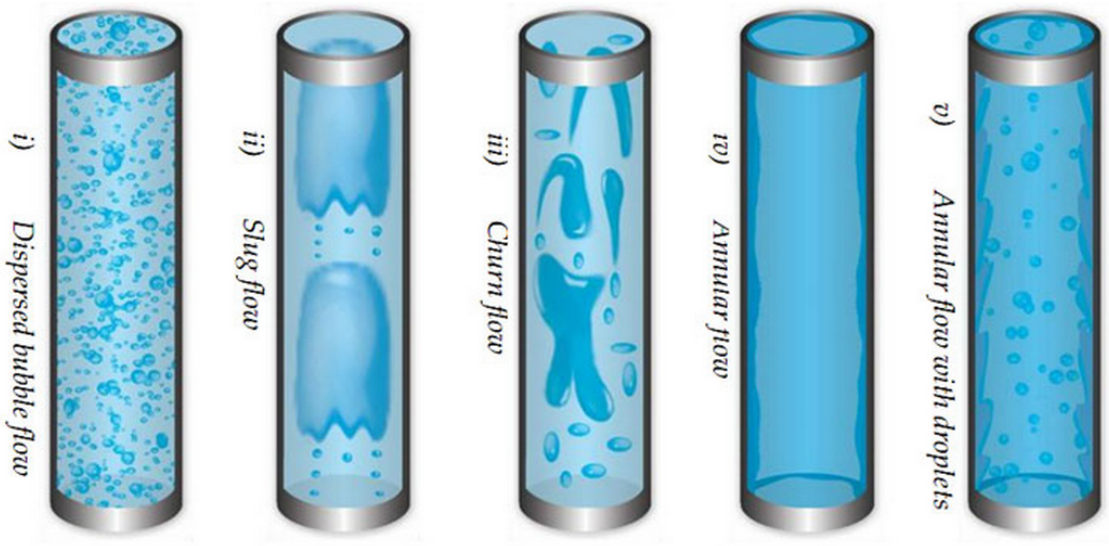


Figure 3.7: Gas-liquid flow-patterns for vertical pipes (retrieved from [12]).

The general pressure gradient equation is

$$\frac{dp}{dz} = \frac{g}{g_c}\rho_s sin\phi + \frac{f\rho_f v_m^2}{2g_c d} + \frac{\rho v_m dv_m}{g_c dz} \tag{3.9}$$

where $\rho_s = \rho_l\ H_L + \rho_g\ H_g$ and the definition for $\rho_s$ and the density term is used in the acceleration component.

$$\frac{dp}{dz} = \left(\frac{dp}{dz}\right)_{el} + \left(\frac{dp}{dz}\right)_{f} + \left(\frac{dp}{dz}\right)_{acc} \tag{3.10}$$

The pressure drop caused by elevation change depends on the density of the two-phase mixture and is usually calculated using a liquid holdup value. Friction losses require evaluation of a two-phase friction factor. Acceleration is sometimes negligible and is usually calculated only for high flow velocities. Many correlations have been developed for predicting two-phase flowing pressure gradients that differ in the manner used to calculate these three components of the total pressure gradient. Some investigators chose to assume that gas and liquid phases travel at the same velocity (no slippage between phases) for evaluating the mixture density and evaluate only a friction factor empirically. Others developed methods for calculating both liquid hold up and friction factor and some chose divide the flow conditions into patterns and developed separate correlations for each flow regime.

Figure 3.8 shows flow regime pattern both injection and production of the fluid. Predicting the flow regimes that occur at a given location in a well is extremely important. The empirical correlation or mechanistic model used to predict flow behavior varies with flow pattern. Droplet flow, also known as mist flow, happens at the wellhead during steam-only injection. In this flow, the gas phase is continuous and the bulk of the liquid is entrained as droplets in the gas phase. The pipe wall is coated with a liquid film, but the gas phase predominantly controls the pressure gradient [13, 14, 23, 46].

Annular mist flow also as known as annular droplet flow occurs right after the mist flow and is characterized by the axial continuity of the gas phase in a central core with the liquid flowing downward, both as a thin film along the pipe wall and as dispersed droplet in the core. [13, 14, 23, 46].

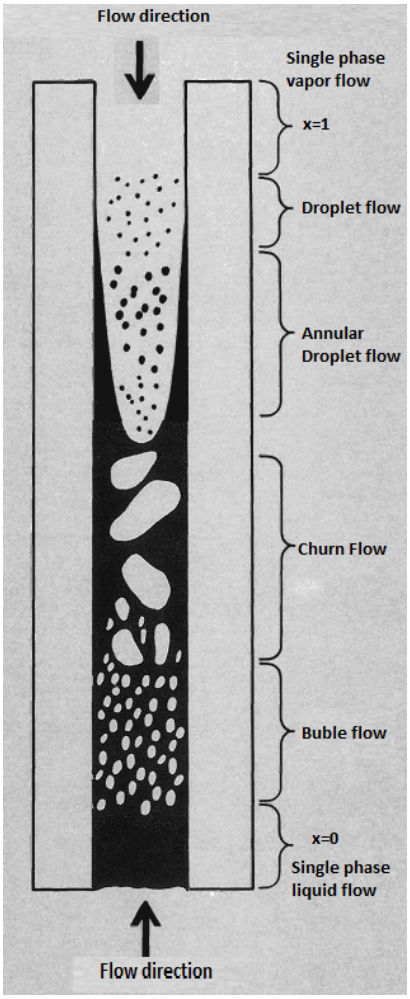


Figure 3.8: Vertical downward two-phase flow [33].

Churn flow is the change of continuous gas phase to continuous liquid phase. There is clear distinction between gas bubbles and liquid phase like gas phase trapped into largebubbles. Neither phase appears to be continuous. [13, 14, 23, 46].

During slug flow, the pipe is almost completely filled with the liquid and free gas phase is present in small bubbles. The bubbles move at different velocities and except for their density, have little effect on the pressure gradient. The wall of the pipe always contacts with the liquid phase [13, 14, 23, 46].

The correlations addressed in this study are discerned from each other by taking into account both the slippage effect and flow patterns. Parameters are calculated in two-phase flow requires knowledge of several parameters such as liquid holdup, superficial velocity of both gas and liquid phases, viscosity of both phases, slip velocity and no-slip velocity values. Here we are going to give equations of them.

**Liquid Holdup and Slippage Effect**

When two or more phases are present in a pipe, they tend to flow at different

in-situ velocities. These in-situ velocities depend on the density and viscosity of each phase. Typically the phase that is less dense flows faster than the other. This causes a "slip" effect between the phases. As a consequence, the in-situ volume fractions of each phase (under flowing conditions) differ from the input volume fractions of the pipe. Liquid holdup is defined as the ratio of the volume of a pipe segment occupied by liquid to the volume of the pipe segment. That is

$$H_L = \frac{volume \quad of \quad liquid \quad in \quad a \quad pipe \quad segment}{volume \quad of \quad pipe \quad segment} \tag{3.11}$$

Liquid holdup is a fraction that varies from zero for all gas flow to one for all liquid flow. The remainder of the pipe segment is of course occupied by gas, that is referred to as gas holdup or gas fraction. That is

$$H_g = 1 - H_L \tag{3.12}$$

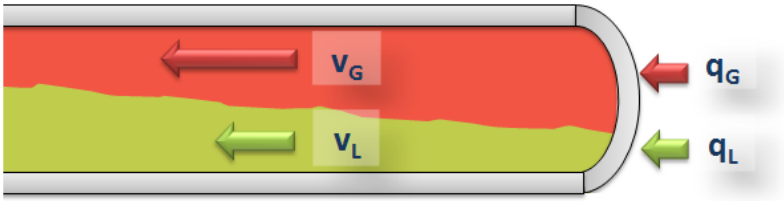


Figure 3.9: Liquid Holdup and Slippage effect representation (retrieved from[4]).

**No – Slip Liquid Holdup**

No-slip holdup, sometimes called input liquid content, is defined as the ratio of the volume of liquid in a pipe segment divided by the volume of the pipe segment which would exist if the gas and liquid traveled at the same velocity (no-slippage). It can

be calculated directly from the known liquid and gas from rates as

$$C_L = \frac{q_L}{q_L + q_g} \tag{3.13}$$

$$C_g = 1 - C_L = \frac{q_g}{q_L + q_g} \tag{3.14}$$

**Velocity**

Many two-phase flow correlations are based on a variable called superficial velocity. The superficial velocity of a fluid phase is defined as the velocity which that phase would exhibit if it flowed through the total cross section of the pipe alone. Superficial velocity for the gas phase is

$$v_{sg} = \frac{q_g}{A} \tag{3.15}$$

Actual gas velocity is

$$v_g = \frac{q_g}{AH_g} \tag{3.16}$$

Superficial velocity for liquid phase is

$$v_{sL} = \frac{q_L}{A} \tag{3.17}$$

The actual liquid velocity is

$$v_s = \frac{q_L}{AH_L} \tag{3.18}$$

The two-phase mixture velocity is

$$v_m = v_{sL} + v_{sg} \tag{3.19}$$

The slip velocity is

$$v_s = v_g - v_L = \frac{v_{sg}}{H_g} - \frac{v_{sL}}{H_L} \tag{3.20}$$

The no-slip holdup is

$$C_L = \frac{v_{sL}}{v_m} \tag{3.21}$$

**Viscosity**

Viscosity of the both saturated water and saturated steam is calculated based on the correlation of from Liang et al. [32].

For saturated water viscosity

$$\begin{aligned} \mu_w &= exp[0.484045 - 3.1115 * 10^{-2} * T^{0.95} + 1.3192 * 10^{-4} * T^{1.9} \\ &\quad -2.2934 * 10^{-7} * T^{2.85}] \end{aligned} \tag{3.22}$$

For saturated steam viscosity

$$\begin{aligned} \mu_s &= 0.0085 + exp[-7.0661 + 2.1106 * 10^{-2} * T - 7.2085 * 10^{-5} * T^2 \\ &\quad +1.0111 * 10^{-7} * T^3] \end{aligned} \tag{3.23}$$

### 3.3.1 Modified Beggs and Brill Model

For multiphase flow, many of the published correlations are applicable for "vertical flow" only, while others apply for "horizontal flow" only. Not many correlations apply to the whole spectrum of flow situations that may be encountered in oil and gas operations, namely uphill, downhill, horizontal, inclined and vertical flow. The Beggs and Brill [3, 7, 14, 39] correlation, is one of the few published correlations capable of handling all these flow directions. It was developed using 1" and 1-1/2" sections of pipe that could be inclined at any angle from the horizontal.

The Beggs and Brill multiphase correlation deals with both the friction pressure loss and the hydrostatic pressure difference. First the appropriate flow regime for

the particular combination of gas and liquid rates (Segregated, Intermittent or Distributed) is determined. The liquid holdup, and hence, the in-situ density of the gas-liquid mixture is then calculated according to the appropriate flow regime, to obtain the hydrostatic pressure difference. A two-phase friction factor is calculated based on the "input" gas-liquid ratio and the Moody friction factor table using Colebrook equation. From this the friction pressure loss is calculated using "input" gas-liquid mixture properties.

#### 3.3.1.1 Flow-Pattern Determination

The Beggs and Brill correlation needs to identify the flow pattern at the given flowing conditions in order to calculate the liquid holdup and friction pressure drop. For this purpose, the Beggs and Brill correlation makes use of a horizontal flow pattern map built based on the Froude number of the mixture ($F_{rm}$) and input liquid content (no-slip liquid holdup, $C_L$).

In order to build the flow map, the observed flow patterns were grouped as: segregated (stratified, wavy and annular flow), intermittent (plug and slug flow), distributed (bubble and mist flow), and transition (flow pattern included after a modification of the original publication that considers the region between the segregated and intermittent grouped patterns).

The boundaries between these groups of flow patterns appear as curves in a log-log plot in the original publication by Beggs and Brill. This was later revised so that straight lines could be used instead. We use this modified flow pattern map in our calculations. The revised lines that define the boundaries are defined as follows (where * stands for the modification of the original curve to a straight line in a log-log plot)

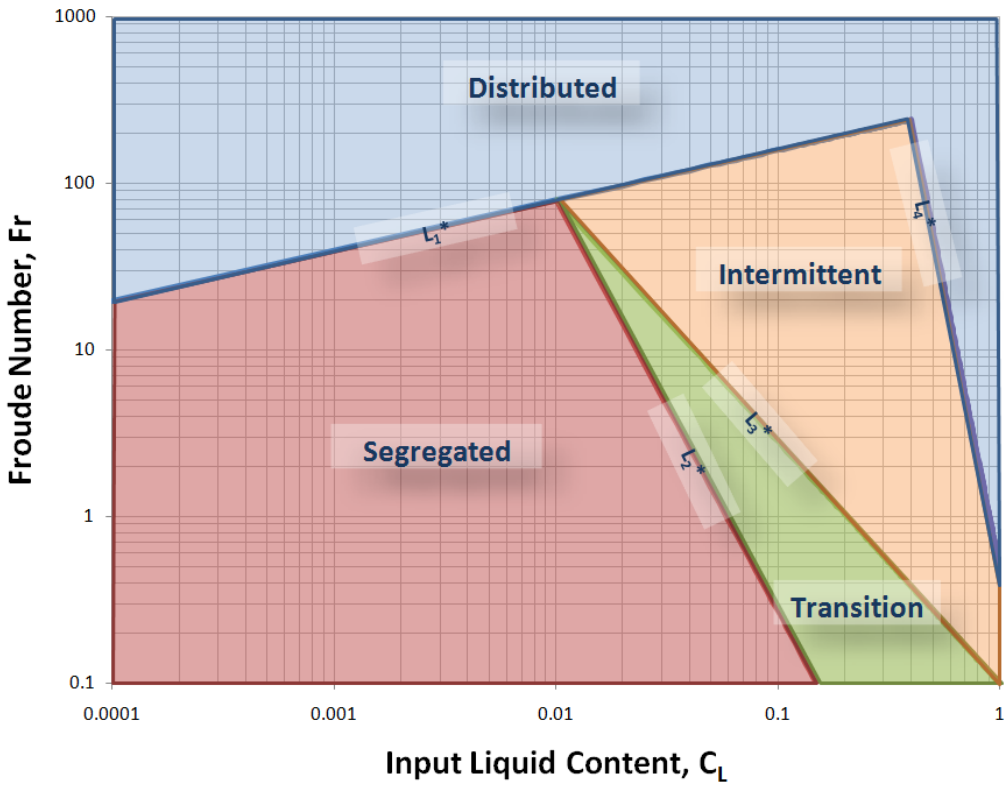


Figure 3.10: Flow Map for the Beggs and Brill Correlation (retrieved from[4]).

$$L_1^* = 316 C_L^{0.302} \tag{3.24}$$

$$L_2^* = 0.0009252 C_L^{-2.4684} \tag{3.25}$$

$$L_3^* = 0.1 C_L^{-1.4516} \tag{3.26}$$

$$L_4^* = 0.5 C_L^{-6.738} \tag{3.27}$$

The identified flow pattern is the one that would exist if the pipe were horizontal. Unless the pipe is actually in the horizontal position, the Beggs and Brill correlation is not able to recognize the actual flow pattern under the given conditions. Therefore, to calculate the liquid holdup, we first determine the liquid holdup for the horizontal

flow, and this value is then corrected for the angle of interest.

The Froude number is a dimensionless number that relates the inertia with respect to the gravitational forces. For a mixture, it is obtained as

$$Fr_m = \frac{V_m^2}{gD} \tag{3.28}$$

Once the input liquid content ($C_L$) and Froude number of the mixture ($F_{rm}$) are determined, the corresponding flow pattern is identified when the following inequalities are satisfied.

$SegregatedFlow$ occurs when $C_L < 0.01$ and $Fr_m < L_1^*$ or $C_L \geq 0.01$ and $Fr_m < L_2^*$ .

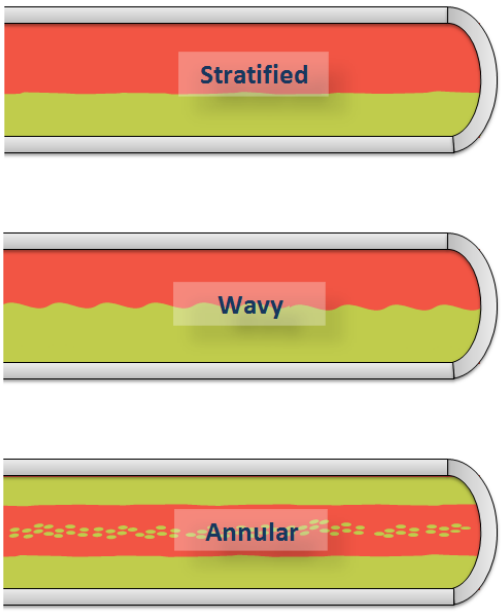


Figure 3.11: Segregated Flow Regime (retrieved from[4]).

$IntermittentFlow$ occurs when $0.01 \leq C_L < 0.4$ and $L_3 < Fr_m \leq L_1^*$ or $C_L \geq 0.4$ and $L_3^* < Fr_m \leq L_4^*$.


Figure 3.12: Intermittent Flow Regime (retrieved from[4]).

*DistributedFlow* occurs when $C_L < 0.4$ and $Fr_m \geq L_1^*$ or $C_L \geq 0.4$ and $Fr_m > L_4^*$.

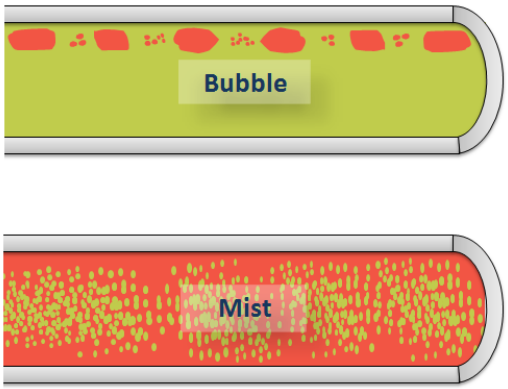


Figure 3.13: Distributed Flow Regime (retrieved from[4]).

*TransitionFlow* occurs when $C_L \geq 0.01$ and $L_2^* < Fr_m < L_3^*$.

#### 3.3.1.2 Hydrostatic Pressure Difference

Once the flow pattern has been determined, the liquid holdup is then calculated. Beggs and Brill divided the liquid holdup calculation into two parts. First, the liquid holdup for horizontal flow, $E_L(0)$, is determined. Afterwards, this horizontal holdup is corrected for inclined flow to obtain the actual holdup, $E_L(\theta)$. The horizontal

holdup must be $E_L(0) \geq C_L$. Therefore, in the event that $E_L(0) < C_L$, the horizontal holdup is set to $E_L(0) = C_L$. The expression used to calculate the horizontal holdup changes per flow pattern group as follows in **MatLab**:

---

**if** $strcmp(Flowpattern,'Segregated')$ **then**
  $E_L(0) \leftarrow \frac{0.98 C_L^{0.4846}}{Fr_m^{0.0868}}$
**else**
  **if** $strcmp(Flowpattern,'Intermittent')$ **then**
    $E_L(0) \leftarrow \frac{0.845 C_L^{0.5351}}{Fr_m^{0.0173}}$
  **end if**
  **if** $strcmp(Flowpattern,'Distributed')$ **then**
    $E_L(0) \leftarrow \frac{1.065 C_L^{0.5824}}{Fr_m^{0.0609}}$
  **end if**
  **if** $strcmp(Flowpattern,'Transition')$ **then**
    $A \leftarrow \frac{L_3^* - Fr_m}{L_3^* - L_2^*}$
    $B \leftarrow 1 - A$
    $E_L(0)_{Segregated} \leftarrow \frac{0.98 C_L^{0.4846}}{Fr_m^{0.0868}}$
    $E_L(0)_{intermittent} \leftarrow \frac{0.845 C_L^{0.5351}}{Fr_m^{0.0173}}$
    $E_L(0)_{Transition} \leftarrow A E_L(0)_{Segregated} + B E_L(0)_{Intermittent}$
  **end if**
**end if**

---

Once the horizontal in-situ liquid volume fraction is determined, the actual liquid volume fraction is obtained by correcting $E_L(0)$ by an inclination factor $B(\theta)$:

$$E_L(\theta) = B(\theta) E_L(0) \tag{3.29}$$

$$B(\theta) = 1 + \beta \left[ sin(1.8\theta) - \frac{1}{3} sin^3(1.8\theta) \right] \tag{3.30}$$

$\beta$ for all type of flow pattern is

$$\beta = (1 - C_L) ln \left[ \frac{4.70 N_{vl}^{0.1244}}{C_L^{0.3692} Fr_m^{0.0978}} \right] \tag{3.31}$$

where $N_v l = 1.938 V_{sl} \left(\frac{\rho_L}{g\sigma}\right)^{\frac{1}{4}}$ and $\beta$ must always be $\geq 0$. Therefore if a negative value of $\beta$ is obtained, $\beta$=0.

Once the actual liquid holdup $E_L(\theta)$ is calculated, the mixture density $\rho_m$ is obtained. Mixture density, in turn, is used to calculate the pressure change due to the hydrostatic head of the vertical component of the pipe

$$\Delta P_{HH} = \frac{\rho_m g L sin(\theta)}{144 g_c} \tag{3.32}$$

#### 3.3.1.3 Frictional Pressure Loss

In order to calculate frictional losses, a normalizing friction factor $f_{NS}$ is used. To determine $f_{NS}$, we utilize the Moody Friction factor calculated using the Colebrook equation. For this purpose, the no-slip Reynolds number is used:

$$Re_{NS} = \frac{\rho_{NS} V_m D}{\mu_{NS}} \tag{3.33}$$

Based on experimental data, Beggs and Brill presented a correlation for the ratio of the two-phase friction factor $f_{tp}$ and the normalizing (no-slip) friction factor resulting in the following exponential equation:

$$f_{tp} = f_{NS} e^S \tag{3.34}$$

The value of S depends on the no-slip and the actual liquid holdup:

$$S = \frac{ln(Y)}{-0.0523 + 3.182(ln(Y)) - 0.8725(ln(Y))^2 + 0.01853(ln(Y))^4} \tag{3.35}$$

where Y = $\frac{C_L}{E_L(\theta)^2}$

1: **if** $Y \geq 1$ and $Y \leq 1.2$ **then**
2: $S \leftarrow ln(2.2Y - 1.2)$
3: **else**
4: $S \leftarrow \frac{ln(Y)}{-0.0523+3.182(ln(Y))-0.8725(ln(Y))^2+0.01853(ln(Y))^4}$
5: **end if**

Finally, the expression for pressure loss due to friction is:

$$\Delta P_f = \frac{2 f_{tp} V_m^2 \rho_{NS} L}{144 g_c} \tag{3.36}$$

### 3.3.2 Aziz, Govier and Fogarasi Model

Fontanilla[19] investigated applicability of the Aziz et al. [29] mechanistically based pressure drop correlation for downwards steam flow. As Fontanilla stated for Aziz et al. [29], this correlation that was strictly developed for upward vertical flow needs some modification in order to apply to downward flow. Those modifications are included in the bubble flow and in the slug flow patterns. Due to the large volume of steam(gas) as compared to the water that is present in most steam injection wells, the annular mist flow pattern is very common.

#### 3.3.2.1 Flow Pattern Determination

In Figure 3.14 we can see the flow-pattern map for different flow types.

$$N_x = V_{Sg} \left(\frac{\rho_g}{0.0764}\right)^{\frac{1}{3}} \left[\left(\frac{72}{\sigma_L}\right)\left(\frac{\rho_L}{62.4}\right)\right]^{\frac{1}{4}} \tag{3.37}$$

$$N_y = V_{SL} \left[\left(\frac{72}{\sigma_L}\right)\left(\frac{\rho_L}{62.4}\right)\right]^{\frac{1}{4}} \tag{3.38}$$

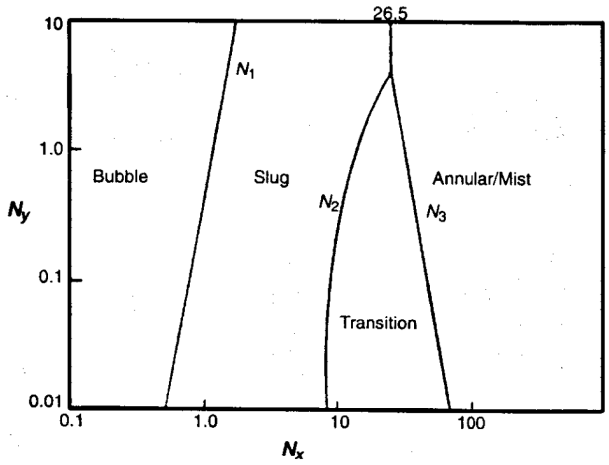


Figure 3.14: Flow Pattern map for Aziz et al. (retrieved from[14]).

In the Figure 3.14 we have several lines that represents flow-pattern transitions and they are defined as:

$$N_1 = 0.51(100N_y)^{0.172} \tag{3.39}$$

$$N_2 = 8.6 + 3.8N_y \tag{3.40}$$

$$N_3 = 70(100N_y)^{-0.152} \tag{3.41}$$

where $v_{SL}$ is in ft per second, $v_S$ is in feet per second, $\rho_g$ is in pounds per cubic feet, $\rho_L$ is in pounds per cubic feet and $\sigma_L$ is in dynes per centimeter.

**Bubble Flow**

The bubble flow pattern is characterized by small bubbles of steam(gas) dispersed in a continuous water phase. In downward flow, the difference in densities of the two phases causes the bubbles to travel at a velocity lesser than the average velocity of the mixture. Bubble flow exists if $N_x < N_1$. Liquid holdup for bubble flow is calculated from

$$H_L = 1 - \frac{v_{Sg}}{v_{bf}} \tag{3.42}$$

where $v_{bf}$ is the rise velocity of small gas bubbles in a flowing liquid. This velocity is

predicted for downward flow as follow

$$v_{bf} = 1.2v_m - v_{bs} \tag{3.43}$$

where the first term is the approximate velocity of the fluid mixture, accounting for the nonuniform velocity and bubble concentration profiles across the cross section, and $v_{bs}$ is the rise velocity of a continuous swarm of small bubbles in a static liquid column. The $v_{bs}$ term is predicted from

$$v_{bs} = 1.41 \left[ \frac{\sigma_L g(\rho_L - \rho_g)}{\rho_L^2} \right]^{\frac{1}{4}} \tag{3.44}$$

The frictional component of the pressure gradient is determined as

$$\frac{\partial p}{\partial Z} = \frac{f \rho_s v_m^2}{2d} \tag{3.45}$$

where $\rho_s$ is determined from equation (4.34) and friction factor from Moody Friction factor calculation using the Colebrook equation[27].

$$\rho_s = \rho_L H_L + \rho_g (1 - H_L) \tag{3.46}$$

$$N_{Re} = \frac{\rho_L v_m d}{\mu_L} \tag{3.47}$$

The acceleration component of the pressure gradient is considered to be negligible for bubble flow.

**Slug Flow**

Slug flow exists if $N_1 < N_x < N_2$ for $N_y < 4$ or $N_1 < N_x < 26.5$ for $N_y \geq 4$.
The liquid holdup for slug flow is also calculated from Eq.(4.30) and Eq.(4.37). For slug flow, however, the bubble-rise velocity in a static liquid column is based on large bubble. Aziz et al.[29] state that

$$v_{bs} = C\sqrt{\frac{gd(\rho_L - \rho_g)}{\rho_L}} \tag{3.48}$$

where C was given by Wallis as

$$C = 0.345\left[1 - e^{(-0.029N_v)}\right]\left[1 - e^{(\frac{3.37-N_E}{m})}\right] \tag{3.49}$$

and

$$N_E = \frac{gd^2(\rho_L - \rho_g)}{\sigma_L} \tag{3.50}$$

$$N_v = \frac{\sqrt{d^3 g\rho_L(\rho_L - \rho_g)}}{\mu_L} \tag{3.51}$$

and m is determined as

```
if N_v ≥ 250 then
    m ← 10
else
    if 250 > N_v > 18 then
        m ← 69 N_v^{-0.35}
    end if
    if N_v ≤ 25 then
        m ← 25
    end if
end if
```

The friction pressure-gradient component for slug flow is determined from

$$\left(\frac{dp}{dZ}\right)_f = \frac{f\rho_L H_L v_m^2}{2d} \tag{3.52}$$

The friction factor is obtained from a Moody friction factor and the Colebrook equation[27]. The Reynolds number is given as

$$N_{Re} = \frac{f\rho_L v_m d}{\mu_L} \tag{3.53}$$

The acceleration pressure-gradient component was considered negligible for slug flow.

**Mist Flow**

Mist flow exists when $N_x > N_3$ for $N_y < 4$ or $N_x > 26.5$ for $N_y > 4$. Aziz et al.[29] recommended the Duns and Ros [28] mist-flow method be used to calculate pressure gradient for this flow pattern.

**Transition Flow**

The transition region exists when $N_2 < N_x < N_3$ for $N_y < 4$. In Figure 4.8, the transition region does not exist for $N_y > 4$. When the transition region is predicted, the pressure gradients must be calculated with both the slug-flow and mist-flow equations. To obtain the pressure gradient, linear interpolation is performed.

$$\frac{dp}{dZ} = A\left(\frac{dp}{dZ}\right)_{slug} + (1-A)\left(\frac{dp}{dZ}\right)_{mist} \tag{3.54}$$

where $A = \frac{N_3 - N_x}{N_3 - N_2}$

#### 3.3.2.2 Modifications

Al-Najjar and Al-Soof [5] showed that improved results could be obtained with Aziz et al. method if the flow pattern map in Figure 3.14 was replaced with the Duns and Ros map. Their conclusion was based on a comparison of the predicted and measured

pressure drops for 80 tests on 15 flowing wells in Iraq.

# Chapter 4

# Effect of Non-Condensable Gas ($N_2$)

In our calculations we used $N_2$ as the non-condensable gas. We explore the partial pressure effect of $N_2$ on downhole steam quality, temperature, pressure and as well as heat loss during the steam injection. Addition of non-condensable gas into our system makes our calculation a little complex [10]. The pressure of the vapor phase is now a sum of steam partial pressure and gas partial pressure:

$$P_{total} = P_{steam} + P_{N_2} \tag{5.1}$$

where $P_{total}$ is the total pressure of the gas phase, $P_{steam}$ is the partial pressure of the steam and $P_{N_2}$ is the partial pressure of the $N_2$. We assume $N_2$ only exists in the vapor phase with steam and has the same temperature as the steam. $N_2$ is assumed not to carry heat, so contribution to the mixture enthalpy is zero. $N_2$, however, provides partial pressure during steam injection. Neglecting the enthalpy of $N_2$ is a good approximation because steam enthalpy is several orders of magnitude larger in comparison to $N_2$.

The total mol fraction of the liquid and gas phase is

$$\sum x_i = 1.0 \tag{5.2}$$

$$\sum y_i = 1.0 \tag{5.3}$$

where x is the liquid mole fraction of the components, y is the vapor mole fraction of the components. Because we have only liquid water in our system inequlibrium with steam and $N_2$, $\sum x_i = 1.0$ is always equal to $x_{water}$.

Calculation of the partial pressure of the gas components is

$$P_{N_2} = y_{N_2} * P_{total} \tag{5.4}$$

$$P_{steam} = y_{steam} * P_{total} \tag{5.5}$$

Suppose we have a system with given injection rate, steam quality, steam temperature or pressure (one determines the other), time and mol fraction of $N_2$. So, mole fraction of steam is found from Eq. 5.3 and $\sum y_2 = y_{N_2} + y_{steam} = 1.0$ yields that $y_{steam} = 1 - y_{N_2}$. With a given undilited steam pressure or temperature (one determines other), we find the total pressure as

$$P_{total} = \frac{P_{steam}}{y_{steam}} = \frac{P_{steam}}{1 - y_{N_2}} \tag{5.6}$$

Once we find total pressure we continue to find other input parameters in our calculation. Total mass of the steam is found as

$$W_{mX} = Wm * t * x \tag{5.7}$$

Having the total mass of the steam in our system, we find the total moles of the steam

as

$$Mole_X = \frac{W_{mX} * 454}{18.02} \tag{5.8}$$

With known steam mole fraction, we find how many moles of $N_2$ is in the system as

$$y_{steam} = \frac{Mole_X}{Mole_X + Mole_{N_2}} \tag{5.9}$$

Because $y_{steam}$ is known and $y_{N_2}$ is known, there is only one unknown in Eq. 5.9. $Mole_{N_2}$ is easily found using Eq. 5.9. The reason we calculated mole of the $N_2$ is because it is not changed entire process. Meaning that mass of the $N_2$ is constant al the time. The only thing is going to change in each interval is that mol fraction of the $N_2$, and it is going to increase due to the condensation of steam. Another important assumption is that the viscosity of mixture of $N_2$ and steam is the as same as the viscosity of the undiluted steam. The equation for viscosity is given by Eq.3.23.

We assume that in two phase flow, cases occur where the gas partial pressure is significant compared to the steam partial pressure. When this is the case the gas and steam act as perfect gases. Thus we use ideal gas law

$$PV = n * R * T \tag{5.10}$$

where P is the total pressure of the system in kilo pascal, n is the mole fraction of the component, R is the universal gas constant 8.314 J/K-mol and T is the temperature in Kelvin, $K =^o C + 273.15$.

Total volume of the steam and $N_2$ is obtained using ideal gas law as

$$V_{steam} = \frac{Mole_X * R * T_{steam}}{P_{steam@initial}} \tag{5.7}$$

$$V_{N_2} = \frac{Mole_{N_2} * R * T_{steam}}{P_{steam@initial}} \tag{5.8}$$

Once steam volume and $N_2$ volume are obtained, it is easy to find density of the total gas mixture. Another, potentially more accurate, method is to obtain the steam molar volume from the steam tables. In either case, the overall volume is found by applying Amagat's law. That is, the volumes of each component add ideally and there is no volume change upon mixing. The density of the gas mixture and liquid mixture are used in our calculation. In each segment of the wellbore, this calculation has to be repeated until steam reaches the reservoir.

# Chapter 5

# Graphical User Interface (GUI)

Our GUI provides several inputs parameters and options that are useful in the calculations. The user can choose different two-phase correlations and get the results as well as choose previous calculation results for post-processing. The theory behind calcualtions is well described in preceding chapters and the Appendix. The overall heat transfer coefficient is implemented both following Willhite's approach[49] and Ramey's time function[42]. This is similar to Fontanilla [19]. This chapter shows how we get the results using our GUI.

**GUI for the Main program**

The GUI is demonstrated with snapshot of the program. The first snapshot gives the background for the program. The second snapshot is about calculations for onshore environment with insulated and without insulated tubing. Also, we provide solutions for the addition of non-condensable gas $N_2$ for both onshore and offshore environments. The third snapshot is the input parameters for the offshore environment. The fourth snapshot is the output tables both onshore and offshore environments. The fifth snapshot is about the post-processing for viewing the results in figures for steam quality, steam pressure, steam temperature and heat loss along the wellbore. All

calculations take into account two-phase flow correlations.

First snapshot of the program is shown Figure 5.1, it is seen that there are several input parameters for specifically steam injection parameters for onshore cases. User can choose different insulation materials and two-phase flow correlations. Figure 5.2 is the similar input parameters except riser radius and sea temperature inputs. User also able to choose insulation materials and two phase flow correlation to calculate steam temperature, steam pressure, steam quality and heat loss values. In third figure that is Figure 5.3, after the calculation is done either for onshore or offshore cases, results are shown this part and user able to save those datas to excel files or clear them. Last one is the Figure 5.4, is post-processing the data that obtained from calculations either onshore or offshore is designed specifically to visualize the results and to save the figures or delete it.

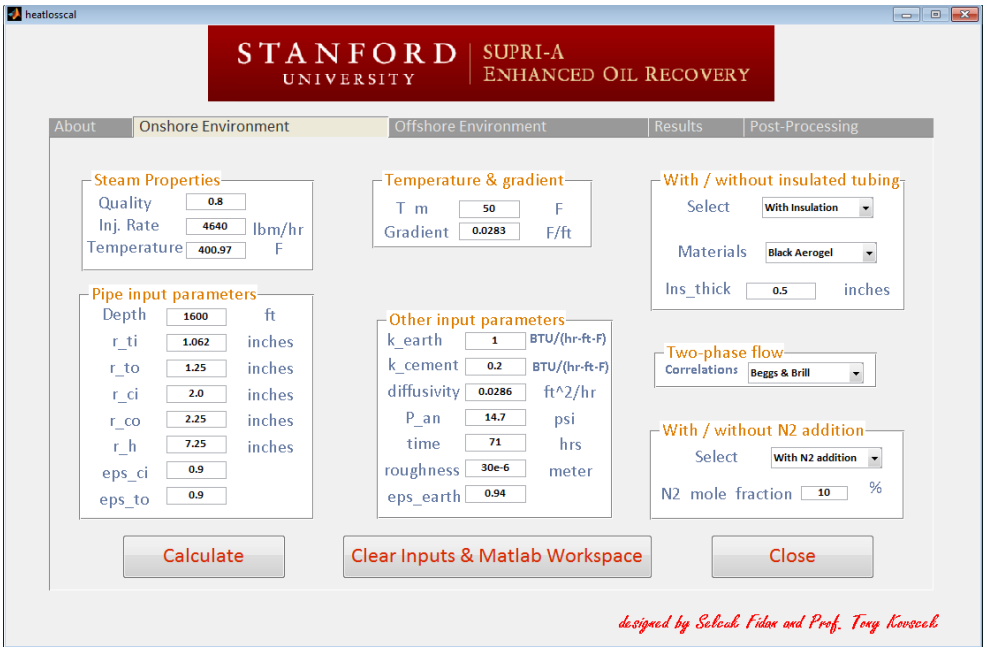


Figure 5.1: User interface developed GUI for onshore calculations.

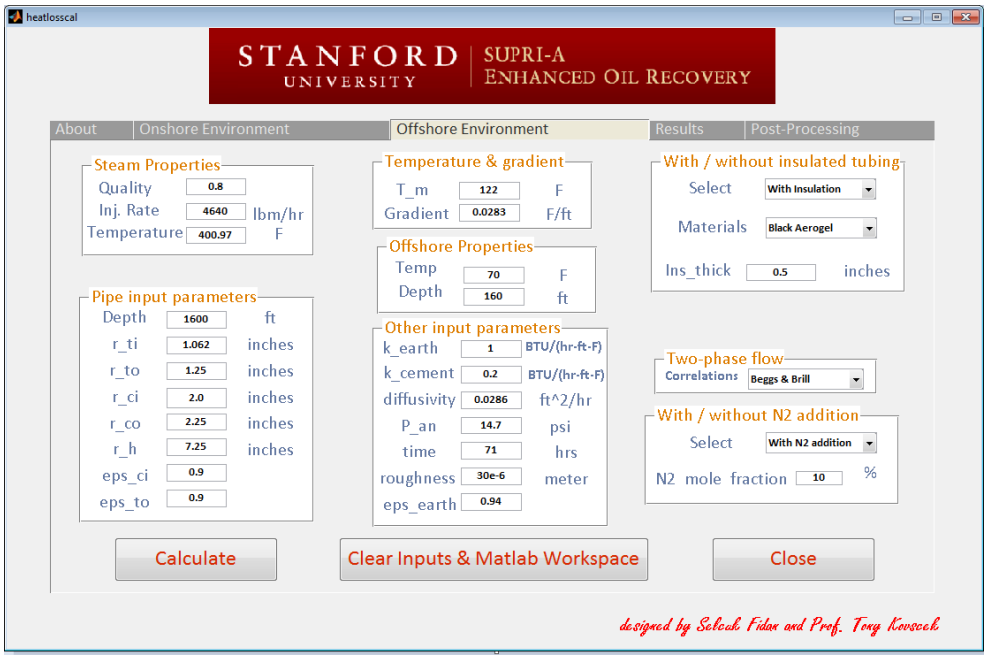


Figure 5.2: User interface developed GUI for offshore calculations.

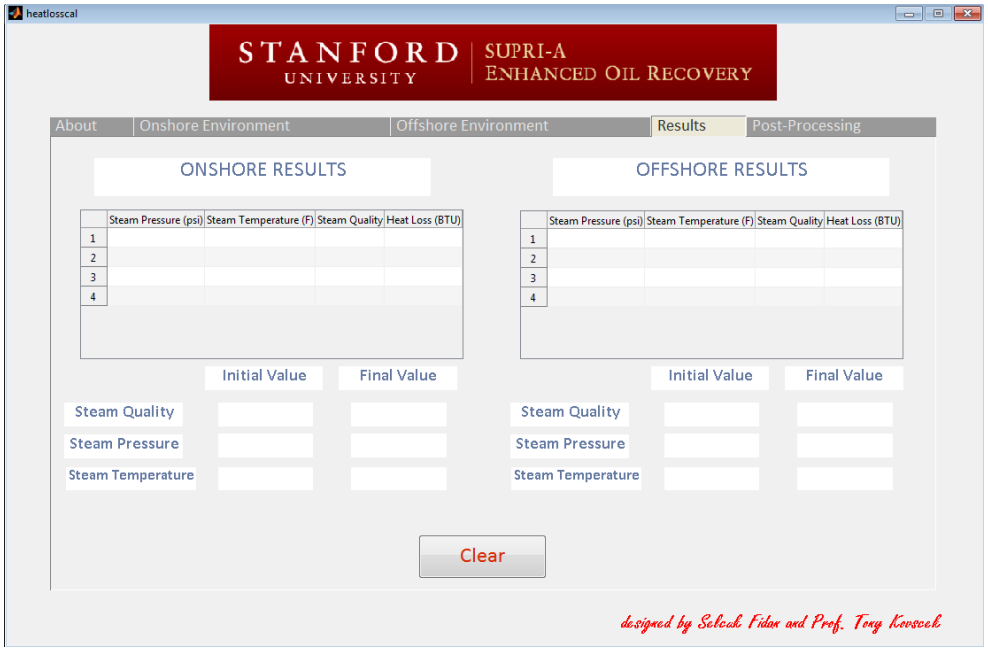


Figure 5.3: User interface developed GUI for both onshore and offshore results.


Figure 5.4: User interface developed GUI post-processing for both onshore and offshore results.

# Chapter 6

# Results and Comparisons

In this part of the study, surface line, sea and sea floor to reservoir heat loss calculations are presented using limited data provided by Prats [41]. We compared our results with Prats's [41] results. It is shown that our results match with Prats's [41] results for surface lines. For injection wells, our results are a little higher than his results. With this we found his minor mistake for onshore injection well and reported here. And then results are extended to 2 field cases [11]. Moreover, non-condensable gas addition calculations are done with different injection rate, steam quality, steam temperature, different depth and different percentage of $N_2$ addition in order to see the sensitivity of steam temperature, steam pressure, steam quality and heat loss.

## 6.1 Examples for heat loss calculation

Examples with known solutions are presented for surface line and onshore calcualtions with insulated or without insulated tubing to verify the new code. There is no example for offshore heat loss calculation, so we take input values from Prats [41] and modify the calculations to illustrate the hole of insulation. This part of results are only considered for heat loss aspects.

### 6.1.1 Example 10.1 from Prats

Steam at 550 $^oF$ is injected through 4-in. N-80 pipe at a rate of 229 B/D. Prats [41] asks "find the steady state heat loss per year per 100 ft of pipe when the pipe is (1) is insulated with 3 in of calcium silicate and (2) not insulated - i.e., bare." The average yearly temperature is 60 $^oF$, and the prevailing winds have an average velocity of 20 mph normal to the injection line. The input parameters are listed in Table 6.1.

$$h_{fc} = \frac{18 v_w^{0.6} r_{ins}^{0.6}}{r_{ins}} \tag{6.1}$$

With insulation, the over all specific thermal resistance is calculated from Eq. 3.2 and plotted into Figure 6.1 and for without insulation plotted into Figure 6.2.

Accordingly, the amount of heat lost from 100-ft length of pipe over a period of 1 year is $Q_l$=1.1581*$10^8$ BTU for the calcium silicate (highest heat loss), for black aerogel heat loss is $Q_l$=2.0302*$10^7$ BTU (lowest heat loss).

Without insulation and at a surface temperature near 550 $^oF$, radiation heat losses are important. The sum of the coefficients of heat transfer due to the radiation and free(or natural) convection for a horizontal pipe is given Table 3.1 for a several pipe sizes and temperatures. Eq. 3.2 is also applied here in order find the heat loss for without insulation case.

Thus, the amount of heat lost from a 100-ft length of pipe over a period of 1 year is: $Q_l$=6.095*$10^9$ BTU when the pipe is bare. Therefore, the insulation reduces heat losses by a factor of about 50 when using calcium silicate, however if you use aerogel it would be 280. Because one barrel of oil is roughly 6.0*$10^6$ BTU, the reduction in yearly heat losses resulting from insulating the pipe amounts to more than 1000 bbl of fuel for a 100-ft length of pipe. When you use calcium silicate you would consume 100 bbl, on the other side when you use aerogel you would consume 16 bbl for 100 ft length surface pipe. When we think about deeper wells using insulation material

should be considered especially aerogel. Table 6.1 is used when we calculate the heat losses for the uninsulated case.

In Example 10.1 with insulations, Prats [41] used calcium silicate as the insulation material and get the heat loss as, $Q_l$=1.16*$10^8$ BTU, over the year. Our result for using calcium silicate is $Q_l$=1.1581*$10^8$ BTU and it is consistent with Prats's example as shown in Figure 6.1. Without insulation, Prats [41] stated that the coefficient of heat transfer due to radiation and forced convection is estimated to be 330 $BTU/ft^2 - D - ^oF$, however, he used 110 $BTU/ft^2 - D - ^oF$ and get the heat loss results over the one year period is $Q_l$=6.21*$10^9$ BTU. In our calculation we find this minor mistake from Prats calculation, and it causes little deviation from the exact results. This shows that the real heat loss from bare tubing is $Q_l$=6.095*$10^9$ BTU as shown in Figure 6.2. Still those results match well.

In Table 6.1, there are several column headings. Abbreviations are explained as "SLwithIns" is the surface line with insulated tubing, "SLwithoutIns" is the surface line without insulated tubing, "SeawithIns" is the offshore case with insulated tubing, "SeawitouthIns" is the offshore case without insulated tubing, "2ResWithIns" is the sea floor to reservoir case with insulated tubing, and "2ResWithoutIns" is the sea floor to reservoir case without insulated tubing.

Table 6.1: Input parameters from Prats [41] as used for different example calculations.

| **Parameters** | **SLwithIns** | **SLwithoutIns** | **SeaWithIns** | **SeaWithoutIns** | **2ResWithIns** | **2ResWithoutIns** |
|---|---|---|---|---|---|---|
| $T_{steam}$ | 550 | 550 | 600 | 600 | 600 | 600 |
| $T_{average}$ | 60 | 60 | 70 | 70 | 100 | 100 |
| $r_{ti}$ | 0.1478 | 0.1478 | 0.14 | 0.14 | 0.14 | 0.14 |
| $r_{to}$ | 0.1667 | 0.1667 | 0.1458 | 0.1458 | 0.1458 | 0.1458 |
| $r_{ins}$ | 0.41467 | No Insulation | 0.2292 | No Insulation | 0.2292 | No Insulation |
| $r_{riserin}$ | 0 | 0 | 0.6 | 0.6 | 0 | 0 |
| $r_{riserout}$ | 0 | 0 | 0.75 | 0.75 | 0 | 0 |
| $h_f$ | 2000 | 2000 | 0 | 0 | 0 | 0 |
| $h_{pi}$ | $\infty$ | $\infty$ | 0 | 0 | 0 | 0 |
| $h_{po}$ | 2000 | 2000 | 0 | 0 | 0 | 0 |
| $\lambda_{pipe}$ | 25 | 25 | 25 | 25 | 0 | 0 |
| $\lambda_{cem}$ | 0 | 0 | 24 | 24 | 24 | 24 |
| $\lambda_{ins}$ | 0.166/24 | No Insulation | 0.166/24 | No Insulation | 0.166/24 | No Insulation |
| $time$ | 365*24 | 365*24 | 21*24 | 21*24 | 21*24 | 21*24 |
| $PipeLength$ | 100 | 100 | 164 | 164 | 1000 | 1000 |
| $\epsilon_{riserin}$ | 0 | 0 | 0.9 | 0.9 | 0 | 0 |
| $\epsilon_{riserout}$ | 0 | 0 | 0.9 | 0.9 | 0 | 0 |
| $\epsilon_{rto}$ | 0 | 0 | 0.9 | 0.9 | 0 | 0 |
| $\epsilon_{riserin}$ | 0 | 0 | 0 | 0 | 0.9 | 0.9 |
| $\epsilon_{riserout}$ | 0 | 0 | 0 | 0 | 0.9 | 0.9 |
| $\epsilon_{rto}$ | 0 | 0 | 0 | 0 | 0.9 | 0.9 |

Table 6.2: Radiation-natural convection coefficient of heat transfer.

| **Diameter** | **130** | **180** | **230** | **280** | **330** | **380** | **480** | **580** | **680** | **780** | **880** | **980** | **1080** | **1180** | **1280** |
|---|---|---|---|---|---|---|---|---|---|---|---|---|---|---|---|
| 0.50 | 50.9 | 59.5 | 66.2 | 74.4 | 81.8 | 90.0 | 107.0 | 127 | 149 | 174 | 202 | 234 | 269 | 307 | 352 |
| 1.00 | 48.7 | 57.1 | 63.6 | 71.5 | 79.0 | 86.9 | 104.0 | 124 | 146 | 171 | 198 | 230 | 265 | 304 | 348 |
| 2.00 | 46.3 | 54.5 | 60.5 | 68.4 | 75.4 | 83.3 | 100.0 | 120 | 141 | 166 | 194 | 225 | 260 | 299 | 343 |
| 4.00 | 44.2 | 51.8 | 57.8 | 65.3 | 72.2 | 79.9 | 96.5 | 116 | 137 | 162 | 189 | 221 | 256 | 294 | 338 |
| 8.00 | 42.2 | 49.4 | 70.1 | 62.4 | 69.4 | 76.8 | 93.1 | 112 | 134 | 158 | 186 | 217 | 252 | 290 | 334 |
| 12.00 | 41.0 | 48.2 | 53.8 | 61.0 | 67.7 | 75.1 | 91.9 | 111 | 132 | 156 | 184 | 215 | 250 | 289 | 332 |
| 24.00 | 39.4 | 46.3 | 51.6 | 58.8 | 65.3 | 72.7 | 88.8 | 108 | 129 | 153 | 180 | 212 | 247 | 286 | 329 |

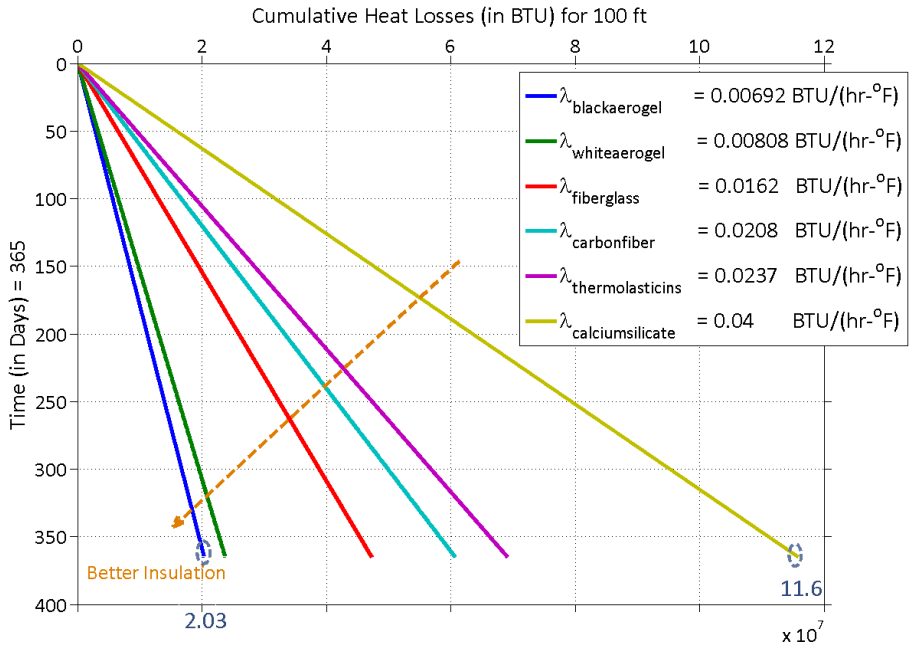


Figure 6.1: Surface lines heat loss calculation with six different insulation materials.

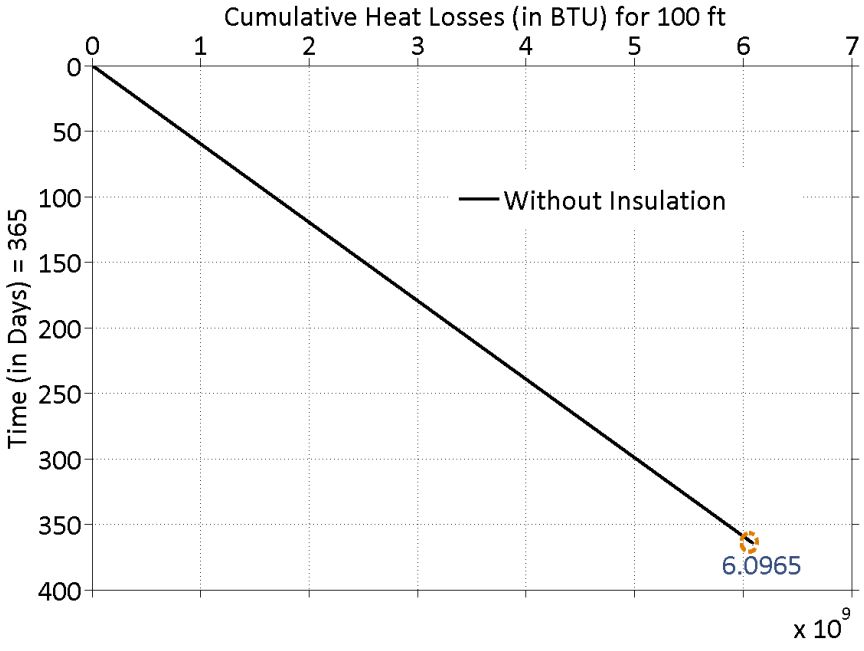


Figure 6.2: Surface Heat Loss calculation without insulation.

### 6.1.2 Example for Offshore

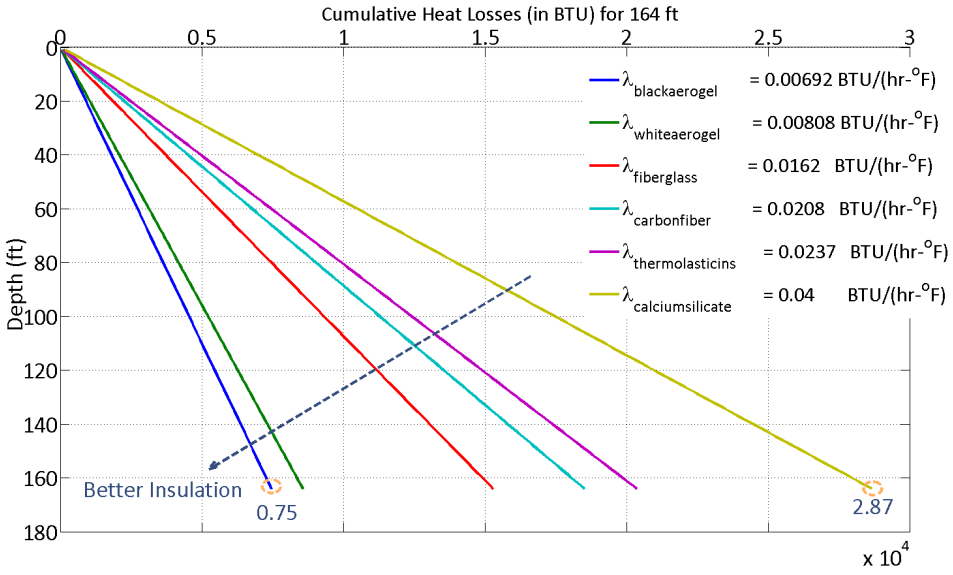


Figure 6.3: Heat loss from sea level to sea floor with six different insulations.

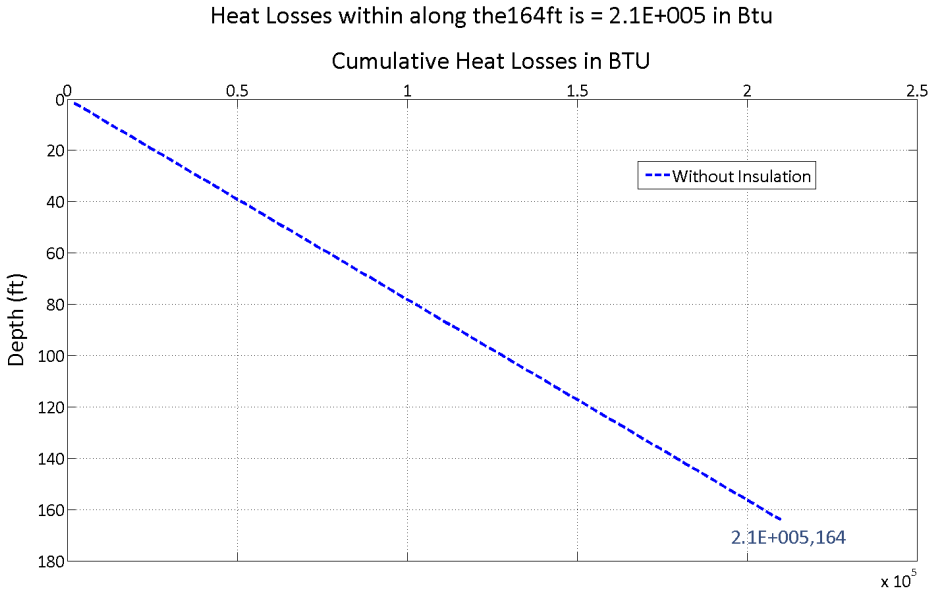


Figure 6.4: Heat loss from sea level to sea floor without insulation.

Under 600 $^oF$, steam injection for offshore heat loss is calculated with insulated material and uninsulated cases. Sea temperature is taken as 70 $^oF$ for 164 $ft$ water depth. This is relatively shallow. Heat loss estimation for 21 days of injection shows that the greatest the thermal conductivity values the greatest the heat losses observed. For instance using calcium silicate $(2.87 * 10^4)$ BTU gives four times more heat loss than black aerogel $(0.75 * 10^4)$ BTU. In addition, the bare tubing $(2.1 * 10^5)$ BTU case also gives about 8 times more heat loss than using lowest thermal conductivity insulation materials. It is clear that for 21 days period heat loss are substantial for uninsulated wells.

### 6.1.3 Example 10.2 from Prats

Steam at 600 $^oF$ is injected down 3.5-in. tubing set on a packer in 9 5/8 -in., 53.5-lbm/ft N-80 casing. The annulus contains a stagnant gas at zero gage pressure at wellhead, and the casing is cemented to surface in a 12-in. hole. The tubing is insulated with 1 in. of calcium silicate, the insulation being held in place and sealed from accidental entry of liquids in the annulus by a very thin sheath of aluminum. A temperature survey in the well indicates a mean surface temperature of 100 $^oF$ over the 1000-ft depth. Estimate the rate of heat loss 21 days after steam injection started, as well as the casing temperature. There is no altered zone near the boreholes. Input parameters are taken from Table 6.1.

Heat transfer across the gas filled annulus is by radiation and natural convection. Radiation is sensitive to the temperature levels and emissivities $(\in)$ of the surfaces. The temperature at the surface of the insulation $(T_{ins})$ and that at the inner radius of the casing $(T_{ci})$, together with the emissivities at these surfaces $(\in_{ins})$ and $(\in_{ci})$, affect the radiation heat losses across the annular space between the insulated casing. The calculation procedure is well explained in the Prats book[41].

Prats [41] assumed that for shallow reservoir temperature change does not vary

much with depth such as 1000 ft. He also stated that when the steam injection happens, shallow reservoir temperature stays constant. This is why using a single value of $R_h$ may provide a close enough estimate of heat losses and wellbore temperatures. This is good approach in terms of calculation and simplicity.

Example 10.2 from Prats [41] got heat loss $Q_l$=4.46*$10^6$ BTU for 21 days that corresponds to an equivalent energy content of 6.0*$10^6$ BTU/bbl of fuel, the daily heat loss from such an insulated well corresponds to less than 1 bbl of fuel. In our calculation we get $Q_l$=4.6*$10^6$ BTU that is slightly different than Prats results that is shown in Figure 6.5. It is because of several input parameters that differs somewhat.

Discussion of heat loss so far, considers the entire well as a unit. It is because of assuming temperature of the fluid does not change with depth for shallow reservoirs. In our program validation we do not assume this and we take into account temperature change along the wellbore.

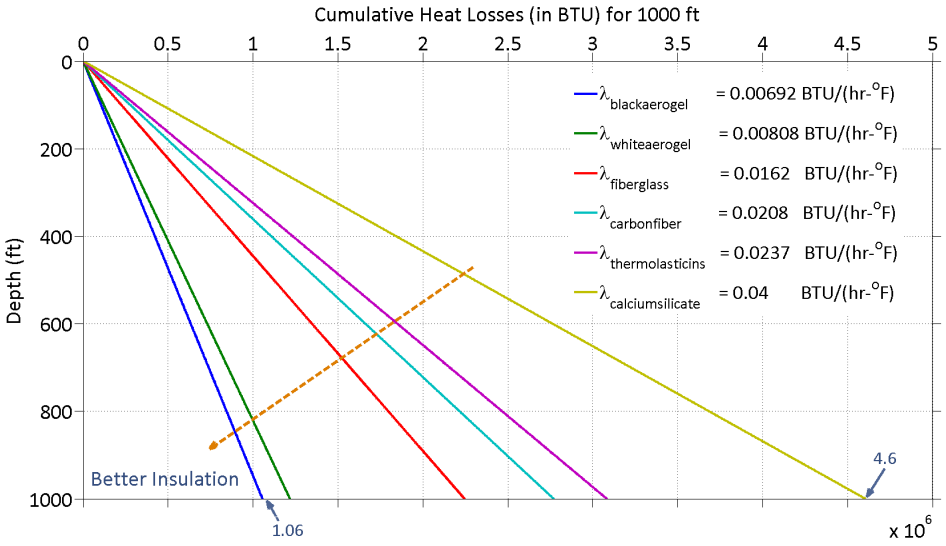


Figure 6.5: Heat loss calculation using different insulation materials based on Example 10.2 from Prats[41].

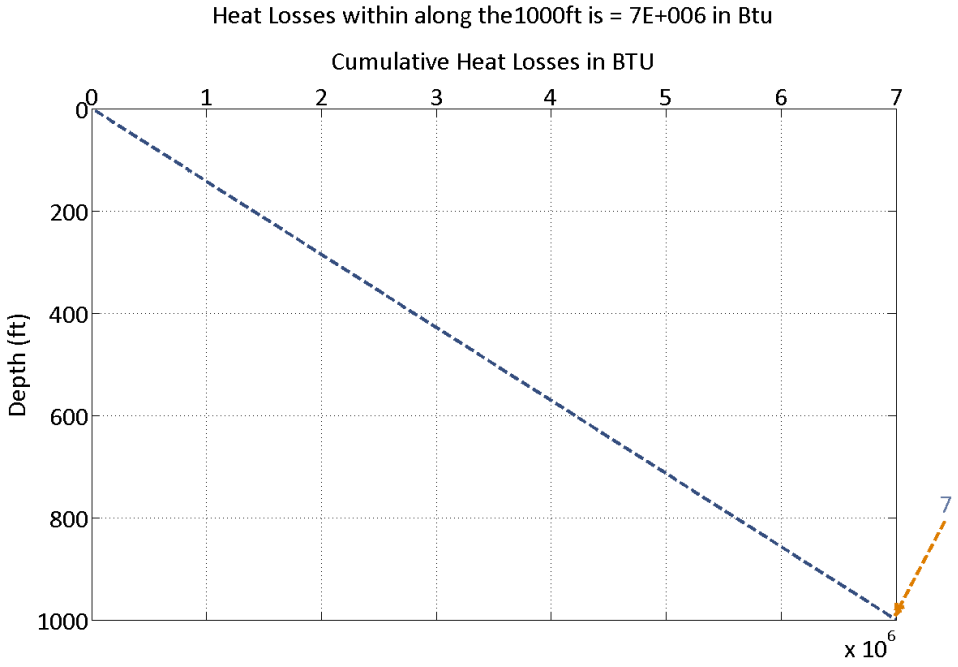


Figure 6.6: Heat loss calculation without using insulation materials based on Example 10.2 from Prats [41].

## 6.2 Program Validation

Table 6.3: Field data parameters for field data 1 and field data 2 [19].

| **Input Parameters** | **Field Data 1** | **Field Data 2** |
|---|---|---|
| $D_{ti}$ | 0.177 | 0.177 |
| $r_{to}$ | 0.104166667 | 0.104166667 |
| $r_{ins}$ | No Insulation | No Insulation |
| $r_{ci}$ | 0.166666667 | 0.166666667 |
| $r_{co}$ | 0.1875 | 0.1875 |
| $r_h$ | 0.6 | 0.6 |
| $k_e$ | 1 | 1 |
| $\alpha_E$ | 0.0286 | 0.0286 |
| $k_{cem}$ | 0.2 | 0.2 |
| $\epsilon_{to}$ | 0.9 | 0.9 |
| $\epsilon_{ci}$ | 0.9 | 0.9 |
| $\epsilon_{EARTH}$ | 0.94 | 0.94 |
| $W_m$ | 4640 | 4850 |
| $x$ | 0.8 | 0.8 |
| $p_{wh}$ | 250 | 250 |
| $T_m$ | 50 | 50 |
| $Depth$ | 1600 | 1600 |
| $P_{an}$ | 14.7 | 14.7 |
| $t$ | 71 | 117 |

There are 2 field cases where steam temperature is reported in the literature [11]. The Martha Bigpond well data is retrieved from the paper. Fontanilla and Aziz [20]

referred to the same field data from Bleakley's paper [11] as field data 1 and 2. These cases are to referred in our calculations as field data 1 and field data 2 as well. Input parameters are tabulated in Table 6.3. Besides Beggs and Brill [13, 14] and Aziz et al. [29], Hasan and Kabir model [23, 40] and the Drift Flux model [21] are applied in our calculations.

After applying the modified Fontanilla[20] approach with modified correlations, we got promising results using the Beggs and Brill [13, 14] approach for multiphase flow with field data 1. The other three correlations also get good agreement with Fontanilla's results as shown in Figure 6.7 and 6.8. When we look at the steam quality versus depth, the Beggs and Brill over predicts the quality values that Fontanilla got for field data 1 in Figure 6.9. The other three correlations that we implemented have almost the same results. It may be because of applying different correlations to get saturated steam properties during calculations.

In Figure 6.10, we can see the heat loss during steam injection is almost same values for the four different correlations of multiphase flow.

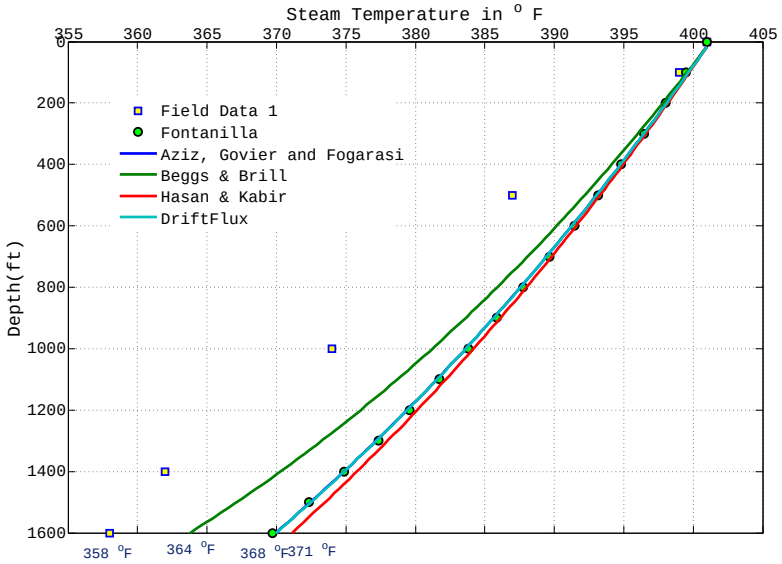


Figure 6.7: Comparison of steam temperature with field data 1 and two-phase correlations.

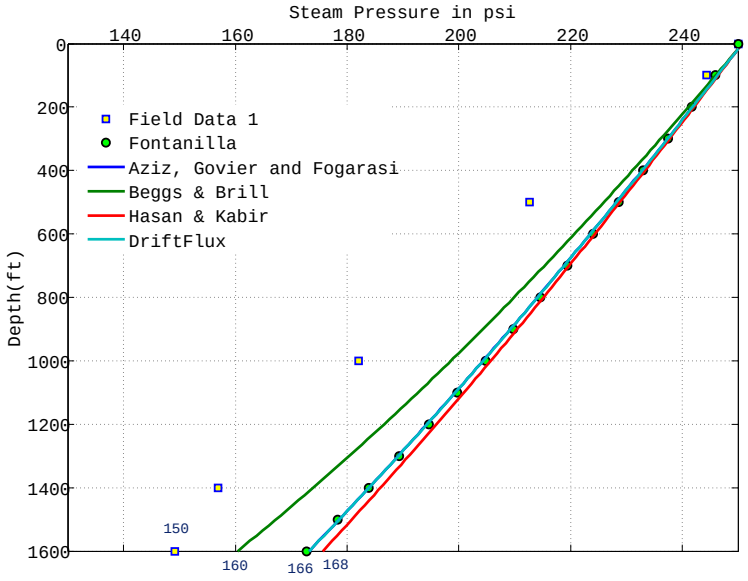


Figure 6.8: Comparison of steam pressure with field data 1 and two-phase correlations.

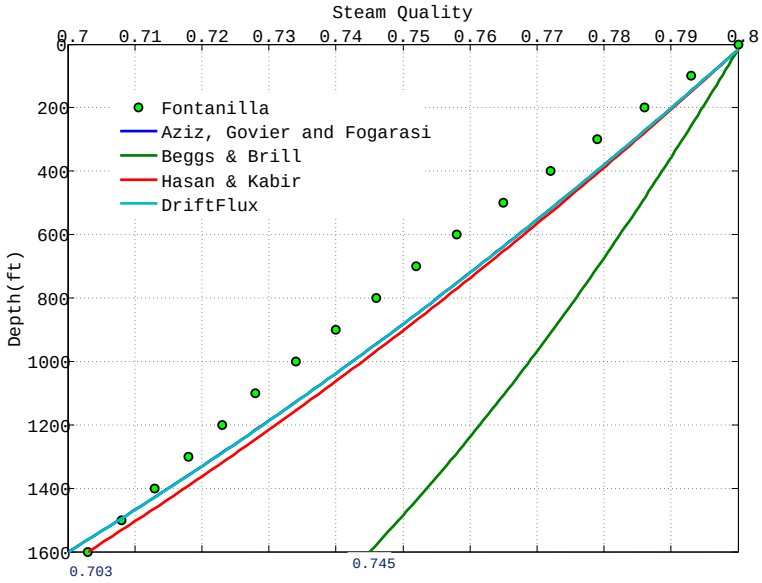


Figure 6.9: Calculated steam quality with different two-phase correlations based on field data 1.

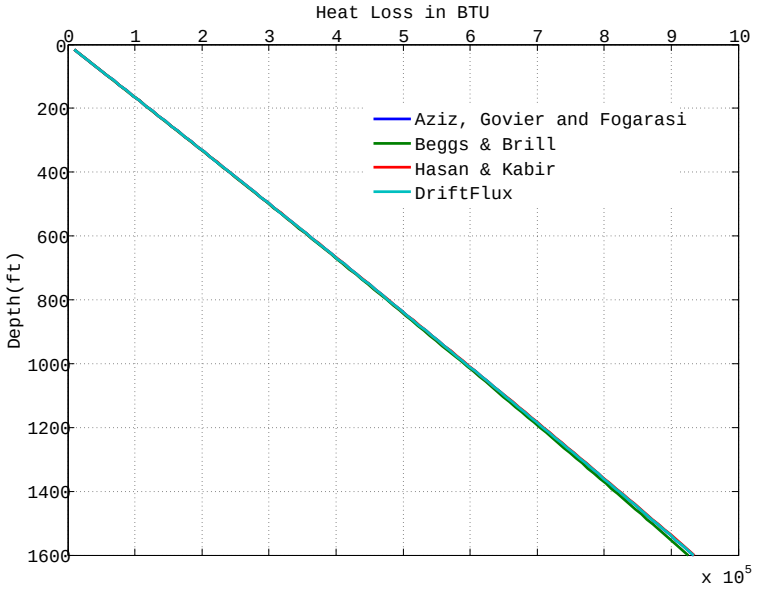


Figure 6.10: Calculated heat loss calculation with insulated tubing based on field data 1.

Figure 6.11 and 6.12 also show results after we run our simulator for field test data 2. Again, we can see that the modified Beggs and Brill method gives a better result than the Fontanillla approach compared to the field data 1. The other three correlations give results similar to Fontanilla's result. Although, we got good results for steam temperature and pressure values for Beggs and Brill, our calculation shows a little overprediction of values for steam quality as shown on Figure 6.13 from Fontanilla's result.

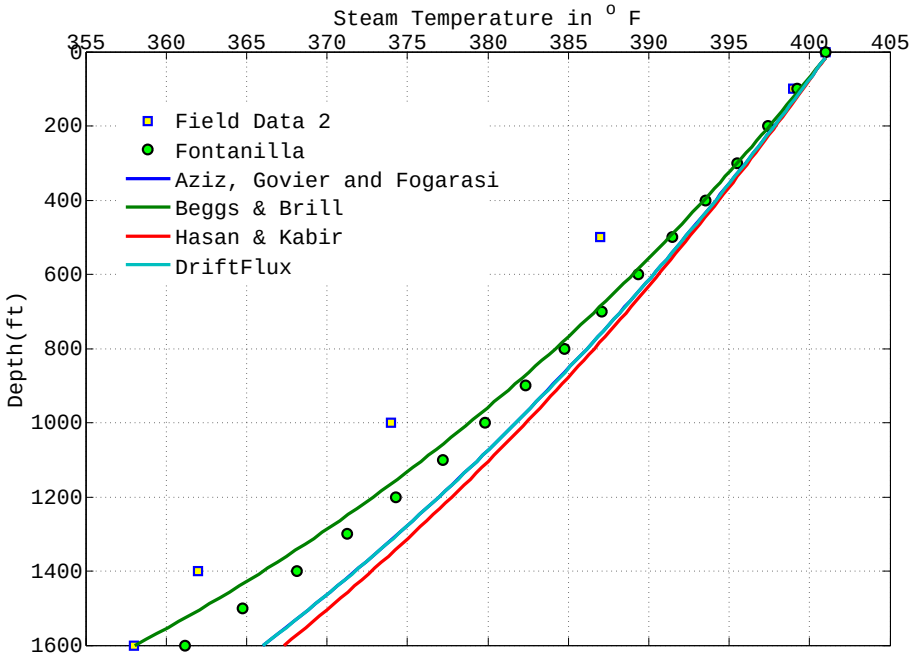


Figure 6.11: Comparison of steam temperature with field data 2 and two-phase correlations.

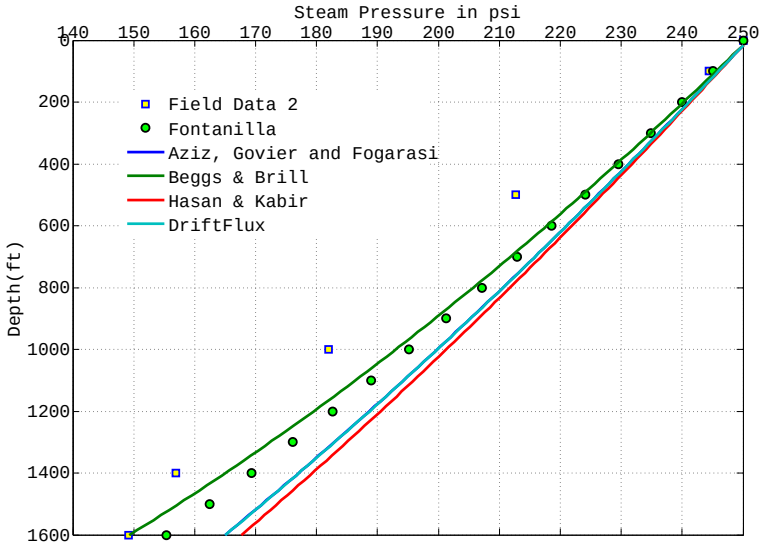


Figure 6.12: Comparison of steam pressure with field data 2 and two-phase correlations.

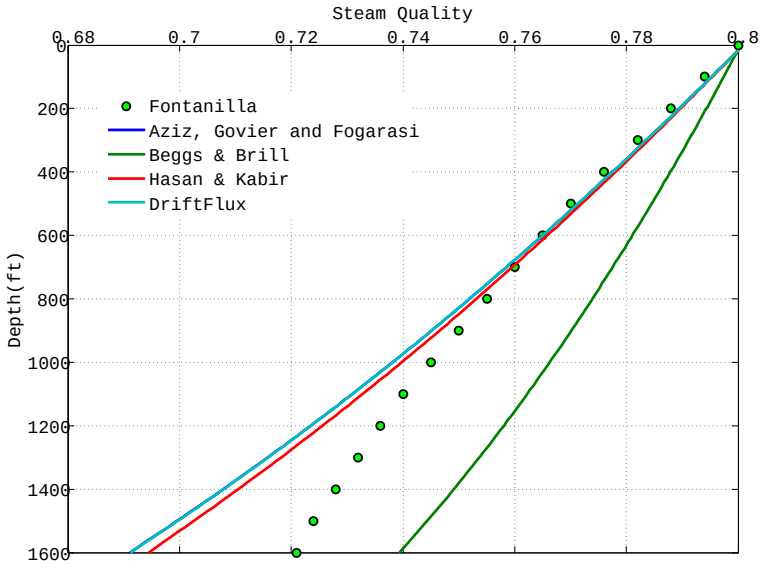


Figure 6.13: Calculated steam quality with different two-phase correlations based on field data 2.

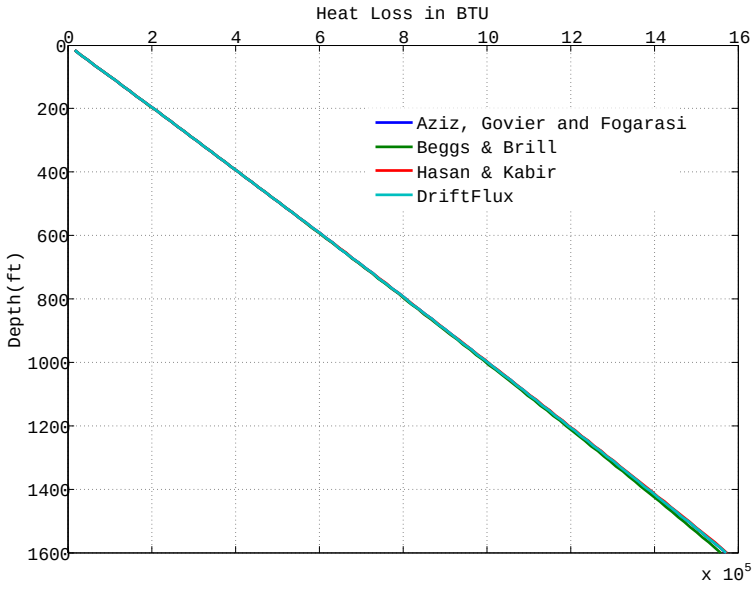


Figure 6.14: Calculated heat loss calculation with insulated tubing based on field data 2.

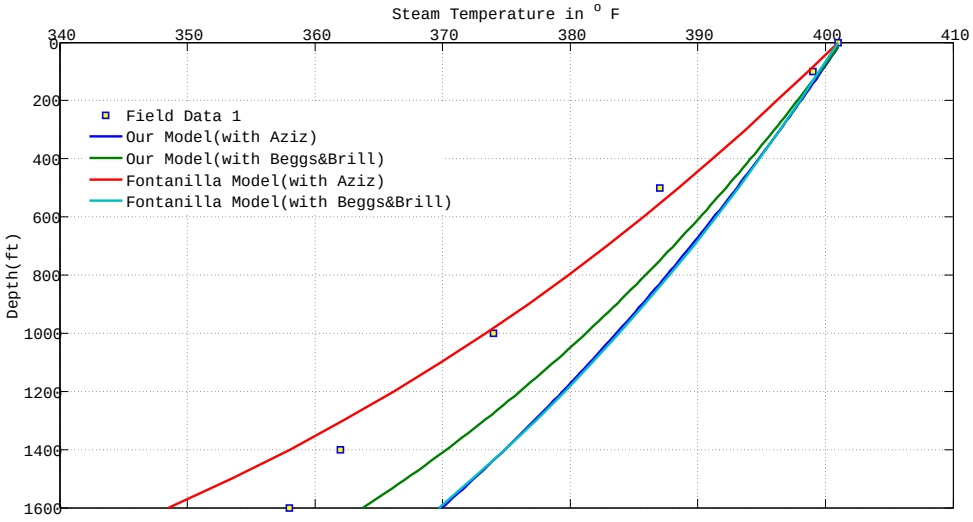


Figure 6.15: Comparison of our model with Fontanilla's model steam temperature with field data 1.

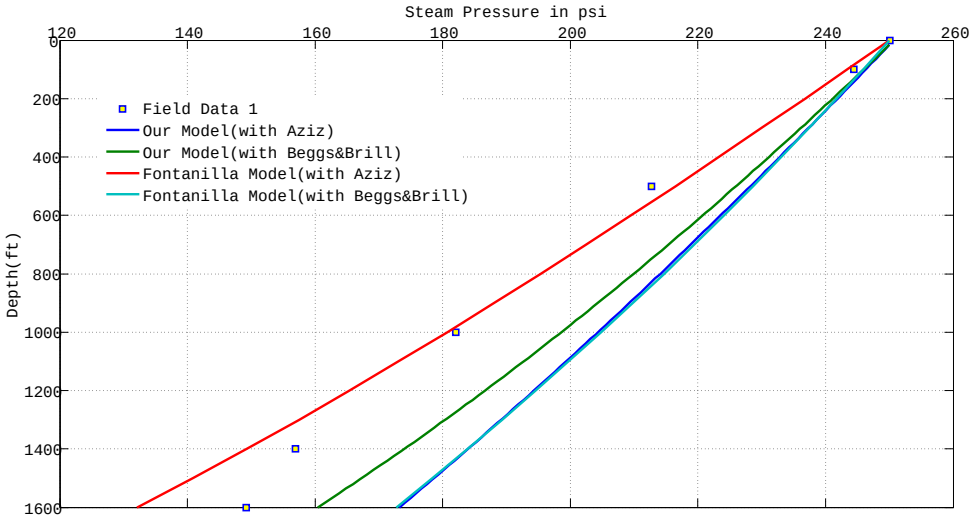


Figure 6.16: Comparison of our model with Fontanilla's model steam pressure with field data 1.

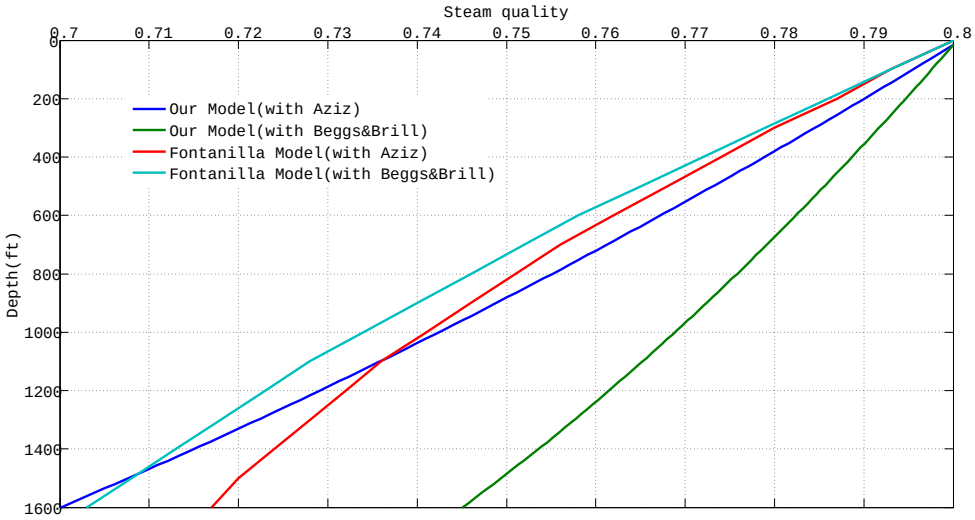


Figure 6.17: Comparison of our model with Fontanilla's model steam quality with field data 1.

When we look at the results that we got for both field data 1 and 2 cases, we had an opportunity to compare the results with Fontanilla's approach. The figures above

for the field data 1, and our implementation of Beggs and Brill correlations starts converging to the real data when we reach the bottom of the wellbore in Figure 6.15. On the other hand Fontanilla's Beggs and Brill implementation has less accurate results than ours. Our model using Aziz et al. has good agreement with Fontanilla's Beggs and Brill results. Looking at the results, Fontanilla's Aziz et al. calculations give almost perfect results with the field data until 1000 ft. Reuslts then deviate from the real values and go out of the range. In Figure 6.16, we can also see the same trend with Figure 6.15. It comes to check steam quality, although we are able to calculate steam quality with given injection rate and input parameters, in the literature we could not find the steam quality data. Therefore we only compare the results we have in our model and Fontanilla's model, in Figure 6.17. We can conclude the comparison saying that the Aziz et al. model starts converging from the beginning and obtains similar values. On the other hand, Beggs and Brill results differ quite a bit between the two methods.

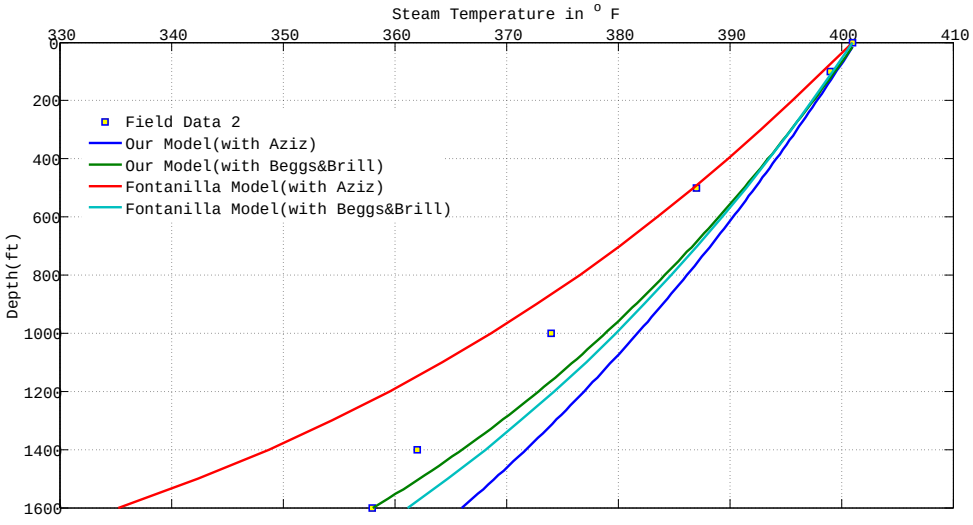


Figure 6.18: Comparison of our model with Fontanilla's model steam temperature with field data 2.

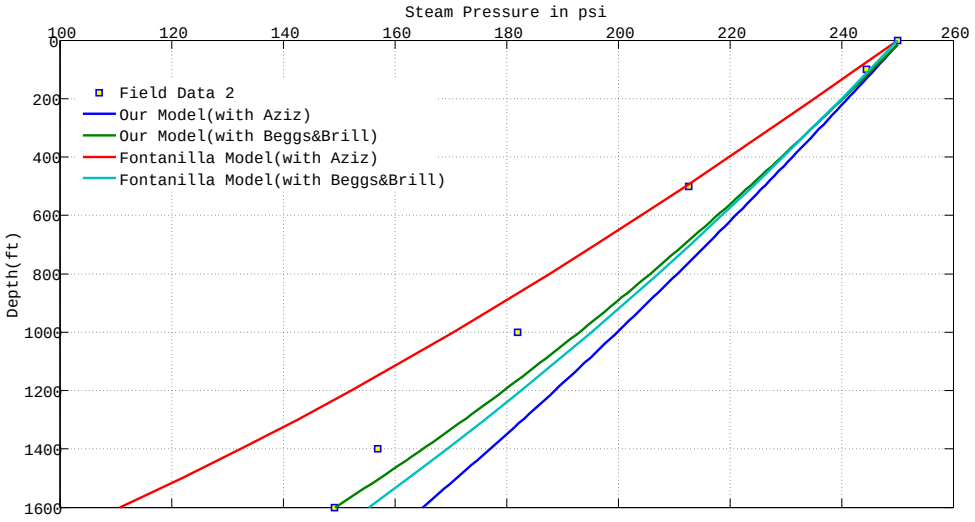


Figure 6.19: Comparison of our model with Fontanilla's model steam pressure with field data 2.

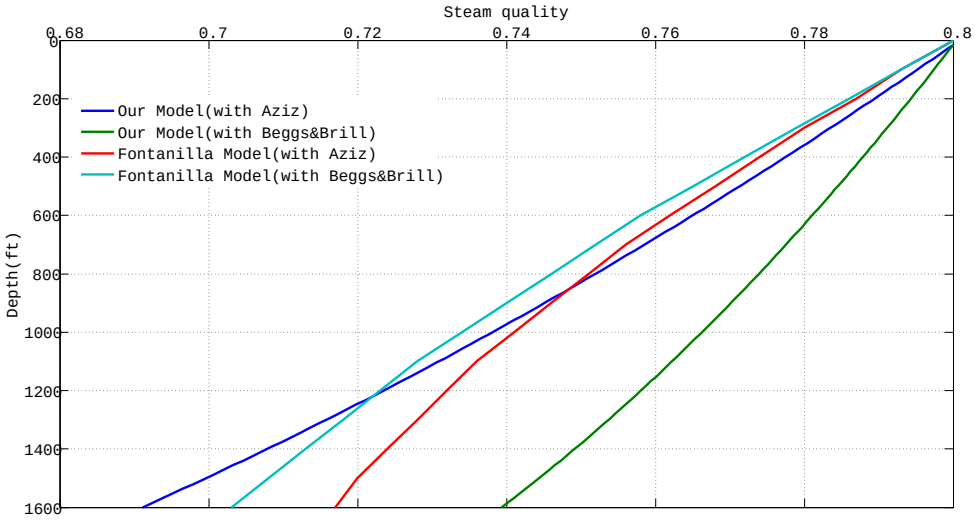


Figure 6.20: Comparison of our model with Fontanilla's model steam quality with field data 2.

In the field data 2, we got the results and plot them as shown in Figures 6.18 - 6.20. In Figure 6.18 our model with Beggs and Brill correlations gives very good agreement

with the real data and converges to the exact value. In contrast, Fontanilla's method with the Beggs and Brill approach gives less accurate results than our model. In our model, the Aziz et al. method, results better match field data as compared to Fontanilla's Aziz et al. approach, however, Fontanilla's Aziz et al. approach initially gives great results and captures almost exact values for several hundreds ft then deviates substantially from the reality. We can also conclude with saying that we improved Fontanilla's approach using several two-phase correaltions. This trends continue in Figure 6.19 with pressure values. The last comparison is steam quality. We can say that our model with Beggs and Brill two-phase flow correlations has less quality drop than Fontanilla's Begss and Brill model in Figure 6.20. The Aziz et al. approach has similar steam quality values in both models.

## 6.3 Onshore environments

For both onshore and offshore environments with insulated or uninsulated tubing input parameters are used for field data 1. The surrounding temperature, however, is taken as 122 $^oF$, time is 1 year and injection rate 4850 lbm/hr similar to the onshore, offshore and non-condensable gas cases. For the offshore part, field data 1 values are used as an input and exception is also used here with additional input for offshore sea temperature is taken as 70 $^oF$.

Results in Figures 6.21 and 6.22 are insulated by black aerogel, and various two-phase correlations are used. Three different steam injection temperatures and two different depths are considered for the onshore environment. Steam temperature, steam pressure, steam quality and heat loss values are investigated. When the steam temperature is 400 $^oF$, the Beggs and Brill two-phase flow correlation model's temperature profile or pressure profile drops dramatically. On the other hand, three other two-phase correlations converge to the same values both on temperature profile

and pressure profile. When we increase injection temperature to 500 $^oF$, the Beggs and Brill two-phase flow correlation model's temperature or pressure profile drops less than the other correlations until 7500 $ft$ then converge to the others. When the depth is greater than 8000 $ft$, it gives a little greater value than other correlations. Interestingly, the behavior of the Beggs and Brill model when the injection temperature increased to 600 $^oF$ gives less temperature drop than all the other three correlations. Figures 6.25 and 6.26 show that with different temperature and depth all the flow regimes have similar values in steam temperature, steam pressure, and steam quality comparing with insulated case. The differences between insulated and uninsulated tubing is the heat loss and steam quality values. Figure 6.23 and Figure 6.27 show results. The steam quality values with insulated tubing when compared to uninsulated tubing cases differ significantly. Without insulation, there is greater heat loss and quality decreases to a greater extent as compared to the insulated case. It is also observed that, the Beggs and Brill model, with increasing injection temperature overpredicts the steam quality values. Figures 6.24 and 6.28 give the information that increasing injection steam temperature causes greater heat loss when comparing 500 $^oF$ and 600 $^oF$ cases.

Similar trends are obtained during the steam injection in an offshore environment as well. Although the offshore depth of 200 $ft$ is relatively shallow and greater pressure drop and temperaure drop for small interval does not really effect the behavior trend of the steam properties at downhole conditions. The greater the steam temperature, the greater steam quality and steam properties are obtained in both cases. The greatest heat loss is obtained using calcium silicate which has greatest thermal conductivity value among the six different insulations. Figures presented in Appendix C also have similar behavior in our example, therefore this explanation will help to understand those figures as well.

### 6.3.1 Examples with Insulation Materials

$UsingBlackAerogel\lambda_{BA} = 0.0069BTU/(ft - hr -^o F)$

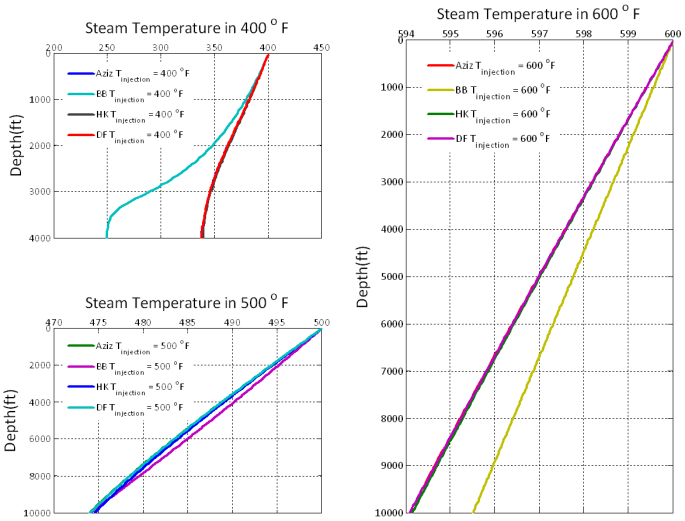


Figure 6.21: Steam temperature distribution for different injection temperature vs depth (ft), 1 year, $T_m = 122\ ^oF$ and injection rate 4850 lbm/hr with using black aerogel.

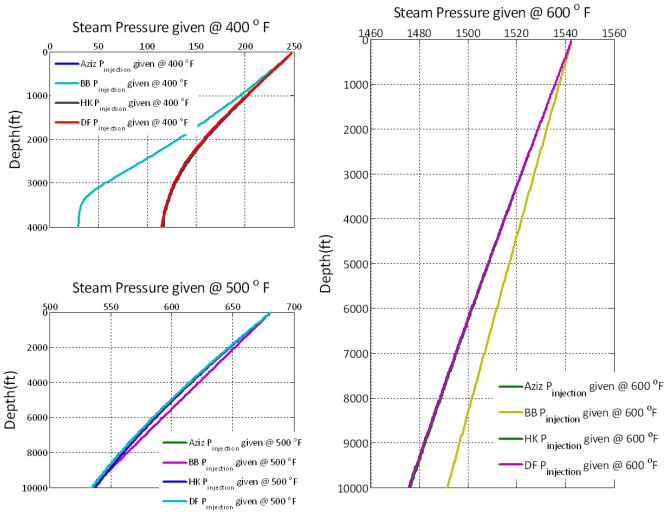


Figure 6.22: Steam pressure distribution for different injection temperature vs depth (ft), 1 year, $T_m = 122\ ^oF$ and injection rate 4850 lbm/hr with using black aerogel.

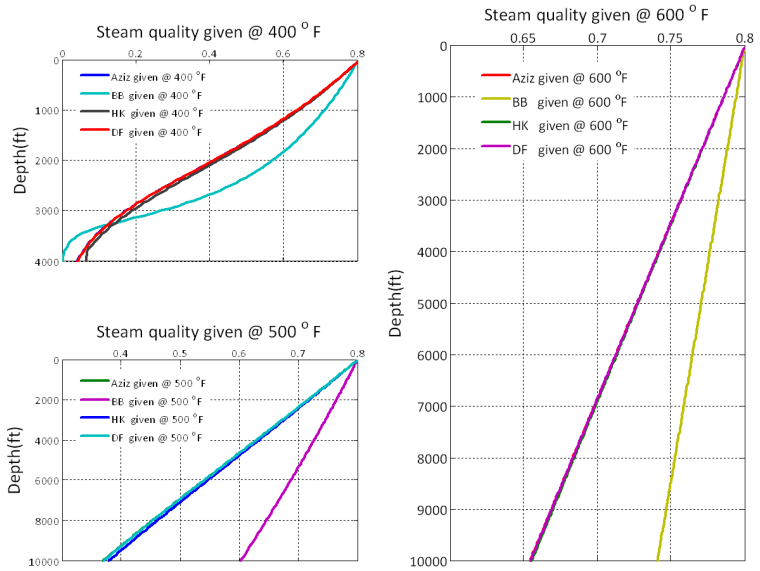


Figure 6.23: Steam quality distribution for different injection temperature vs depth (ft), 1 year, $T_m = 122\ ^oF$ and injection rate 4850 lbm/hr with using black aerogel.

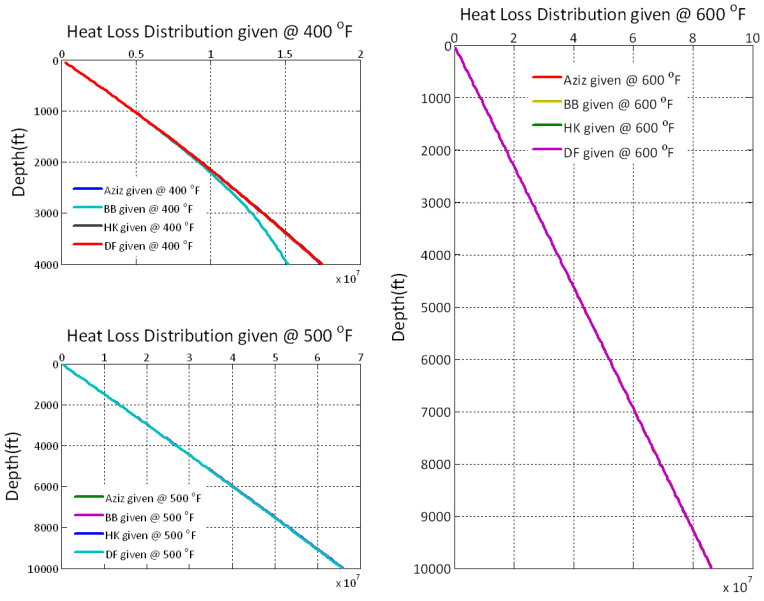


Figure 6.24: Heat loss distribution for different injection temperature vs depth (ft), 1 year, $T_m = 122\ ^oF$ and injection rate 4850 lbm/hr with using black aerogel.

### 6.3.2 Examples without Insulation Materials

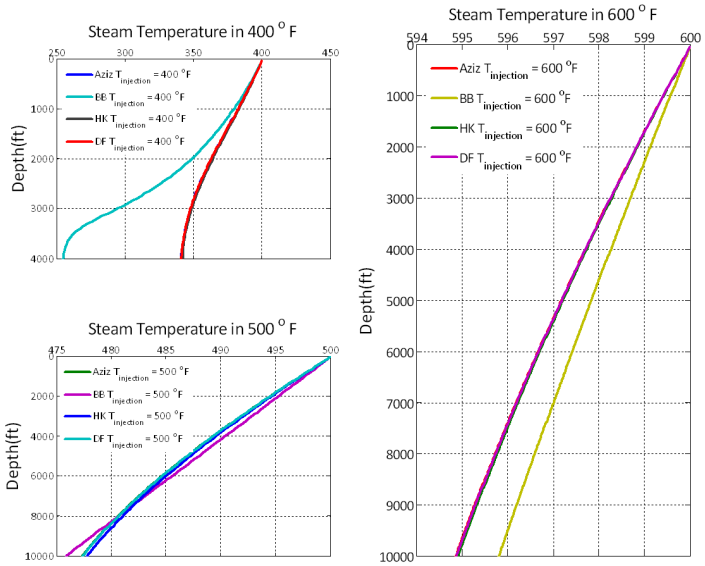


Figure 6.25: Steam temperature distribution , 1 year, $T_m = 122\ ^oF$ and injection rate 4850 lbm/hr without insulation.

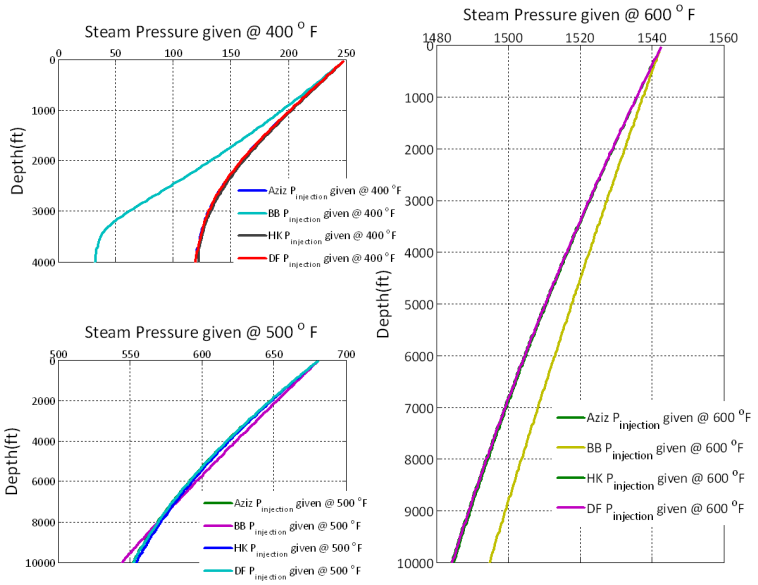


Figure 6.26: Steam pressure distribution, 1 year, $T_m = 122\ ^oF$ and injection rate 4850 lbm/hr without insulation.

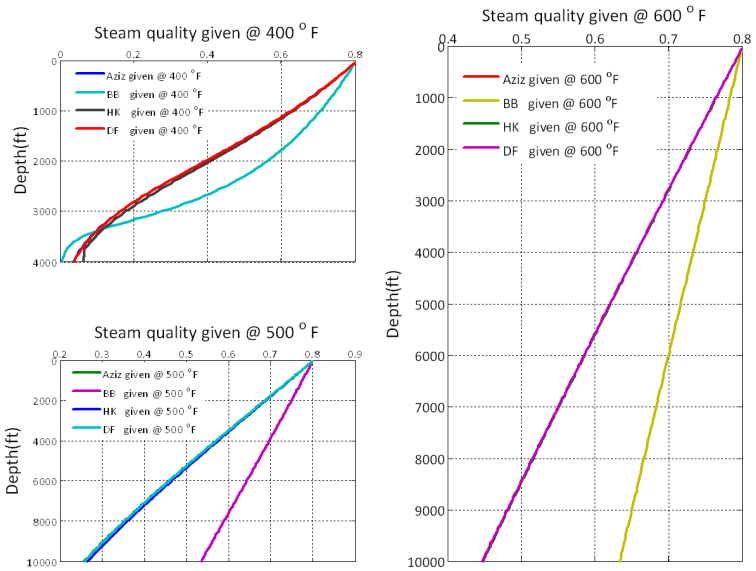


Figure 6.27: Steam quality distribution, 1 year, $T_m = 122\ ^oF$ and injection rate 4850 lbm/hr without insulation.

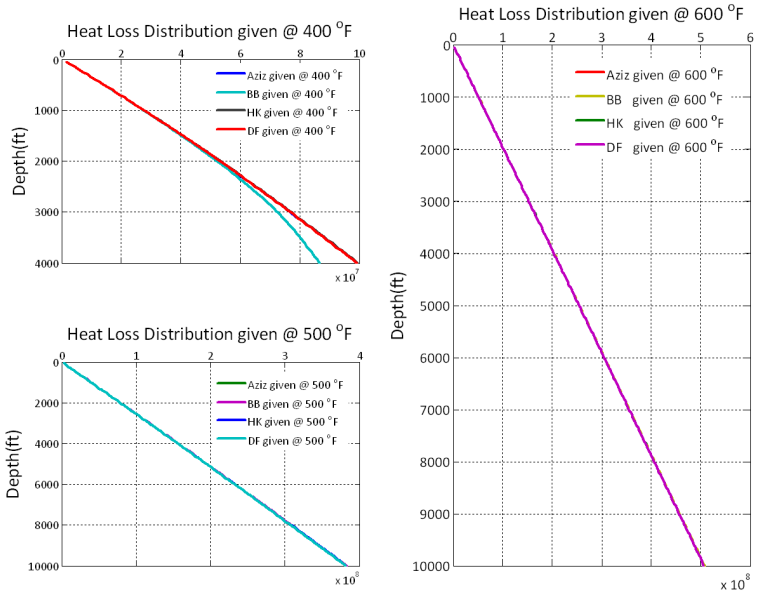


Figure 6.28: Heat loss distribution, 1 year, $T_m = 122\ ^oF$ and injection rate 4850 lbm/hr without insulation.

## 6.4 Offshore Environments

### 6.4.1 Examples with Insulation Materials

$UsingBlackAerogel\lambda_{BA} = 0.0069BTU/(ft - hr -^o F)$

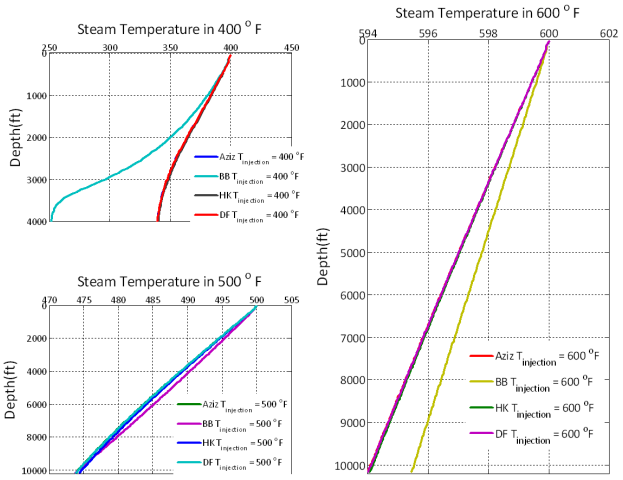


Figure 6.29: Steam temperature distribution for different injection temperature vs depth (ft), 1 year, $T_m = 122\ ^oF$ and injection rate 4850 lbm/hr for black aerogel.

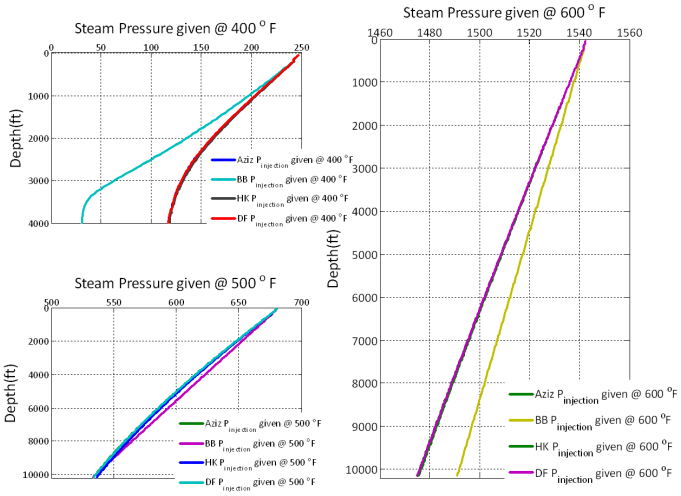


Figure 6.30: Steam pressure distribution for different injection temperature vs depth (ft), 1 year, $T_m = 122\ ^oF$ and injection rate 4850 lbm/hr for black aerogel.

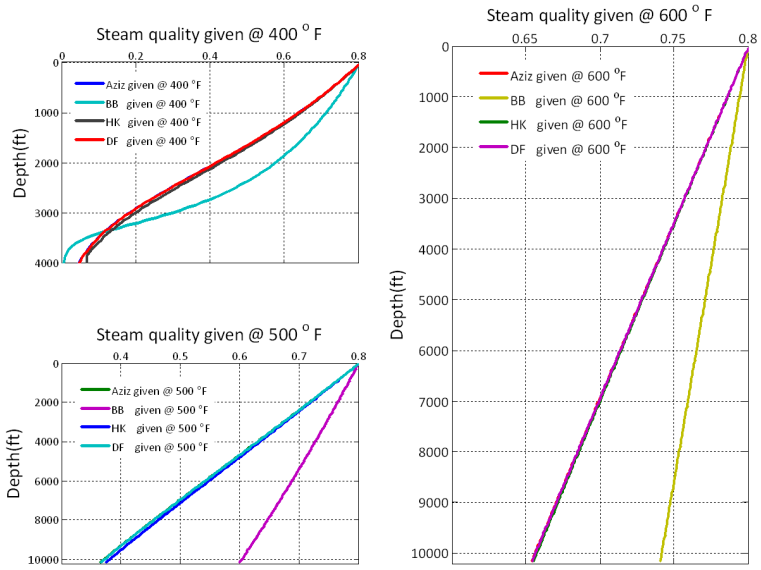


Figure 6.31: Steam quality distribution for different injection temperature vs depth (ft), 1 year, $T_m = 122\ ^oF$ and injection rate 4850 lbm/hr for black aerogel.

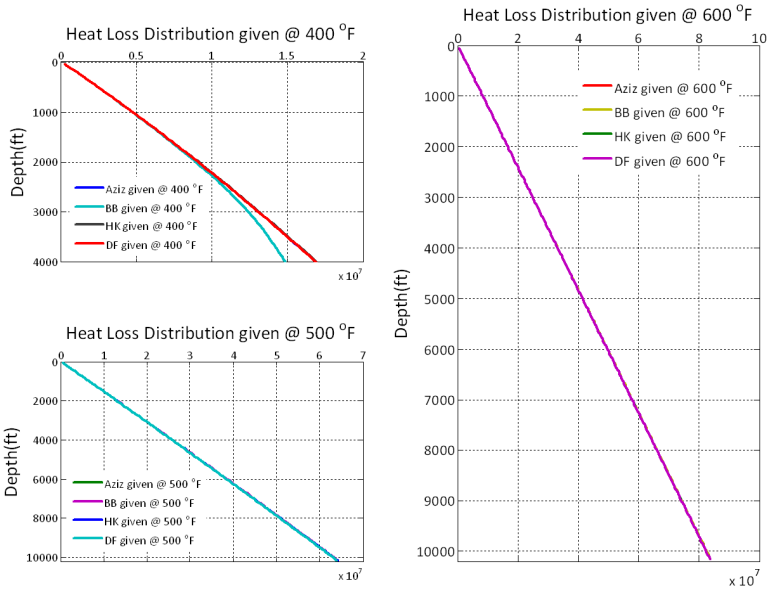


Figure 6.32: Heat loss distribution for different injection temperature vs depth (ft), 1 year, $T_m = 122\ ^oF$ and injection rate 4850 lbm/hr for black aerogel.

### 6.4.2 Examples without Insulation Materials

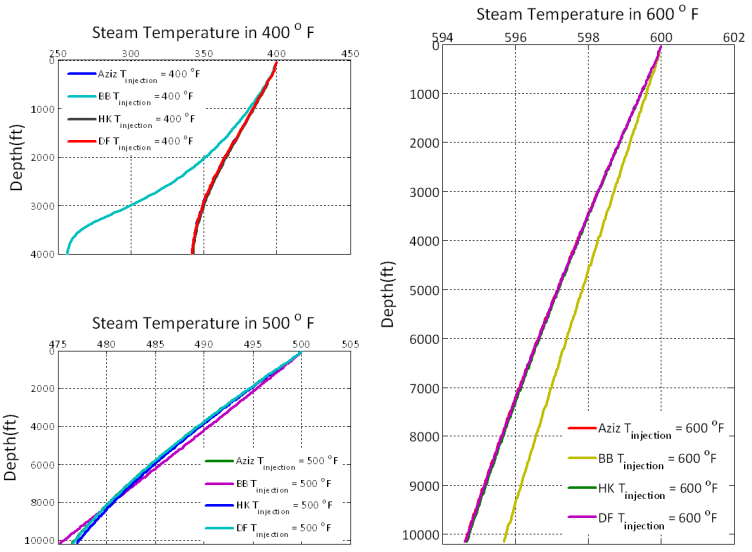


Figure 6.33: Steam temperature distribution, 1 year, $T_m = 122\ ^oF$ and injection rate 4850 lbm/hr without insulation.

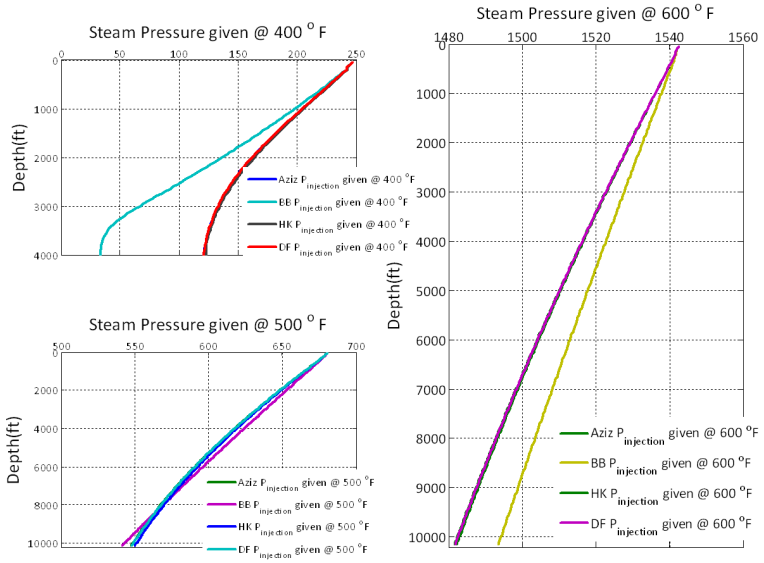


Figure 6.34: Steam pressure distribution, 1 year, $T_m = 122\ ^oF$ and injection rate 4850 lbm/hr without insulation.

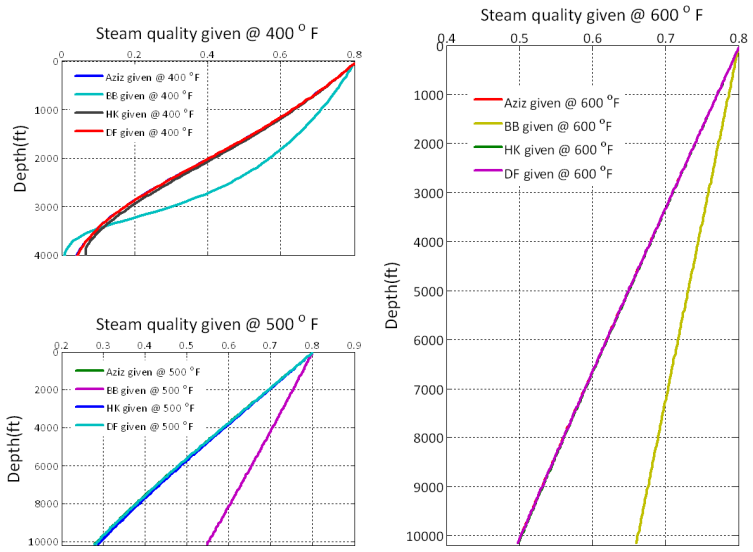


Figure 6.35: Steam quality distribution, 1 year, $T_m = 122\ ^oF$ and injection rate 4850 lbm/hr without insulation.

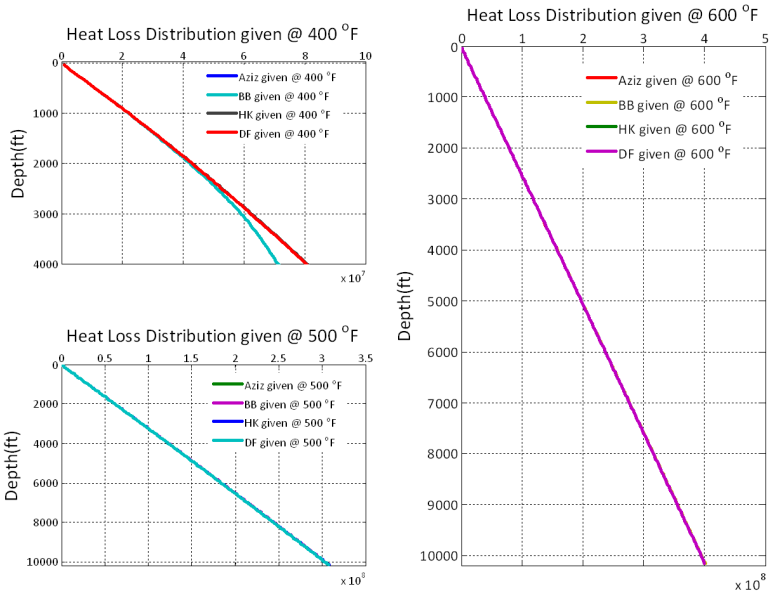


Figure 6.36: Heat loss distribution, 1 year, $T_m = 122\ ^oF$ and injection rate 4850 lbm/hr without insulation.

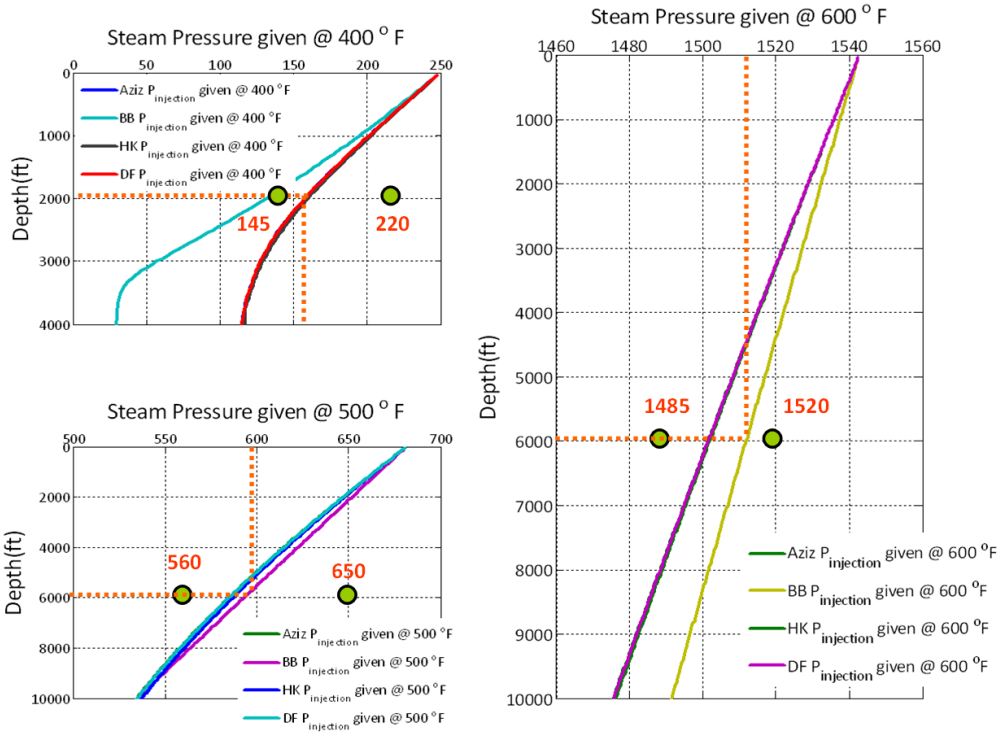


Figure 6.37: Pressure drop distribution and formation pressure (green dots), 1 year, $T_m = 122\ ^oF$ and injection rate 4850 lbm/hr with using black aerogel for onshore.

Reservoir pressure is clearly an important factor governing steam injectors. When we know the formation pressure, we can determine whether we can inject steam and at what temperatures in order to heat the reservoir. For this purpose, we could conceive two different formation pressures at the same depth. One is smaller than steam pressure one is greater than steam pressure on shown Figure 6.37. If formation pressure is greater than steam pressure, steam can not be injected to the reservoir. Greater the steam pressures are obtained with higher temperatures. Having this advantage, steam can be injected with increasing temperature to the formation.

## 6.5 Adding Non-Condensable Gas ($N_2$) in an Onshore environment

### 6.5.1 Examples with Insulation Materials

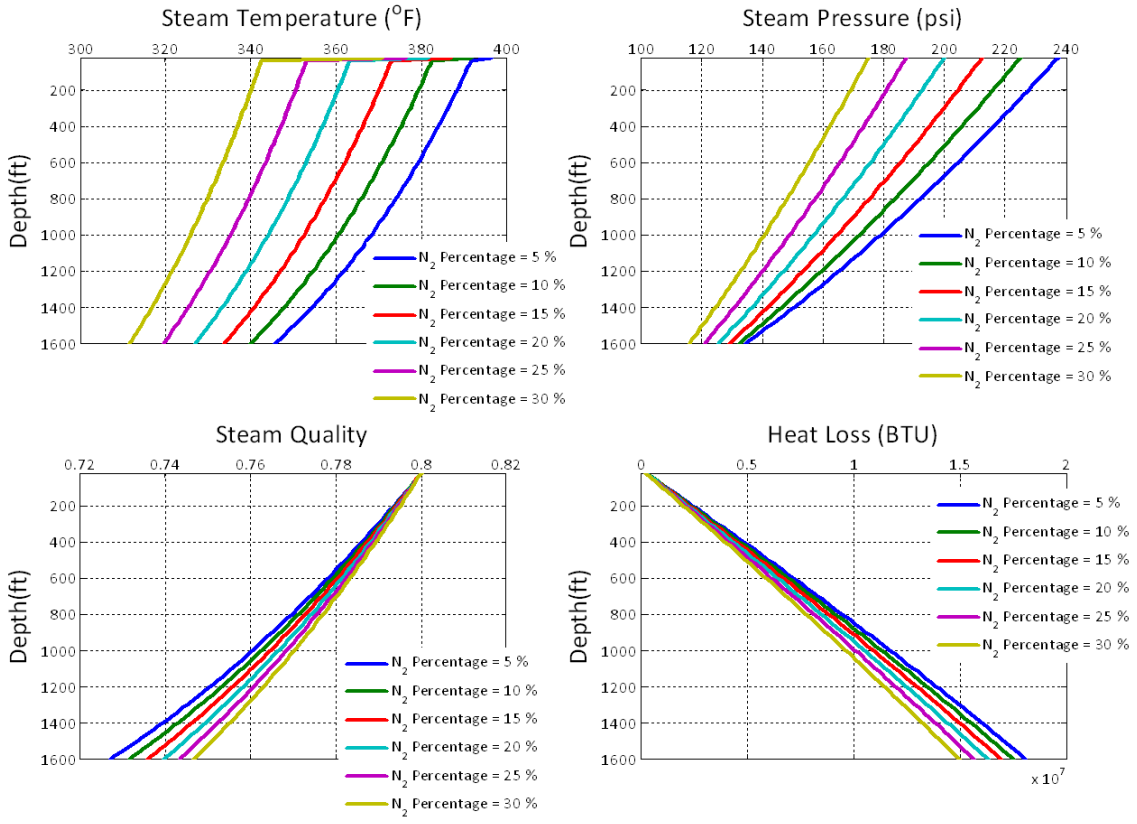


Figure 6.38: With changing $N_2$ molar percentage, 1 year, $T_m = 122\ ^oF$ and injection rate 4850 lbm/hr with using black aerogel.

Non-condensable gas is added to the field data 1 scenerio an input except 122 $^oF$, time is 1 year and injection rate 4850 lbm/hr with modified Beggs and Brill two-phase correlation. First, different $N_2$ molar percentage of steam is added to the steam, starting from 5 % to 30% mol fraction of the steam. In Figure 6.38, the greater $N_2$

in the system gives more partial pressure to the system. The contribution of partial pressure by steam drops significantly and temperature as well. But, steam quality drops less so the heat loss decreases. It has a disadvantage to deliver lower steam temperature to the reservoir in terms of less latent heat addition to the reservoir. Reducing the fraction of $N_2$ in the steam gives greater heat loss and quality drop, however, it increases steam partial pressure and temperature, so more heat is delivered to the reservoir.

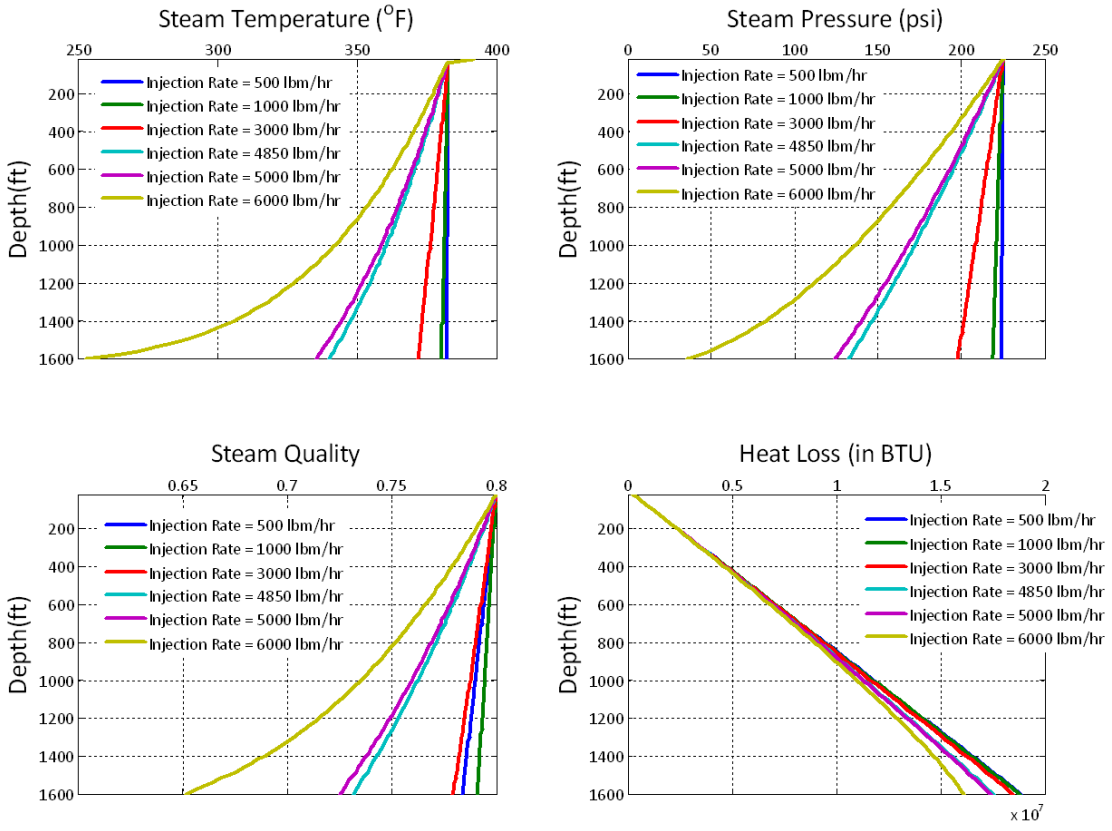


Figure 6.39: With changing injection rate, 1 year, $T_m = 122\ ^oF$ and injection rate 4850 lbm/hr with using black aerogel.

In Figure 6.39, different injection rate is studied with 10% by mole $N_2$ added to the steam. In our calculation, frictional pressure drops have the greatest contribution

to the pressure drop calculation. Frictional pressure drop can be caused by greater injection rate in our case. The greater the injection rate the greater the pressure drop, steam temperature, and steam quality decrease downhole. Increasing injection rate does not yield good results in downward steam injection operations.

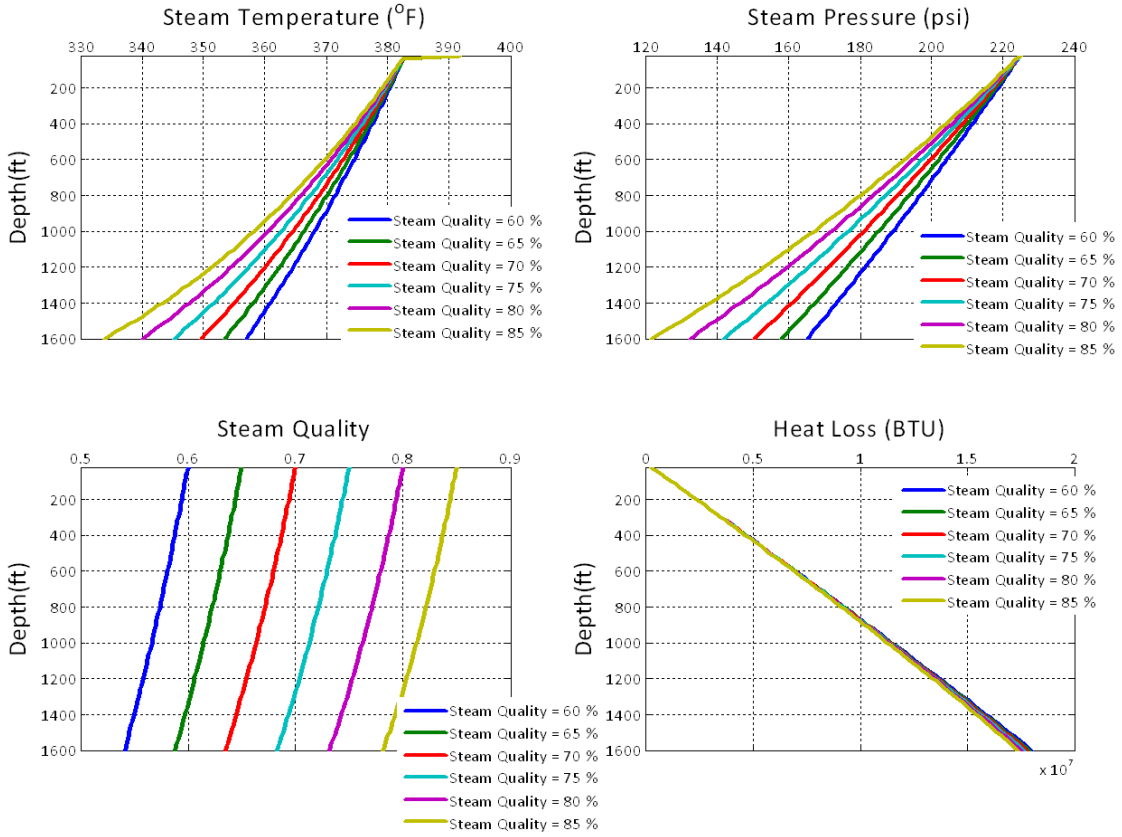


Figure 6.40: With changing steam quality molar percentage , 1 year, $T_m = 122\ ^oF$ and injection rate 4850 lbm/hr with using black aerogel.

Figure 6.40, different steam quality values are conducted in our work with 10% $N_2$. Increasing steam quality yields more pressure and temperature drop in existing cases for non-condensable gas. However, it also yields higher steam quality values when the steam reaches to reservoir with rich quality but poor temperature and pressure values. That may not be good for maintaining the temperature and pressure of the

steam. In the same figure, heat loss values with different steam quality does not vary and have almost same value with different injection quality.

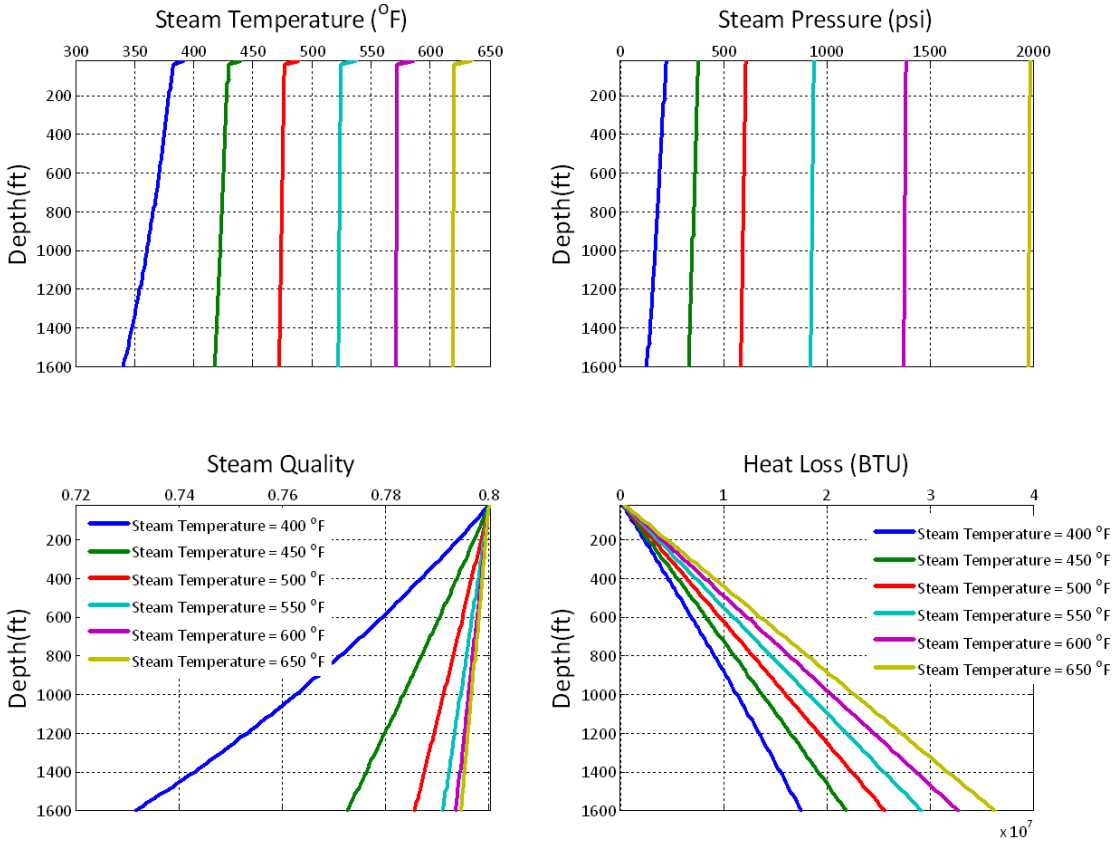


Figure 6.41: With changing injection temperature, 1 year, $T_m = 122\ ^oF$ and injection rate 4850 lbm/hr with using black aerogel.

Steam temperature values are changed in terms of checking the sensitivity of steam quality, steam temperature, steam pressure, and heat loss. In Figure 6.41, increasing steam temperature is caused by increasing steam pressure. Because of this, smaller pressure drop and steam quality change is obtained with highest steam temperature values. The greatest heat loss is observed with the greatest steam injection temperature at 650 $^oF$.

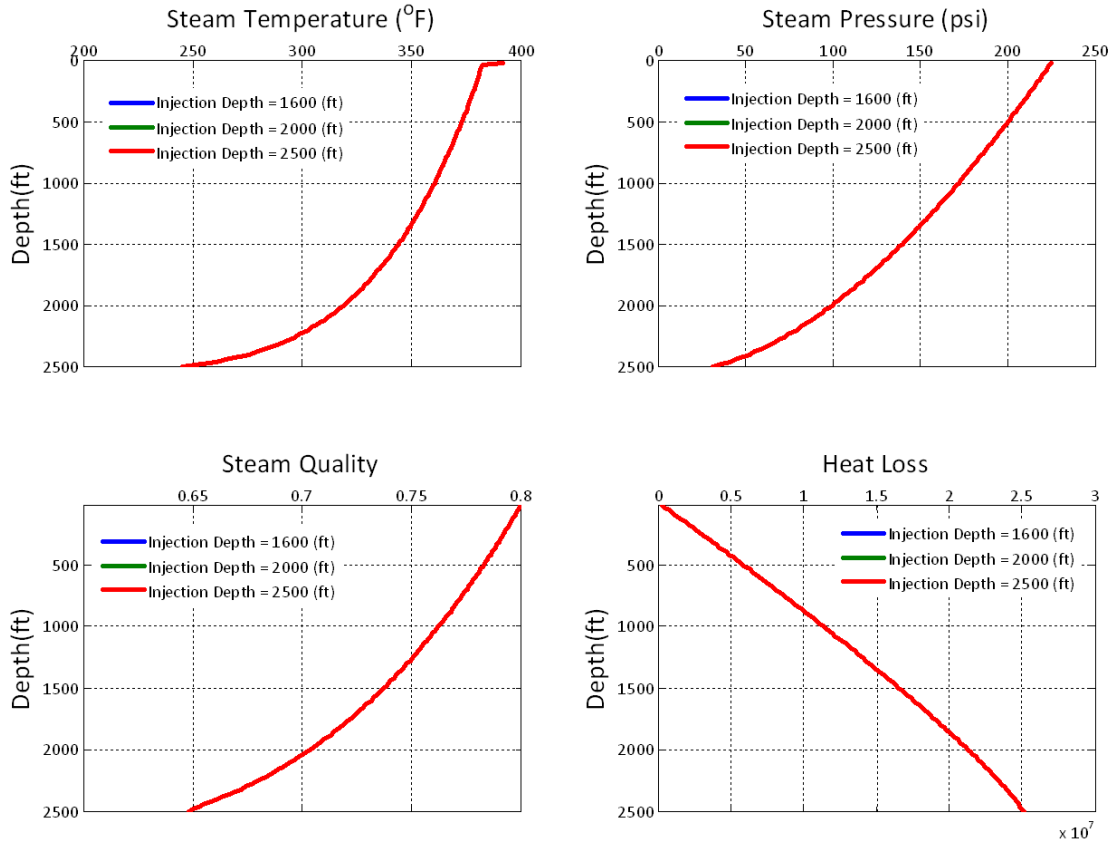


Figure 6.42: With changing injection depth, 1 year, $T_m = 122\ ^oF$ and injection rate 4850 lbm/hr with using black aerogel.

The effect of injection depth is analysed by changing the depth. However, after 2500 $ft$ even if steam quality was high, injection depth could not be increased, because of the significant pressure drop along the tubing. For the different range of depth, all the values are corresponded and follow the same distribution except depth, shown in Figure 6.42.

### 6.5.2 Examples without Insulation Materials

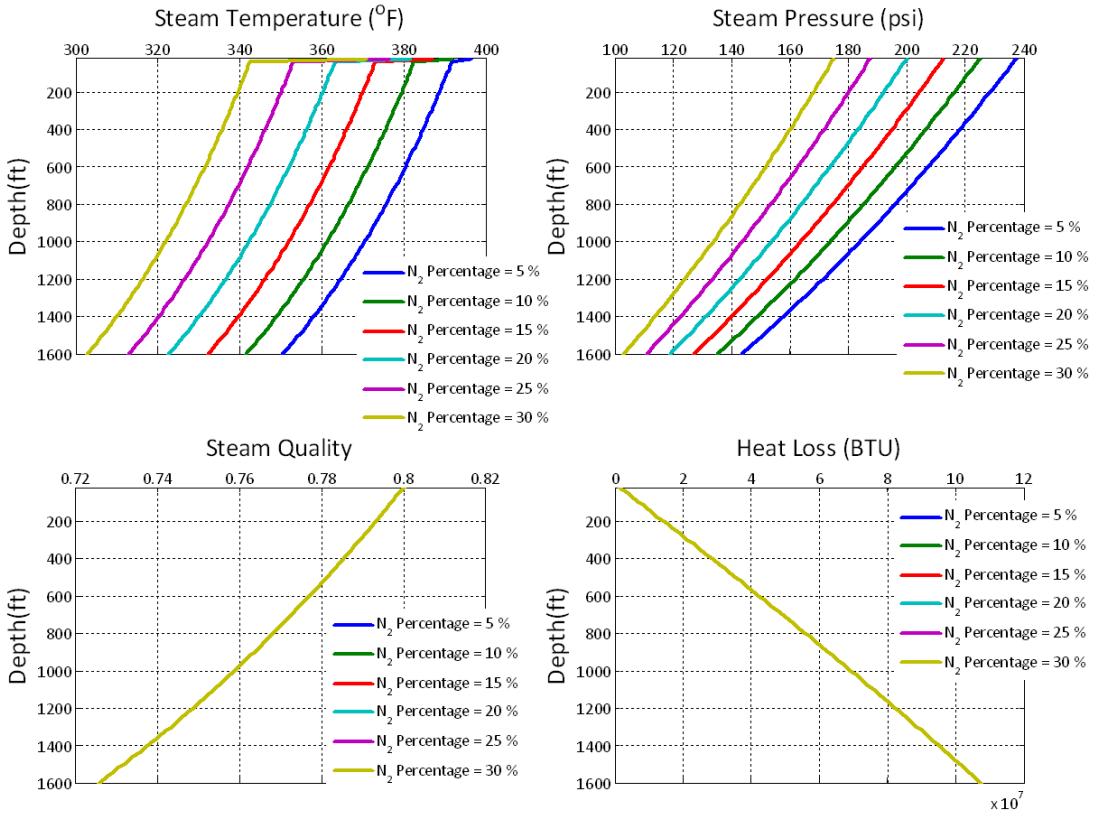


Figure 6.43: With changing $N_2$ molar percentage, 1 year, $T_m = 122\ ^oF$ and injection rate 4850 lbm/hr without insulation.

Same scenerio is also applied for uninsulated tubing as applied to insulated tubing cases. Figure 6.38 and Figure 6.43 has similarities in terms of the greater the mole fraction of $N_2$ we have in the system, the greater pressure drop as well as temperature drop. Another interesting observation is made with comparing to the insulated tubing case. The two temperature and pressure drops curves have slightly higher values than the insulated case when the $N_2$ mole fraction changes 5 %-10%. The other curves have greater pressure drop compaed to the insulated case. However, steam quality drops and heat losses values converge to the same value. Steam quality is less than

comparing with insulated tubing, but heat loss values almost 10 times greater than without insulated case. Using insulated tubing gives advantage instead of bare tubing regarding to less decrease with several parameters.

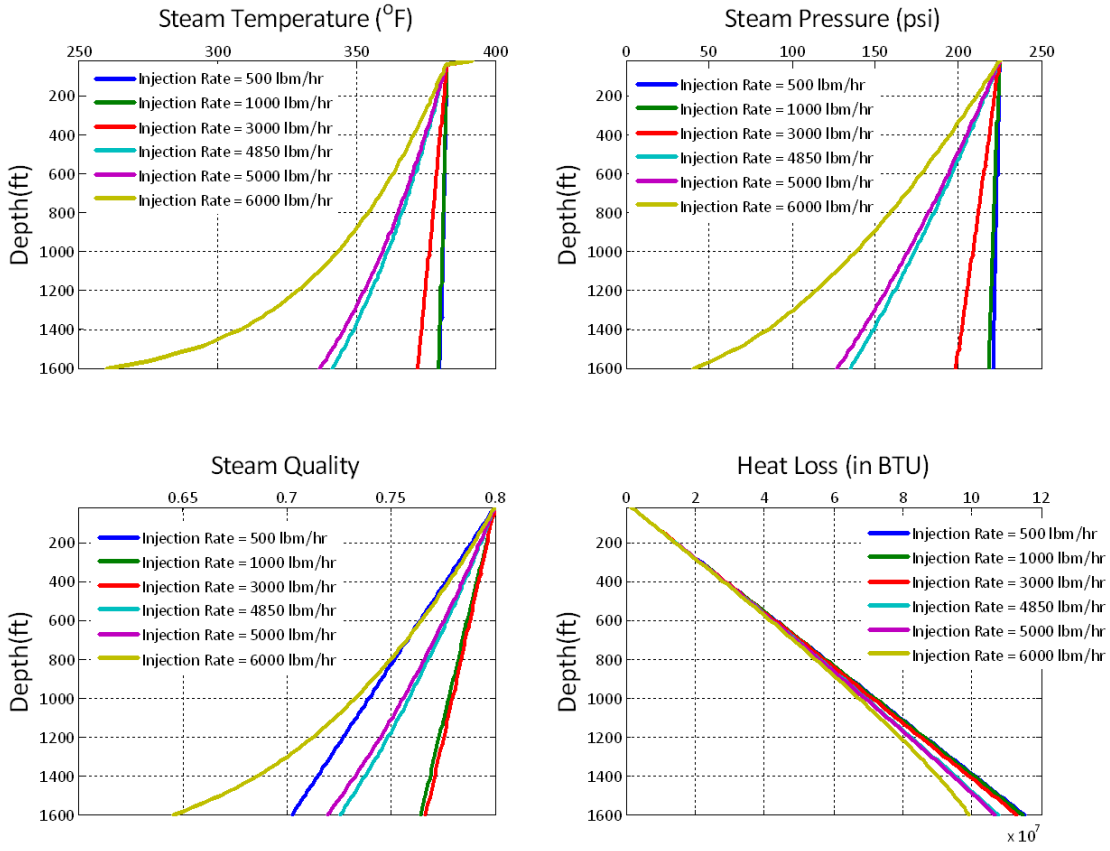


Figure 6.44: With changing injection rate, 1 year, $T_m = 122\ ^oF$ and injection rate 4850 lbm/hr without insulation.

In Figure 6.44, different injection rate is studied with 10% $N_2$ mol fraction of non-condensable gas as shown in Figure 6.39. In our calculation frictional pressure drops have highest contribution to the pressure drop calculation. Frictional pressure drop can be caused by more injection rate in our case. The greater the injection rate greater the pressure drop, steam temperature and and steam quality drop are observed. Increasing injection rate does not yield good results in downward steam

injection operations. There is a greater decrease of steam quality, steam pressure, steam temperature and greater heat losses. Similar trends are seen with insulated tubing except more heat loss and more quality drops are calculated without insulated tubing.

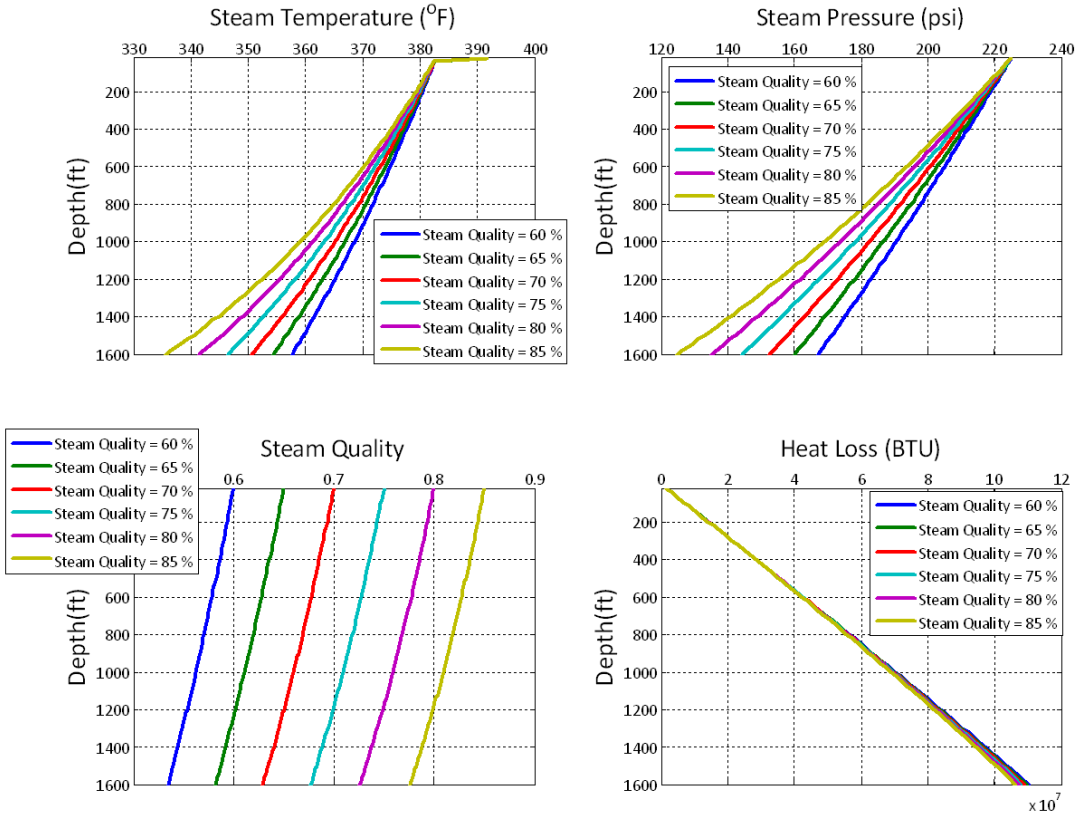


Figure 6.45: With changing steam quality molar percentage , 1 year, $T_m = 122\ ^oF$ and injection rate 4850 lbm/hr without insulation.

Figure 6.45, shows different steam quality values are conducted in our work using uninsulated tubing with 10% $N_2$. Steam quality and steam pressure or temperature values are inversely proportional. When steam quality increase steam pressure change decrease more as well as steam temperature in existing cases for non-condensable gas, and vise versa. However, it also yields higher steam quality values when the steam

reaches to reservoir with rich quality but poor temperature and pressure values. That may not be good for maintaining the temperature and pressure of the steam. In the same figure, heat loss values with different steam quality does not vary and have almost same values with different injection quality. Even if we have greatest liquid water content for the lowest steam quality, the pressure drop is the smallest. The contribution of water to the pressure drop is dependent on the slippage effect value and of course it is going to give little bit higher value than lowest water content on density of the mixture. However, the main contribution for frictional pressure drop values is mixture velocity of the components. In this case, the greater the steam quality we have in the system, the greater the mixture superficial velocity. This is the main explanation for the why pressure drop is dramatically for the greatest steam quality value. For example, I have checked three things : the total density of the mixture, mixture velocity and frictional pressure drop values for both cases and saw that mixture velocity is higher @ x = 0.85, than @ x = 0.6 almost two times. Mixture density of x = 0.6 is 1.2 times higher than x = 0.85, frictional pressure drop for x = 0.85 is almost 2.5 times higher than x = 0.6 case. Therefore, mixture velocity contribution in two-phase flow calculations have highest impact on frictional pressure drop, so total pressure drop increase more.

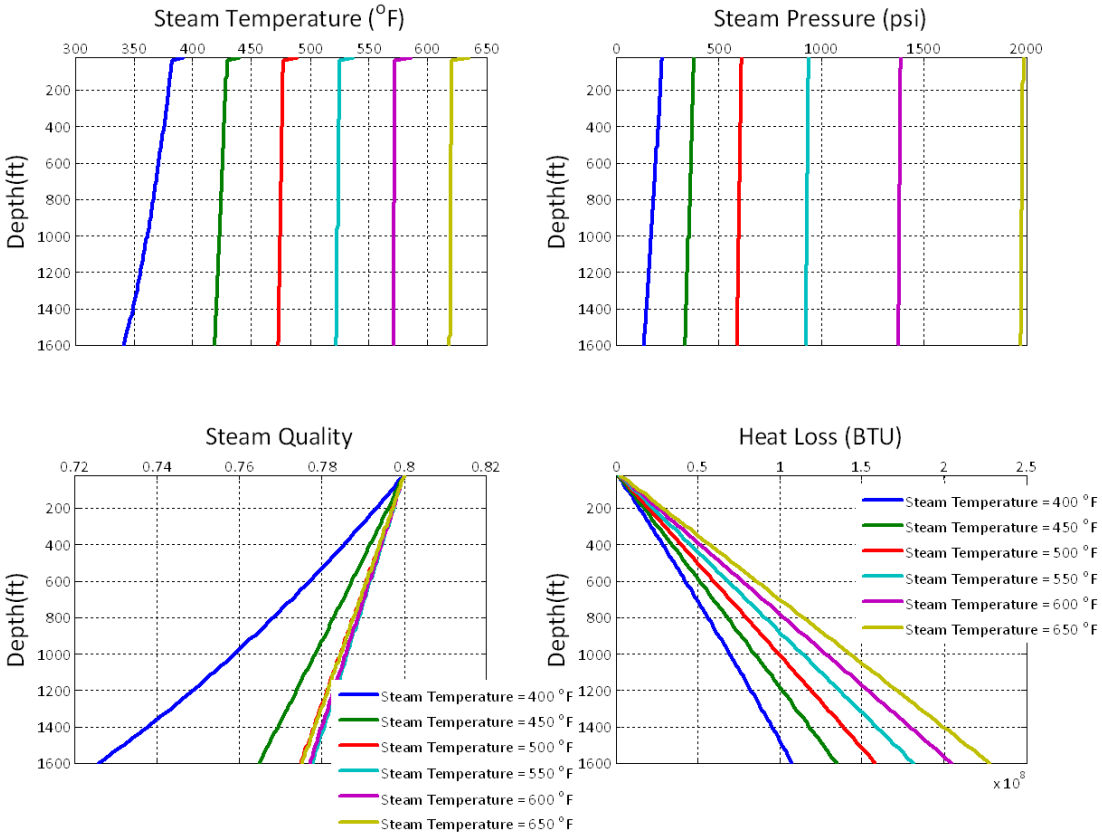


Figure 6.46: With changing injection temperature, 1 year, $T_m = 122\ ^oF$ and injection rate 4850 lbm/hr without insulation.

Steam temperature values are changed in terms of checking the sensitivity of steam quality, steam temperature, steam pressure and heat loss. In Figure 6.46, increasing steam temperature is caused by increasing steam pressure. Because of this less pressure drop and steam quality change obtained with highest steam temperature values. The greatest heat loss is observed with the greatest steam injection temperature with 650 $^oF$. With the insulated case, it is discerned that lowest steam quality, steam pressure, and steam temperature change found with greatest steam injection temperature. Without insulated tubing case, it is seen that the trend of heat loss values is almost 10 times greater as compared to the insulated case. Without insulated

case less steam quality decreases when the temperature 550 $^oF$, the other higher two values have corresponding values.

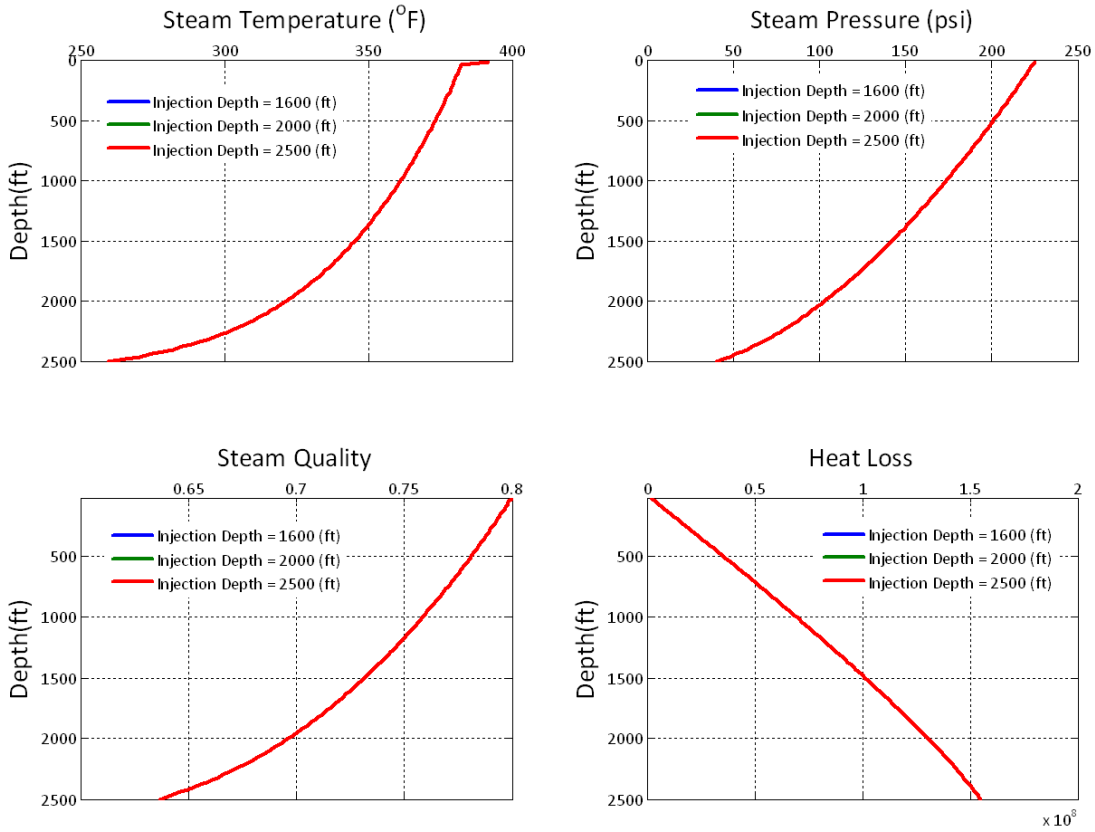


Figure 6.47: With changing injection depth, 1 year, $T_m = 122\ ^oF$ and injection rate 4850 lbm/hr without insulation.

Changing depth under non-condensable gas with using uninsulated tubing is studied by changing the depth ranging from 1600 $ft$ to 2500 $ft$. Again, a similar trend is shown in Figure 6.47 using insulated tubing. However, even if values seems closer for the two different cases, heat loss values are always much greater as compared to the insulated case.

## 6.6 Adding Non-Condensable Gas ($N_2$) in an Offshore environment

Similar observation of steam temperature, pressure, quality and heat loss are obtained with onshore environment, except for initial pressure drop is greater for offshore environment in both insulated and uninsulated cases. For example, Figure 6.38 and Figure 6.48 steam pressure, steam temperature, steam quality are similar except heat losses, on Figure 6.48 heat loss values corresponds on one line, Figure 6.39 and Figure 6.49, Figure 6.40 and Figure 6.50, Figure 6.41 and Figure 6.51, and Figure 6.42 and Figure 6.52 have similar trends between onshore cases and offshore cases with insulated tubing. This observation continues for uninsulated tubing cases as well. For instance, Figure 6.43 and Figure 6.53, Figure 6.44 and Figure 6.54, Figure 6.45 and Figure 6.55, Figure 6.46 and Figure 6.56, and Figure 6.47 and Figure 6.57 have similar trends between onshore cases and offshore cases with uninsulated tubing.

### 6.6.1 Examples with Insulation Materials

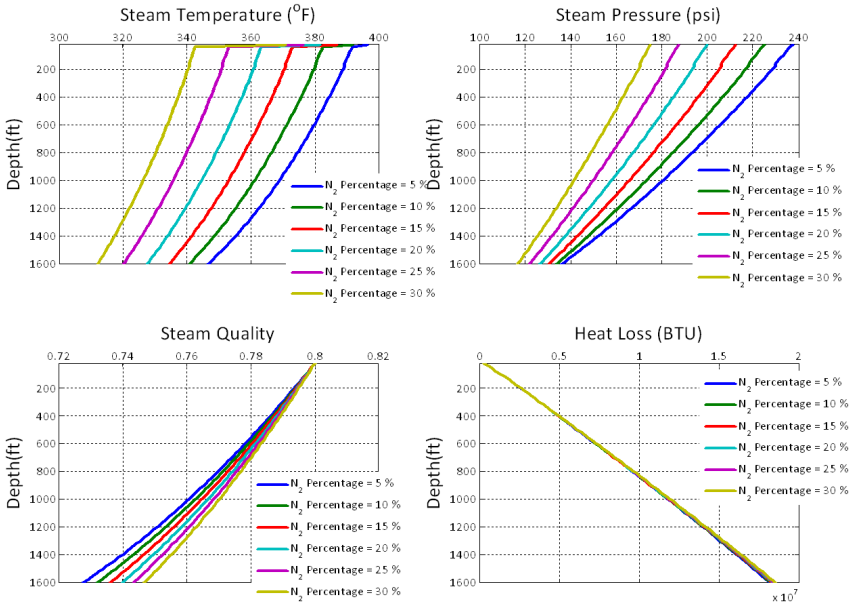


Figure 6.48: With changing $N_2$ molar percentage, 1 year, $T_m = 122\ ^oF$ and injection rate 4850 lbm/hr with using black aerogel.

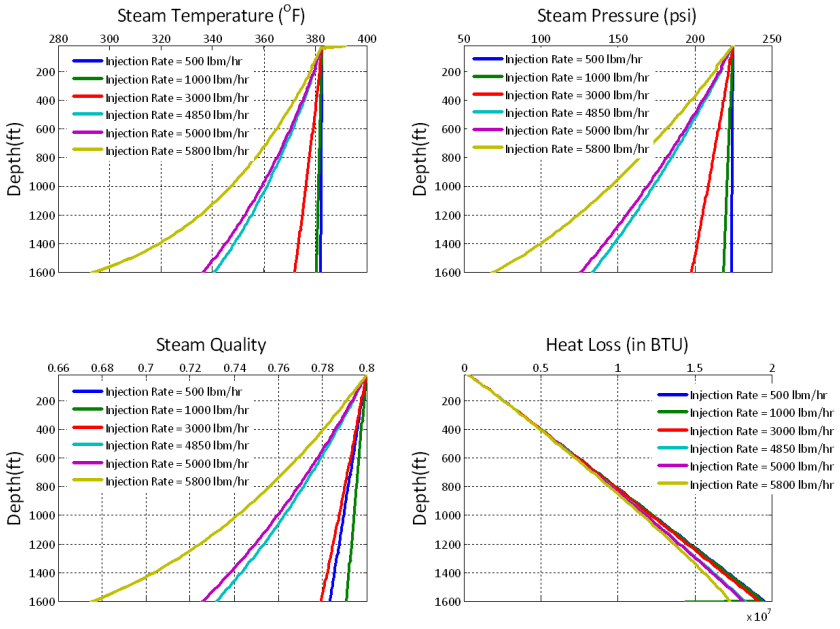


Figure 6.49: With changing injection rate, 1 year, $T_m = 122\ ^oF$ and injection rate 4850 lbm/hr with using black aerogel.

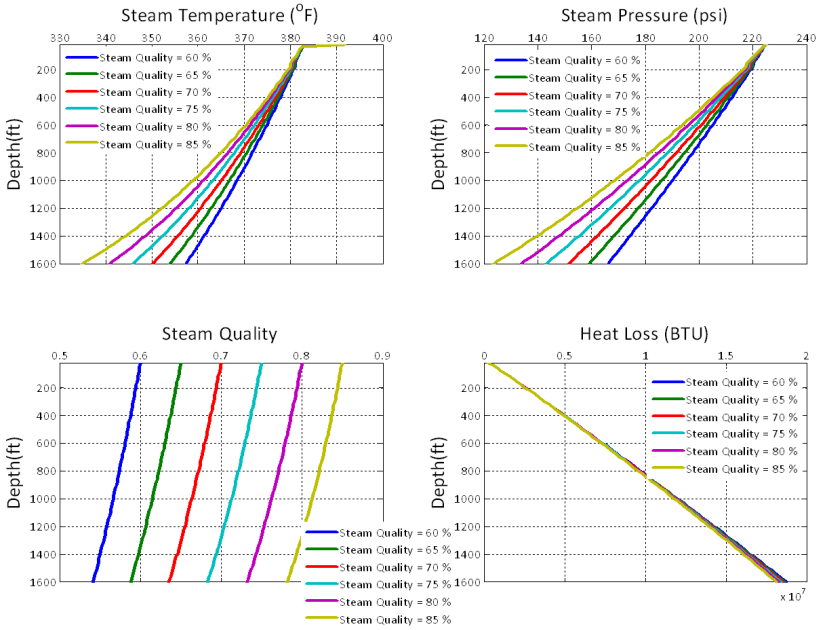


Figure 6.50: With changing steam quality molar percentage , 1 year, $T_m = 122\ ^oF$ and injection rate 4850 lbm/hr with using black aerogel.

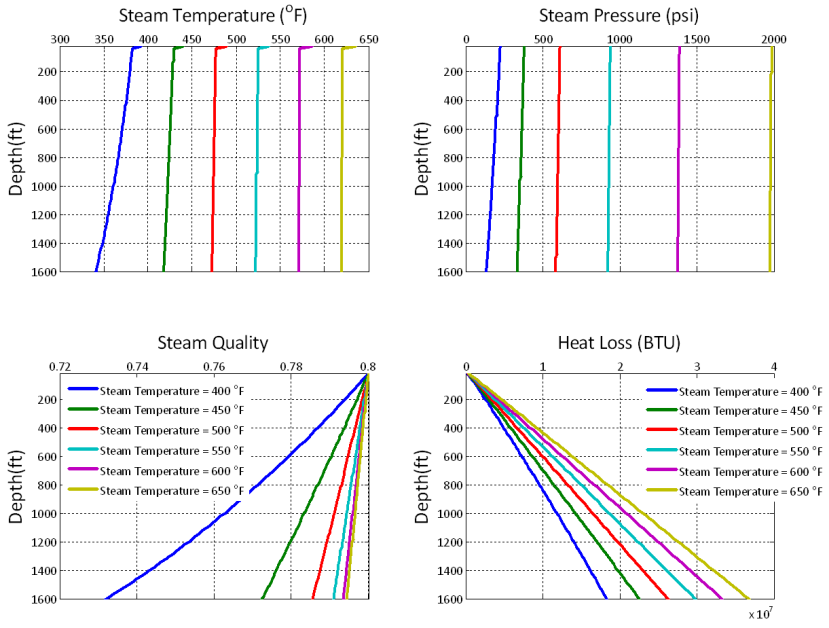


Figure 6.51: With changing injection temperature, 1 year, $T_m = 122\ ^oF$ and injection rate 4850 lbm/hr with using black aerogel.

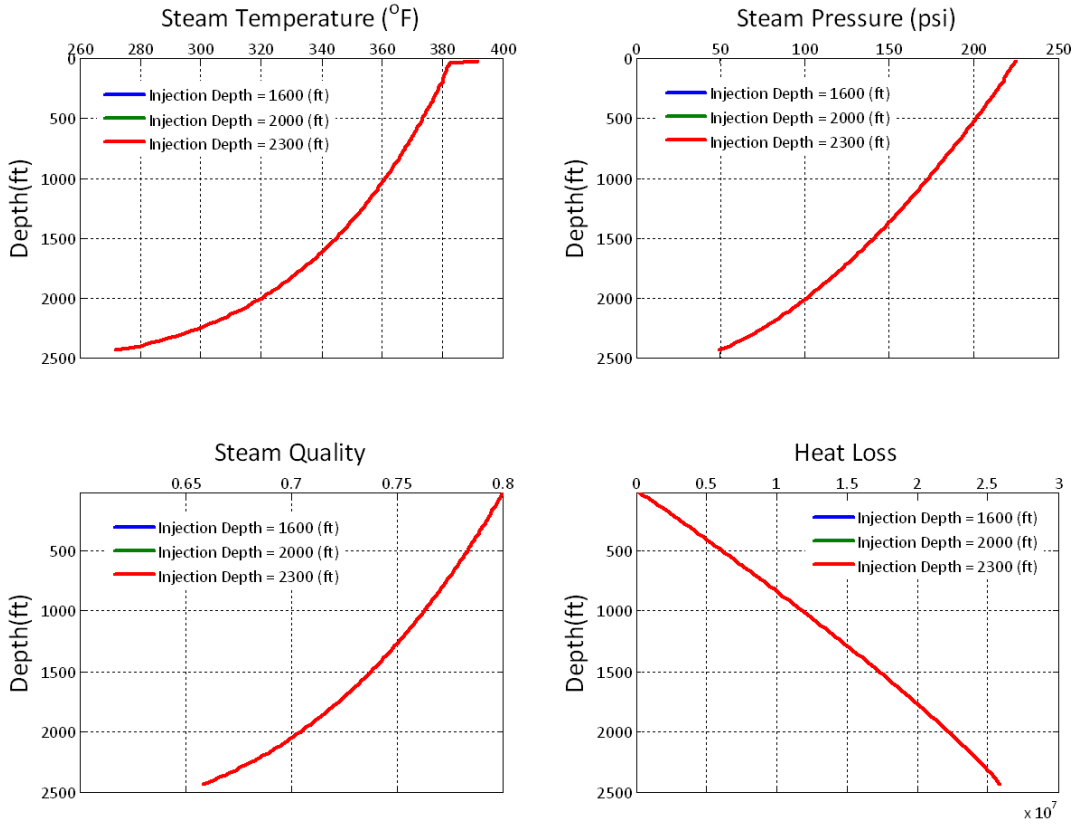


Figure 6.52: With changing injection depth, 1 year, $T_m = 122\ ^oF$ and injection rate 4850 lbm/hr with using black aerogel.

### 6.6.2 Examples without Insulation Materials

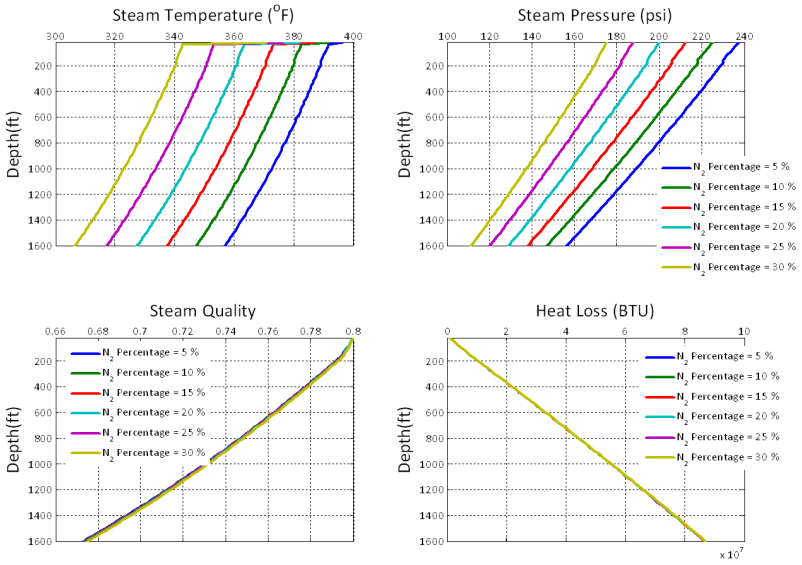


Figure 6.53: With changing $N_2$ molar percentage, 1 year, $T_m = 122\ ^oF$ and injection rate 4850 lbm/hr without insulation.

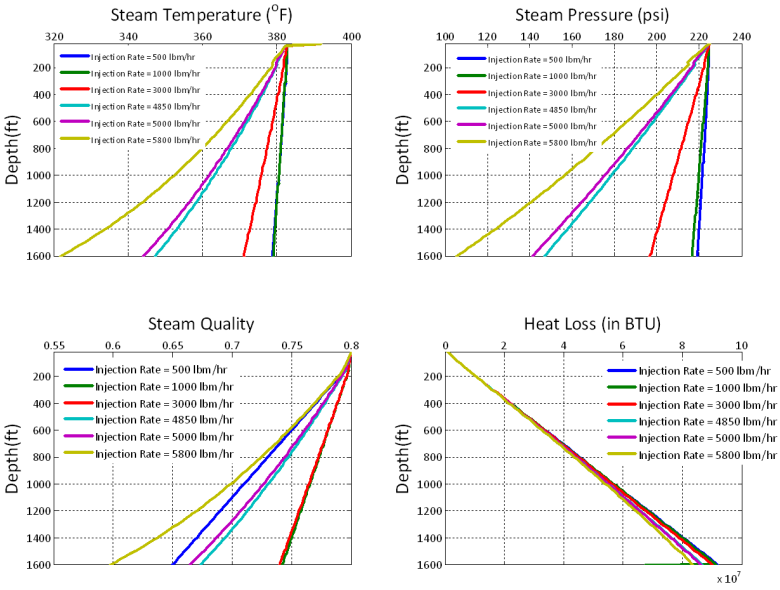


Figure 6.54: With changing injection rate, 1 year, $T_m = 122\ ^oF$ and injection rate 4850 lbm/hr without insulation.

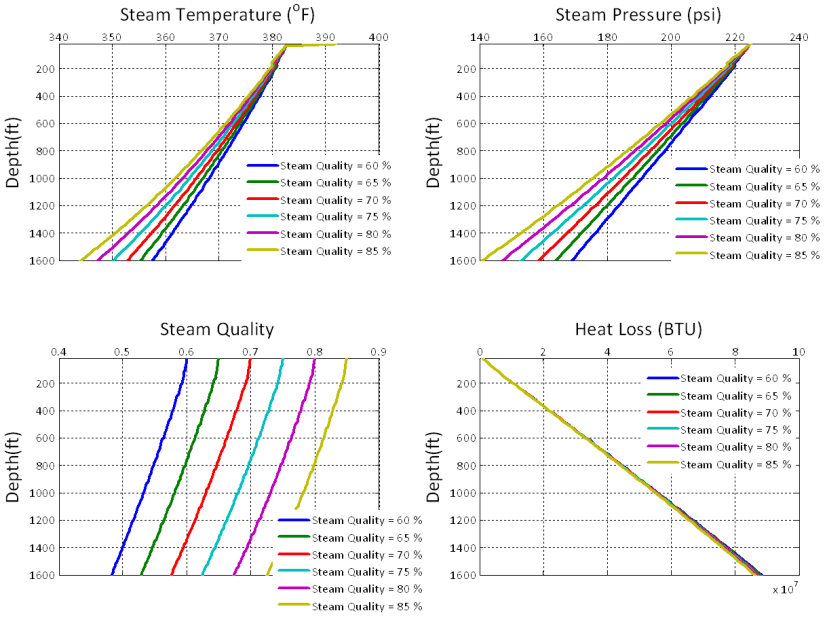


Figure 6.55: With changing steam quality molar percentage , 1 year, $T_m = 122\ ^oF$ and injection rate 4850 lbm/hr without insulation.

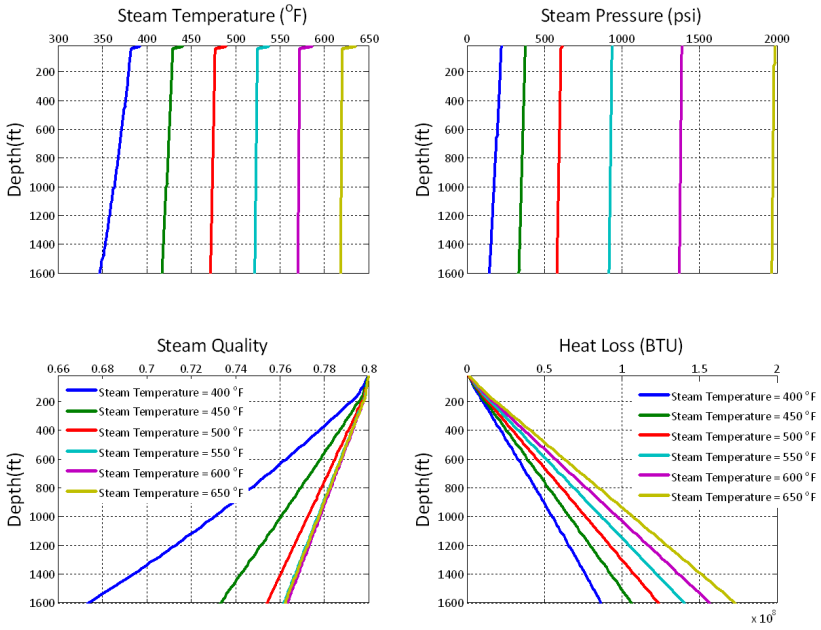


Figure 6.56: With changing injection temperature, 1 year, $T_m = 122\ ^oF$ and injection rate 4850 lbm/hr without insulation.

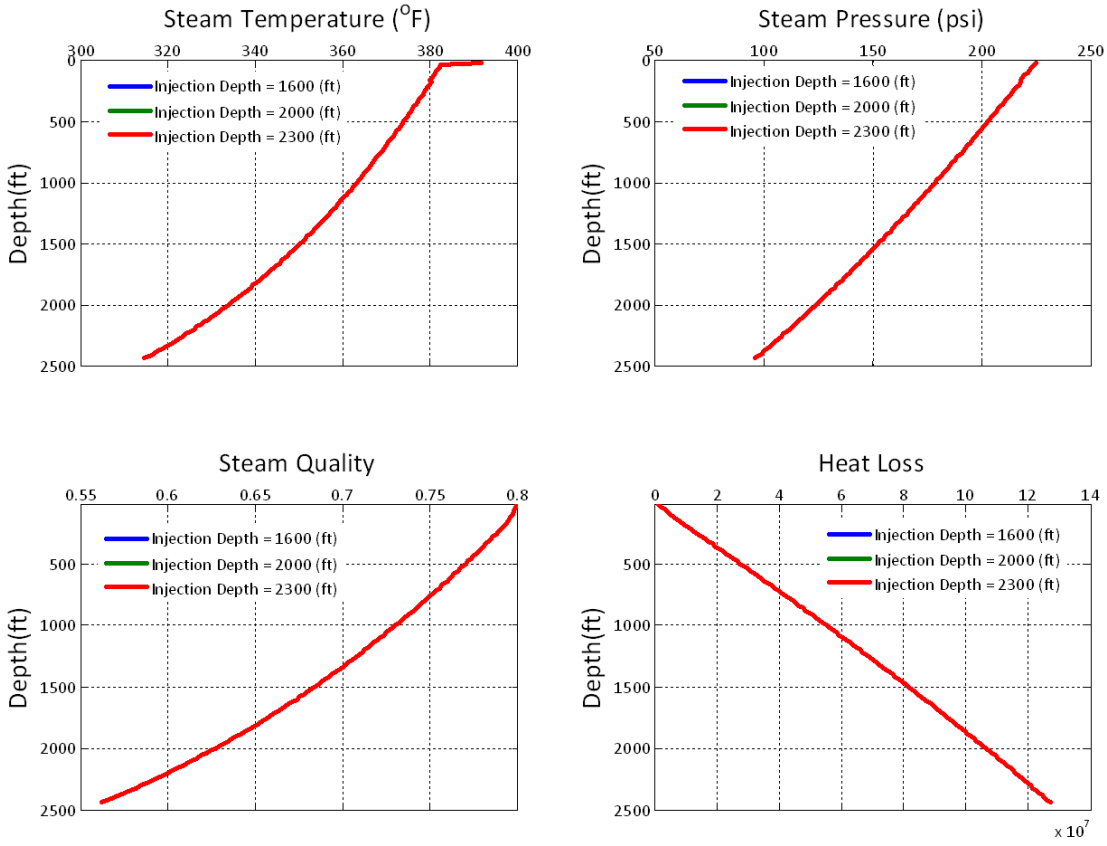


Figure 6.57: With changing injection depth, 1 year, $T_m = 122\ ^oF$ and injection rate 4850 lbm/hr without insulation.

# Chapter 7

# Summary, Conclusions and Future Work

## 7.1 Summary

In this thesis, we have presented an approximate, but accurate, solution for heat losses from steam injectors in both onshore and offshore environments. Solutions take into account pressure drop, heat loss, and multiphase flow. We compared our solution with two field cases and got good agreement. We improved the solution provided by Fontanilla[19] by using more accurate correlations. We made our offshore scenerio calculation taking into account seawater thermo physical properties in order to create a more realistic solution.

We used properties that are characteristics of six different insulation materials that are 1) black aerogel, 2) white aerogel, 3) fiberglass, 4) carbon fiber, 5) thermolastic insulation and 6) calcium silicate [34] with four different correlations for frictional pressure drop in the tubing: Aziz et al. [29], Beggs and Brill [3, 7, 14, 39], Hasan and Kabir [23, 37, 40] , and Drift Flux[21] and gave the results in results section. When the thermal conductivity of the insulation material increases, pressure drop

increases, steam quality drops, and we lose more heat to the surroundings. Heat loss and steam quality are highly related with the steam temperature and steam pressure. In order to see this, we used three different wellhead temperatures of $400^oF$, $500^oF$, and $600^oF$ and plotted the results.

In our calculations, although we saw that Beggs and Brill gives good approximation with the field data 1-2 in temperature, pressure calculations obtained over predicted steam quality results based on Fontanilla's approach. As we know each well has unique characteristics and production or completions history that makes predictions a little bit harder. Therefore, in order to get more accurate simulation results, more published field data is needed.

## 7.2 Conclusions

1. Heat transfer equations are developed by making an analogy with circuits for offshore application and simple heat loss calculation is done with insulated and uninsulated tubing. Uninsulated tubing gives 8 times higher heat loss when compared to the worst insulation material and 30 times more heat loss with compared to the best insulation material. The lower the thermal conductivity, the lesser the heat loss to the surroundings.

2. The Fontanilla and Aziz approach is augmented and tested against the two field cases. With improved two-phase flow correlations, a better estimation of temperature profile is obtained with the Fontanilla and Aziz approach. Pressure and temperature distribution values converged to the field data 1 and 2, with using the Beggs and Brill model. However, Beggs and Brill overpredicts steam quality values with compared to Fontanilla's results. The other two-phase correlations give similar values with Fontanilla's results in terms of comparing steam quality. Four different two-phase flow correlations yield almost same heat loss

results in both field cases.

3. Field data of steam quality values are not available in the literature. The calculated steam quality values based on all the investigated two-phase flow correlations are compared with the results of Fontanilla and Aziz. The Beggs and Brill model yields higher steam quality values, while all the other models yield similar results with the base Fontanilla and Aziz calculation.

4. Using insulation materials only affected heat losses and steam quality for both onshore and offshore environments using insulated or uninsulated tubing. Having low thermal conductive material such as black aerogel provides significantly less heat loss and steam quality decrease over the length of the well. Onshore and offshore results for both insulated or uninsulated cases showed similar trends in steam quality, steam pressure, steam temperature and heat loss profiles.

5. A GUI is developed for users to make the calculation faster, and see the other parameters effect on steam injection operations.

6. Formation pressure is important for both onshore and offshore steam injection operations. One case is studied for two different environments, and it is shown that when the formation pressure is greater than steam injection pressure at given depth steam can not be delivered to the reservoir. Therefore, formation pressure importance is emphasized in Figure 6.37.

7. The use of non-condensable gas, $N_2$, is added to steam is explored. Sensitivity analysis of the different parameters are conducted. Identical wellhead steam injection temperature values for offshore insulated tubing are considered with addition of 10 % $N_2$ to steam and a pure steam only case. We observed that having 10 % $N_2$ increases steam quality value around 8 %, decreases saturated

steam pressure around 20 %, and decreases heat loss around 2 %. For uninsulated tubing cases, increasing $N_2$ mole fraction does not change the bottom-hole steam quality and yielded greater overall heat loss. The trend with different non-condensable gas mole fraction, different steam quality, different injection rate, different depth and different injection temperature values are similar both insulated and uninsulated cases in for onshore and offshore environments. Greater the steam injection rate caused greater overall heat loss. Changing depth do not have any contribution on both insulated tubing and uninsulated tubing cases. The greatest effect on bottom-hole conditions of steam quality is observed with the highest wellhead steam temperature. Increasing steam temperature leads to greater heat loss, because the temperature difference between the well and the formation is greater. At the same time, the greater the injection temperature the greater the pressure values and the smaller the change on steam pressure and steam temperature.

## 7.3 Future Work

For future work, in order to expand of understanding of the physics of the problem, more field data has to be provided by the industry. With this more accurate results can be obtained. Sensitivity analysis and optimization can be done with different injection temperature, rate, time, steam quality and depth, in order to find best combination with regarding cost constraints and technology.

# Nomenclature

Abbreviations

| | |
|---|---|
| 2ResWithIns | Sea floor to the reservoir with insulation |
| 2ResWithoutIns | Sea floor to the reservoir without insulation |
| SeaWithIns | Offshore cases with insulation |
| SeaWithoutIns | Offshore cases without insulation |
| SLWithIns | Surface line with insulation |
| SLWithoutIns | Surface line without insulation |
| HSE | health, safety and environment |
| VIT | vacuum insulated tubing |

Symbols

| | |
|---|---|
| $a$ | geothermal gradient, $^oF/ft$ |
| $A$ | area,$ft^2$ |
| $B(\theta)$ | inclination factor |
| $C_L$ | no-slip liquid holdup |
| $\dot{Q}_{ls}$ | rate of heat loss per unit length of pipe in |
| $dp$ | pressure change, $psi$ |
| $dQ$ | heat loss to the surrounding, $BTU/lb$ |
| $dq$ | heat loss to the surrounding, $BTU/lb$ |
| $E_L(0)$ | horizontal liquid holdup |
| $E_L(\theta)$ | actual liquid holdup |
| $f$ | friction factor, $dimensionless$ |
| $f(tD)$ | time conduction function also known as Ramey function |
| $f_{tp}$ | two-phase friction factor, $dimensionless$ |

| | |
|---|---|
| $f_{NS}$ | no slip friction factor, *dimensionless* |
| $F_{rm}$ | Froud number of mixture |
| $g$ | acceleration due to gravity, $4.17e-8\ ft/hr^2$ |
| $Gr$ | Grashoff's number |
| $h$ | enthalpy, $BTU/lb$ |
| $h_f$ | film coefficient of heat transfer of the pipe, $BTU/ft^2-hr$ |
| $h_{fc}$ | coefficient of heat transfer forced convection, , $BTU/ft^2-hr$ |
| $h_{pipe}$ | coefficient of the heat transfer of pipe, $BTU/ft^2-hr$ |
| $h_{c,an}$ | radiation and convection coefficient of heat transfer, $BTU/ft^2-hr$ |
| $H_L$ | liquid holdup density |
| $J$ | mechanical equivalent of heat, $778\ ft-lb_f/BTU$ |
| $L$ | length, $ft$ |
| $k$ | thermal conductivity of the material, $BTU/(ft-hr-^oF)$ |
| $khc$ | effective thermal conductivity of the annular fluid, $BTU/(ft-hr-^oF)$ |
| $kha$ | actual thermal conductivity of the annular fluid, $BTU/(ft-hr-^oF)$ |
| $KE$ | kinetic energy, $BTU/lb$ |
| $N_{Re}$ | Reynolds number |
| $P$ | pressure, $psi$ |
| $PE$ | potential energy, $BTU/lb$ |
| $Pr$ | Prandtl's number |
| $q_g$ | gas flow rate, $ft^3/hr$ |
| $r_{ti}$ | inner radius of the tubing, $ft$ |
| $r_{to}$ | outer radius of the tubing, $ft$ |
| $r_{ins}$ | insulation radius of the tubing, $ft$ |
| $r_{ci}$ | inside radius of the casing, $ft$ |
| $r_{co}$ | outside radius of the casing, $ft$ |
| $r_h$ | wellbore radius, $ft$ |

| | |
|---|---|
| $r_{Ea}$ | radius of the altered zone in the earth near the well, $ft$ |
| $R$ | Reynolds number |
| $R_h$ | specific thermal resistance |
| $R_{NS}$ | no-slip Reynolds number |
| $t$ | time, $hrs$ |
| $T$ | temperature, $^oF$ |
| $Ta$ | absolute temperature, $^oR =^o F + 460$ |
| $T_A$ | ambient temperature of the atmosphere, $^oF$ |
| $T_b$ | bulk temperature of the fluid in the pipe, $^oF$ |
| $Tm$ | mean surface temperature, $^oF$ |
| $U$ | overall coefficient of heat transfer, $BTU/hr - ft^2 -^o F$ |
| $v$ | specific volume, $ft^3/lb$ |
| $v_w$ | wind velocity, $mph$ |
| $V$ | velocity, $ft/hr$ |
| $v_{sg}$ | superficial velocity for gas phase, $ft/hr$ |
| $v_g$ | actual velocity for gas phase, $ft/hr$ |
| $v_{sL}$ | superficial velocity for liquid phase, $ft/hr$ |
| $v_s$ | actual velocity for liquid phase, $ft/hr$ |
| $v_m$ | mixture velocity, $ft/hr$ |
| $Wm$ | steam injection rate, $lb/hr$ |
| $X$ | steam quality, $fraction\ by\ weight$ |
| $z$ | elevation or depth, $ft$ |

Greek Symbols

| | |
|---|---|
| $\alpha_E$ | thermal diffusivity of the earth, $ft^2/hr$ |
| $\epsilon$ | blackbody emissive power, $BTU/hr - ft^2$ |

| | |
|---|---|
| $\epsilon_{ins}$ | emissivity of the insulation material , $BTU/hr - ft^2$ |
| $\epsilon_{ci}$ | emissivity of the casing , $BTU/hr - ft^2$ |
| $\lambda_{pipe}$ | thermal conductivity of the pipe,$BTU/(ft - hr -^o F)$ |
| $\lambda_{ins}$ | thermal conductivity of the insulation,$BTU/(ft - hr -^o F)$ |
| $\lambda_{cem}$ | thermal conductivity of the cement,$BTU/(ft - hr -^o F)$ |
| $\lambda_{Ea}$ | thermal conductivity of the altered zone,$BTU/(ft - hr -^o F)$ |
| $\lambda_E$ | thermal conductivity of the unaltered zone,$BTU/(ft - hr -^o F)$ |
| $\mu_s$ | gas viscosity,$lb/ft - hr$ |
| $\mu_w$ | liquid viscosity,$lb/ft - hr$ |
| $\rho_l$ | gas density, $lbm/ft^3$ |
| $\rho_l$ | liquid density, $lbm/ft^3$ |
| $\rho_s$ | slip mixture density, $lbm/ft^3$ |
| $\rho_{NS}$ | no-slip mixture density, $lbm/ft^3$ |
| $\sigma$ | Stefan Boltzman constant, $0.1714e - 8\ BTU/(hr - ft^2 -^o R^4)$ |
| $\theta$ | angle from horizontal, $-90$ |

# Appendix A

# Derivation of the Equations

## A.1 Total Energy Equation

In Appendix A, all the equations are listed that are adapted and modified from the work that was done by Fontanilla and Aziz [19]. For a constant injection rate the continuity equation may be written as

$$\frac{d}{dz}\rho_{tp}V_m r_{ti}^2 = 0 \tag{A.1.1}$$

where, $\rho_{tp}$ is the two-phase density (lb/ft$^3$), $V_m$ is the mixture velocity (ft/hr), and $r_{ti}$ is the inside tubing radius (ft).

The energy conservation equation may be derived by taking a differential element $\Delta$z of the tubing as in Figure A.1:

Energy In (BTU/lb) = Energy Out (BTU/lb)

$$h_{m_1} + \frac{z_1}{J} + \frac{V_{m_1}^2}{2gJ} = h_{m_2} + \frac{z_2}{J} + \frac{V_{m_2}^2}{2gJ} \tag{A.1.2}$$

where, $h_{m_1}$ is the mixture enthalpy at point 1 (BTU/lb), $z_1$ is the elevation at point 1 (ft), J is the mechanical equivalent of heat = 778 (ft-$lb_f$/BTU), $V_{m_1}$ is the mixture

velocity at point 1 (ft/hr), g is the acceleration due to the gravity = 4.17*$10^8$ (ft/$hr^2$), $h_{m_2}$ is the mixture enthalpy at point 2 (BTU/lb), $z_2$ is the elevation at point 2 (ft), $V_{m_2}$ is the mixture velocity at point 2 = $V_{m_1} + dV_m$ (ft/hr), dQ is the heat loss to the surroundings, BTU/lb.

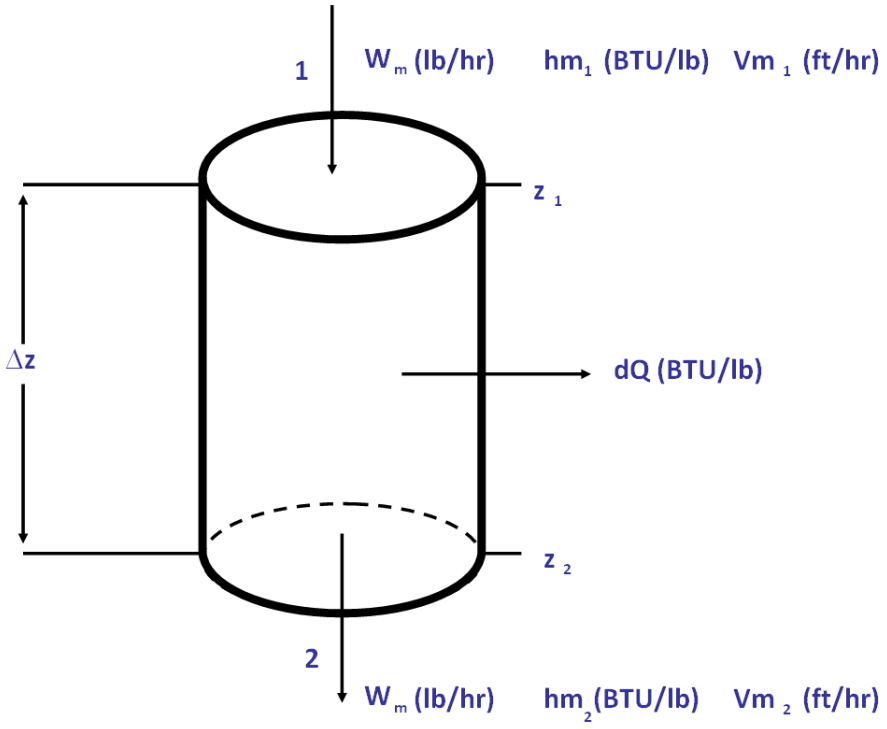


Figure A.1: Schematic view of tubing element in our calculation.

Transferring the L.H.S. of Eq. A.1.2 to the R.H.S. and assuming $dV_m^2$ is negligible we have,

$$h_{m_2} - h_{m_1} + \frac{z_2 - z_1}{J} + \frac{V_{m_1 dV_m}}{gJ} + dQ = 0 \tag{A.1.3}$$

$$\Delta\text{Enthalpy} + \Delta\text{PE} + \Delta\text{KE} + \text{Heat Loss to Surrounding} = 0$$

The sign of the second term, ΔPE, is correct only if the elevation decreases downward. In the present problem for the seafloor to reservoir, the surface is the datum plane and the elevation increases downward, so we need to affix a negative sign before the

term.

$$dh_m + \frac{dz}{J} + \frac{V_{m_1 dV_m}}{gJ} + dQ = 0 \tag{A.1.4}$$

dividing by dz

$$\frac{dh_m}{dz} + \frac{1}{J} + \frac{V_{m_1}}{gJ} + \frac{dV_m}{dz} + \frac{dQ}{dz} = 0 \tag{A.1.5}$$

The kinetic energy term in Eq. A.1.5 may be expanded as :

$$V_{m_1} = V_{SL} + V_{SG} = G_L v_L + G_g v_g \tag{A.1.6}$$

where, $V_{SL}$ is the superficial liquid velocity (ft/hr), $V_{SG}$ is the superficial gas velocity (ft/hr), $G_L$ is the liquid mass flux rate (lb/hr-$ft^2$), $v_L$ is the specific volume of liquid ($ft^3$/lb), $G_g$ is the gas mass flux rate (lb/hr-$ft^2$), $v_g$ is the specific volume of gas ($ft^3$/lb). Its equivalent differential form is

$$dV_m = G_L dv_L + G_g dv_g \tag{A.1.7}$$

Therefore we have

$$\frac{V_{m_1}}{gJ}\frac{dV_m}{dz} = \frac{1}{gJ}\left[v_L G_L^2 \frac{dV_L}{dz} + v_L G_L G_g \frac{dV_g}{dz} + v_g G_g G_L \frac{dV_L}{dz} + v_g G_g^2 \frac{dV_g}{dz}\right] \tag{A.1.8}$$

Substituting Eq. A.1.8 in to Eq. A.1.5

$$\frac{dh_m}{dz} - \frac{1}{J} + \frac{1}{gJ} + \frac{V_{m_1}}{gJ} + \left[v_L G_L^2 \frac{dV_L}{dz} + v_L G_L G_g \frac{dV_g}{dz} + v_g G_g G_L \frac{dV_L}{dz} + v_g G_g^2 \frac{dV_g}{dz}\right] + \frac{dQ}{dz} = 0 \tag{A.1.9}$$

## A.2 Mechanical energy balance or the Extended Bernoulli Equation

The basis for any fluid flow calculation is the mechanical energy balance for the flowing fluid between two points. Because there is no external work done on or by the fluid, a steady-state mechanical energy balance equation in differential form may be written for 1 $lb_m$ of fluid as:

$$144\frac{dp}{\rho_{tp}} + dz + \frac{v_{m_1} dv_m}{g} + dW_f = 0 \tag{A.2.1}$$

where $dp$= $P_2$-$P_1$ is the change in pressure (lb/in$^2$), $\rho_{tp}$ is the two-phase density (lb/ft$^3$), $dz$=$z_2$-$z_1$ is the change in elevation (ft), $v_{m_1}$ is the mixture velocity at point 1 (ft/hr), $dv_m$ is the change in mixture velocity (ft/hr), g is the acceleration due to gravity = 4.17*10$^8$ (ft/hr$^2$), $dW_f$ is the frictional drag (ft). We again have to affix a negative sign on the second term because the elevation increases downward. Multiplying Eq. A.2.1 by $\frac{\rho_{tp}}{dz}$, we have

$$144\frac{dp}{dz} - \rho_{tp} + \frac{\rho_{tp} v_{m_1}}{g}\frac{dv_m}{dz} + \rho_{tp}\frac{dW_f}{dz} = 0 \tag{A.2.2}$$

or 144$\frac{dp}{dz}$-$\frac{dp}{dz}$ elevation of PE+$\frac{dp}{dz}$ acceleration or KE+$\frac{dp}{dz}$ friction = 0

Substituting Eq. A.1.9 into Eq. A.2.2, we have

$$144\frac{dp}{dz} - \rho_{tp} + \frac{\rho_{tp}}{g}\left[v_L G_L^2 \frac{dV_L}{dz} + v_L G_L G_g \frac{dV_g}{dz} + v_g G_g G_L \frac{dV_L}{dz} + v_g G_g^2 \frac{dV_g}{dz}\right] + \left(\frac{dP}{dz}\right)_{friction} \tag{A.2.3}$$

The mixture enthalpy $h_m$ is a function of steam quality X and pressure P (psia).

$$h_m = f(X, P) \tag{A.2.4}$$

The specific volume of liquid (water) and gas (steam) are just functions of pressure P (psia). $V_L$ = g (P),$V_g$ = h (P) thus we can write

$$\frac{dh_m}{dz} = \frac{\partial h_m}{\partial X}\frac{dX}{dz} + \frac{\partial h_m}{\partial P}\frac{dP}{dz} \tag{A.2.5}$$

$$\frac{dv_g}{dz} = \frac{\partial v_g}{\partial P}\frac{dP}{dz} \tag{A.2.6}$$

$$\frac{dv_L}{dz} = \frac{\partial v_L}{\partial P}\frac{dP}{dz} \tag{A.2.7}$$

Substituting Eq. A.2.5, Eq. A.2.6, and Eq. A.2.7 into Eq. A.1.9 yields:

$$\frac{\partial h_m}{\partial X}\frac{dX}{dz} - \frac{\partial h_m}{\partial P}\frac{dP}{dz} - \frac{1}{J} + \frac{1}{gJ}\frac{dP}{dz}\left[v_L G_L^2\frac{\partial V_L}{\partial P} + v_L G_L G_g\frac{\partial V_g}{\partial P} + v_g G_g G_L\frac{\partial V_L}{\partial P} + v_g G_g^2\frac{\partial V_g}{\partial z}\right] + \frac{dQ}{dz} = 0 \tag{A.2.8}$$

Substituting Eq. A.2.6, and Eq. A.2.7 into Eq. A.2.3 we have:

$$144\frac{dP}{dz} - \rho_{tp} + \frac{\rho_{tp}}{g}\frac{dP}{dz}\left[v_L G_L^2\frac{\partial V_L}{\partial P} + v_L G_L G_g\frac{\partial V_g}{\partial P} + v_g G_g G_L\frac{\partial V_L}{\partial P} + v_g G_g^2\frac{\partial V_g}{\partial P}\right] + \left(\frac{dP}{dz}\right)_{friction} = 0 \tag{A.2.9}$$

Solving for $\frac{dP}{dz}$ in Eq. A.2.9,

$$\frac{dP}{dz} = \frac{\rho_{tp} - \left(\frac{dP}{dz}\right)_{friction}}{144 + \frac{\rho_{tp}}{g}\left[v_L G_L^2\frac{\partial V_L}{\partial P} + v_L G_L G_g\frac{\partial V_g}{\partial P} + v_g G_g G_L\frac{\partial V_L}{\partial P} + v_g G_g^2\frac{\partial V_g}{\partial P}\right]} \tag{A.2.10}$$

Solving for $\frac{dX}{dz}$ in Eq. A.2.8 yields,

$$\frac{dX}{dz} = \frac{1}{\frac{dh_m}{dX}}\left[-\frac{\partial h_m}{\partial P}\frac{dP}{dz} + \frac{1}{J} - \frac{1}{gJ}\frac{dP}{dz}\left(v_L G_L^2\frac{\partial V_L}{\partial P} + v_L G_L G_g\frac{\partial V_g}{\partial P} + v_g G_g G_L\frac{\partial V_L}{\partial P} + v_g G_g^2\frac{\partial V_g}{\partial P}\right) - \frac{dQ}{dz}\right] \tag{A.2.11}$$

Eq. A.2.10 and Eq. A.2.11 are two simultaneous, first order ordinary differential equations to be solved for pressure (P) and quality (X). Besides these we need to find

a method to calculate $\frac{dQ}{dz}$.

## A.3 Evaluation of Heat Loss to the Surrounding

In order to solve Eq. A.2.11, we need to know $\frac{dQ}{dz}$ (BTU/lb-ft) which is the heat loss to the surroundings.

$$dQ = \frac{dq}{W_m} \tag{A.3.1}$$

dQ is the change in heat loss by fluid (BTU/lb), dq is the change in heat loss rate (BTU/hr), $W_m$ is the steam injection rate (lb/hr)

Because we have a pseudo steady state heat flow conditions in the wellbore, the rate of heat conduction from the fluid to cement-formation interface (hole) is expressed:

$$\frac{dq}{dz} = 2\pi r_{to}(T_f - T_h) \tag{A.3.2}$$

A representation of the problem for three parts of our system will be analyzed and we refer those figures here again. Figure 3.1 refers to surface lines, Figure 3.4 refers to sea level to sea floor and Figure 3.9 refers to sea floor to reservoir heat loss calculation with insulated or not. Three figures and having two options each of them gives six different heat loss calculation procedures. We adapted the surface line heat losses from Prats and the rest of theprocedures are based on Willhite's approach that was discussed in chapter 3. The radius r and overall heat transfer coefficient U used in Eq. A.3.2 is based on any reference point. In the present case, the outer tubing surface was chosen as the reference plane. From Ramey[42], the rate of heat conduction into the earth is expressed as,

$$\frac{dq}{z} = \frac{2\pi k_e(T_h - T_e)}{f(t)} \tag{A.3.3}$$

where: $T_e$ is the temperature of the earth ( $^o$F), $k_e$ is the thermal conductivity of the

earth (BTU/hr-ft-$^o$F), f(t) is the time conduction function.

Because the rate of heat conduction from the fluid to the cement formation interface (hole) must equal the rate of heat conduction into the earth, Eq. A.3.2 and Eq. A.3.3 may be equated to obtain an expression for $T_h$:

$$T_h = \frac{r_{to}U_{to}f(t)T_f + k_eT_e}{r_{to}U_{to}f(t) + k_e} \tag{A.3.4}$$

Substituting Eq. A.3.4 and Eq. A.3.1 into Eq. A.3.2 we have:

$$\frac{dQ}{dz} = \frac{2\pi r_{to}U_{to}}{W_m}\left[T_f\frac{r_{to}U_{to}f(t)T_f + k_eT_e}{r_{to}U_{to}f(t) + k_e}\right] \tag{A.3.5}$$

If the geothermal gradient is provided, the temperature of the earth, $T_e$, is given by $T_e$=$T_m$+az, otherwise it assumes constant value. $T_m$ is the mean surface temperature ($^o$F), a is the geothermal gradient (($^o$F)/ft), z is the depth (ft). When we substitute the temperature of the earth into Eq. A.3.5 we have:

$$\frac{dQ}{dz} = \frac{2\pi r_{to}U_{to}}{W_m}\left[T_f\frac{r_{to}U_{to}f(t)T_f + k_e(T_m + az)}{r_{to}U_{to}f(t) + k_e}\right] \tag{A.3.6}$$

## A.4 Determination of the $U_{to}$ and $T_{ci}$

To obtain $\frac{dQ}{dz}$ (Eq. A.3.6), we need to know $U_{to}$ which is the overall heat transfer coefficient or the overall coefficient of conductance. The overall heat transfer conductance $U_{to}$ may be evaluated by writing expressions for the heat flow through the various components of the injector. The rate of heat conductance from the fluid to the cement-formation (hole) interface is given by A.3.2. The rate of the heat transfer between the flowing fluid and the inside tubing is given as:

$$\frac{dq}{dz} = 2\pi r_{ti}h_f(T_f - T_i) \tag{A.4.1}$$

where $h_f$ is the film coefficient for heat transfer based on the inside surface area of the tubing. Heat flow through the tubing wall, insulation, casing wall, and the cement sheath occurs by conduction. Integrating Fourier's law of heat conduction over the thickness of the tubing wall we write:

$$\frac{dq}{dz} = \frac{2\pi k_{tub}}{ln(\frac{r_{to}}{r_{ti}})}(T_{ti} - T_{to}) \tag{A.4.2}$$

Integrating Fourier's law of heat conduction over the thickness of the insulation yields:

$$\frac{dq}{dz} = \frac{2\pi k_{ins}}{ln(\frac{r_{ins}}{r_{to}})}(T_{to} - T_{ins}) \tag{A.4.3}$$

There are three modes of heat transfer present in the casing annulus.

1. heat conduction through the fluid in the annular space.

2. natural convection of fluid

3. radiation

Heat transfer by natural convection in the annulus is caused by fluid motion resulting from the variation of density with temperature. Hot fluid near the tubing and insulation is less dense than the fluid in the center of the annulus and tends to rise. On the other hand, the fluid near the casing wall is cooler and denser than that in the center of the annulus and tends to fall. When a body is heated, radiant energy is emitted at a rate dependent on the temperature of the body. The amount of radiant energy transported between the tubing/insulation and casing depends on the view the surfaces have of each other and their emitting and absorbing characteristics. To account for these three modes of heat transfer, it is convenient to define the heat rate through the annulus in terms of heat transfer coefficients $h_c$ (natural convection and

conduction) and $h_r$ (radiation), as:

$$\frac{dq}{dz} = 2\pi r_{to}(h_c + h_r)(T_{ins} - T_{ci}) \tag{A.4.4}$$

The heat conduction through the casing wall is given as:

$$\frac{dq}{dz} = \frac{2\pi k_{cas}}{ln(\frac{r_{co}}{r_{ci}})}(T_{ci} - T_{co}) \tag{A.4.5}$$

The heat conduction throught the cement sheath is given as:

$$\frac{dq}{dz} = \frac{2\pi k_{cem}}{ln(\frac{r_h}{r_{co}})}(T_{co} - T_h) \tag{A.4.6}$$

Note that:

$$T_f - T_h = (T_f - T_{ti}) + (T_{ti} - T_{to}) + (T_{to} - T_{ins}) + (T_{ins} - T_{ci}) + (T_{ci} - T_{co}) + (T_{co} - T_h) \tag{A.4.7}$$

Solving for the temperature differences

$$T_f - T_h = \frac{\frac{dq}{dz}}{2\pi r_{to} U_{to}} \tag{A.4.8}$$

$$T_f - T_{ti} = \frac{\frac{dq}{dz}}{2\pi r_{ti} h_f} \tag{A.4.9}$$

$$T_{ti} - T_{to} = \frac{\frac{dq}{dz}}{2\pi k_{tub}} ln\left(\frac{r_{to}}{r_{ti}}\right) \tag{A.4.10}$$

$$T_{to} - T_{ins} = \frac{\frac{dq}{dz}}{2\pi k_{ins}} ln\left(\frac{r_{ins}}{r_{to}}\right) \tag{A.4.11}$$

$$T_{ins} - T_{ci} = \frac{\frac{dq}{dz}}{2\pi r_{to}(h_c + h_r)} \tag{A.4.12}$$

$$T_{ci} - T_{co} = \frac{\frac{dq}{dz}}{2\pi k_{cas}} ln\left(\frac{r_{co}}{r_{ci}}\right) \tag{A.4.13}$$

$$T_{co} - T_h = \frac{\frac{dq}{dz}}{2\pi k_{cem}} ln\left(\frac{r_h}{r_{co}}\right) \tag{A.4.14}$$

Substituting Eqs. A.4.9 - 4.14 into the Eq. A.4.7 we will have:

$$T_f - T_h = \frac{\frac{dq}{dz}}{2\pi}\left[\frac{1}{r_{ti}h_f} + \frac{ln\left(\frac{r_{to}}{r_{ti}}\right)}{k_{tub}} + \frac{ln\left(\frac{r_{ins}}{r_{to}}\right)}{k_{ins}} + \frac{1}{r_{to}(h_c + h_r)} + \frac{ln\left(\frac{r_{co}}{r_{ci}}\right)}{k_{cas}} + \frac{ln\left(\frac{r_h}{r_{co}}\right)}{k_{cem}}\right] \tag{A.4.15}$$

An equation for $U_{to}$ is found by comparing Eq. A.4.8 and Eq. A.4.15

$$\frac{1}{r_{to}U_{to}} = \left[\frac{1}{r_{ti}h_f} + \frac{ln\left(\frac{r_{to}}{r_{ti}}\right)}{k_{tub}} + \frac{ln\left(\frac{r_{ins}}{r_{to}}\right)}{k_{ins}} + \frac{1}{r_{to}(h_c + h_r)} + \frac{ln\left(\frac{r_{co}}{r_{ci}}\right)}{k_{cas}} + \frac{ln\left(\frac{r_h}{r_{co}}\right)}{k_{cem}}\right] \tag{A.4.16}$$

Therefore,

$$U_{to} = \left[\frac{r_{to}}{r_{ti}h_f} + \frac{r_{to}ln\left(\frac{r_{to}}{r_{ti}}\right)}{k_{tub}} + \frac{r_{to}ln\left(\frac{r_{ins}}{r_{to}}\right)}{k_{ins}} + \frac{1}{(h_c + h_r)} + \frac{r_{to}ln\left(\frac{r_{co}}{r_{ci}}\right)}{k_{cas}} + \frac{r_{to}ln\left(\frac{r_h}{r_{co}}\right)}{k_{cem}}\right]^{-1} \tag{A.4.17}$$

The thermal conductivity of the tubing and casing steel ($k_{tub} = k_{cas} = 25 BTU/hr - ft -^o F$) is considerably higher than that for the other materials in the wellbore (insulation = 0.02 to 0.06 BTU/hr-ft-$^oF$ and cement = 0.2 to 0.6 BTU/hr-ft-$^oF$). Therefore, its relative contribution in Eq. A.4.17 is small and can be neglected ($T_{ti} = T_{to}$ and $T_{ci} = T_{co}$).

Also the film coefficient $h_f$ for steam and water are high enough (500 to 4000 BTU/hr-$ft^2$-$^oF$) to justify the assumption of infinite film coefficient ($T_f = T_{ti}$). Thus Eq. A.4.17 simplifies to Eq. A.4.18

$$U_{to} = \left[ \frac{r_{to} ln\left(\frac{r_{ins}}{r_{to}}\right)}{k_{ins}} + \frac{1}{(h_c + h_r)} + \frac{r_{to} ln\left(\frac{r_h}{r_{co}}\right)}{k_{cem}} \right]^{-1} \tag{A.4.18}$$

## A.5 Determination of the Convection Heat Transfer Coefficient

Before $U_{to}$ can be calculated in Eq. A.4.18, the convection coefficient $h_c$ and the radiation $h_r$ must be evaluated. Heat transfer per unit length by conduction and free convection in the annulus is given if there is no insulation;

$$\frac{dq_c}{dz} = \frac{2\pi k_{hc}}{ln\left(\frac{r_{ci}}{r_{to}}\right)} \tag{A.5.1}$$

if there is an insulation;

$$\frac{dq_c}{dz} = \frac{2\pi k_{hc}(T_{ins} - T_{ci})}{ln\left(\frac{r_{ci}}{r_{to}}\right)} \tag{A.5.2}$$

We can also express Eq. A.5.1 and Eq. A.5.2 may also be expressed if there is no insulation as:

$$\frac{dq_c}{dz} = 2\pi r_{to} h_c (T_{to} - T_{ci}) \tag{A.5.3}$$

if there is a insulation:

$$\frac{dq_c}{dz} = 2\pi r_{ins} h_c (T_{ins} - T_{ci}) \tag{A.5.4}$$

Combining Eq. A.5.1 with Eq. A.5.3 and Eq. A.5.2 with Eq. A.5.4 we will have if there is no insulation,

$$h_c = \frac{khc}{r_{to} ln\left(\frac{r_{ci}}{r_{to}}\right)} \tag{A.5.5}$$

if insulation present;

$$h_c = \frac{khc}{r_{ins} ln\left(\frac{r_{ci}}{r_{ins}}\right)} \tag{A.5.6}$$

The effective thermal conductivity of the annular fluid (khc) is related to the actual thermal conductivity of the annular fluid (kha) as a function of the Grashoff number and Prandtl number.

$$khc = (kha)(0.049)(GrPr)^{0.333}(Pr)^{0.074} \tag{A.5.7}$$

where: Gr is the Grashoff's number, if there is no insulation

$$Gr = \frac{(r_{ci} - r_{to})^3 g\rho_{an}^2 \beta(T_{to} - T_{ci})}{\mu_{an}^2} \tag{A.5.8}$$

if there is an insulation

$$Gr = \frac{(r_{ci} - r_{ins})^3 g\rho_{an}^2 \beta(T_{ins} - T_{ci})}{\mu_{an}^2} \tag{A.5.9}$$

Pr is the Prandtl's number

$$Pr = \frac{C_{an}\mu_{an}}{kha} \tag{A.5.10}$$

where $C_{an}$ is the specific heat of the annular fluid and $\mu_{an}$ is the viscosity of the annular fluid with given pressure in the annulus. $\beta$ ($^oR^{-1}$) is the coefficient of volume expansion. For ideal gas, $\beta$ is the reciprocal average absolute annulus temperature.

$$\beta = \frac{1}{(T_{an} + 460)} \tag{A.5.11}$$

where: $T_{an}$ if there is no insulation

$$T_{an} = \frac{T_{to} + T_{ci}}{2} \tag{A.5.12}$$

if there is an insulation

$$T_{an} = \frac{T_{ins} + T_{ci}}{2} \tag{A.5.13}$$

## A.6 Determination of the Radiation Heat Transfer Coefficient

Radiation heat transfer problems can be represented by "radiation networks" as in Carslaw and Jaeger and Herrera, et al.. The following developments are only for bare tubings but an equivalent equation which can be used for calculation of $h_r$ for tubings with insulation is also given. The tubing and the casing surfaces which exchange heat with each other may be modelled by resistances in series as shown in Fontanilla's thesis [19]. Here we are going to give the equations for $h_r$ with insulation and without insulation. So $h_r$ without insulation

$$h_r = \frac{(Ta_{to} + Ta_{ci})(Ta_{to}^2 + Ta_{ci}^2)\sigma}{\frac{1}{\epsilon_{to}} + \frac{r_{to}}{r_{ci}}\left[\frac{1}{\epsilon_{ci}} - 1\right]} \tag{A.6.1}$$

$h_r$ with insulation

$$h_r = \frac{(Ta_{ins} + Ta_{ci})(Ta_{ins}^2 + Ta_{ci}^2)\sigma}{\frac{1}{\epsilon_{ins}} + \frac{r_{ins}}{r_{ci}}\left[\frac{1}{\epsilon_{ci}} - 1\right]} \tag{A.6.2}$$

## A.7 Computational Procedure for $U_{to}$

In order to calculate $h_c$, $h_r$ and hence $U_{to}$, we need to know the temperature of the inside casing $T_{ci}$ and the temperature at the outer insulation $T_{ins}$. Since we need to

know $T_{ci}$ and $T_{ins}$ (which are unknown) to solve for $h_c$, $h_r$ and $U_{to}$, a trial and error or an iterative solution is required to determine the proper combination of $U_{to}$, $T_{ci}$ and $T_{ins}$. Before describing the iteration procedure, the equations to be used the iteration are developed. The equation for $T_{ins}$ is obtained from Eq. (A.4.3):

$$T_{ins} = T_{to} - \frac{\frac{dq}{dz} ln\left(\frac{r_{ins}}{r_{to}}\right)}{2\pi k_{ins}} \tag{A.7.1}$$

The equation for $T_{co}$ is obtained from Eq. (A.4.6):

$$T_{ins} = T_h + \frac{\frac{dq}{dz} ln\left(\frac{r_h}{r_{co}}\right)}{2\pi k_{cem}} \tag{A.7.2}$$

Substituting this expression for $T_{co}$ in Eq. (A.4.5), and solving for $T_{ci}$, we have:

$$T_{ci} = T_h + \frac{\frac{dq}{dz} ln\left(\frac{r_{co}}{r_{ci}}\right)}{2\pi k_{cas}} + \frac{\frac{dq}{dz} ln\left(\frac{r_h}{r_{co}}\right)}{2\pi k_{cem}} \tag{A.7.3}$$

Substituting Eq. (A.3.2) for $\frac{dq}{dz}$ in Eq. (A.7.3) and solving for $T_{ci}$

$$T_{ci} = T_h + r_{to}U_{to}(T_f - T_h) + \left[\frac{ln\frac{r_{co}}{r_{ci}}}{k_{cas}} + \frac{ln\frac{r_h}{r_{co}}}{k_{cem}}\right] \tag{A.7.4}$$

By neglecting the thermal resistance of the film, tubing, and casing, Eq. (A.7.4) reduces to :

$$T_{ci} = T_h + \frac{r_{to}U_{to}ln\frac{r_h}{r_{co}}}{k_{cem}}(T_{to} - T_h) \tag{A.7.5}$$

The hole temperature ($T_h$) can be obtained from Eq. (A.3.4) derived earlier.

$$T_h = \frac{r_{to}U_{to}f(t)T_f + k_eT_e}{r_{to}U_{to}f(t) + k_e} \tag{A.7.6}$$

The first thing to do is to assume an arbitrary value for $\frac{dq}{dz}$ and calculate an initial $T_{ins}$ from Eq. (A.7.1). Then set $T_{ci}$ equal to the geothermal temperature ($T_e$). Having values for $T_{ins}$ and $T_{ci}$; $h_r$, $h_c$, $U_{to}$, and f(t) can be calculated. $T_h$ is then solved using Eq. (A.7.6). Then a new value of $T_{ci}$ is calcualted using Eq. (A.7.5). The old and new casing temperatures are compared at this point. If the absolute value of their difference is greater than a tolerable amount, say 1 $^o$F, the old casing temperature is incremented by 70 percent of the difference. The model then uses this new casing temperature. To obtain a corresponding $T_h$ based on the new $T_{ci}$, solving for $T_h$ in Eq. (A.7.6) yields:

$$T_h = \frac{T_{ci}k_{cem} - r_{to}ln\frac{r_h}{r_{co}}T_{to}}{k_{cem} - r_{to}U_{to}ln\frac{r_h}{r_{co}}} \tag{A.7.7}$$

Using the new $T_h$ from Eq. (A.7.7), we calculate $\frac{dq}{dz}$ from Eq. (A.3.2). Calculate the new $T_{ins}$ from Eq. (A.7.1) using the new$\frac{dq}{dz}$, $T_{ins}$ and $T_{ci}$. The iteration is continued until convergence is obtained.

In summary, the iteration procedure is as follows:

1. Assume an arbitrary value for old $\frac{dq}{dz}$ and calculate the old $T_{ins}$ from Eq. (A.7.1).

2. Set $T_{ci}$ equal to the geothermal temperature $T_e$ and call this the old $T_{ci}$

3. Calculate $h_r$ from Eq. (A.6.2), $h_c$ from Eq. (A.5.6) $U_{to}$ from Eq. (A.4.18) and f(t) from Eq. (A.8.1) knowing the old $T_{ins}$ and the old $T_{ci}$

4. Calculate the old $T_h$ from Eq. (A.3.4)

5. Calculate the new $T_{ci}$ using Eq. (A.7.5).

6. The old $T_{ci}$ and new $T_{ci}$ are compared. if |new$T_{ci}$ - old$T_{ci}$ | $> 1$, the old $T_{ci}$ is incremented by 70 percent of the absolute value of the difference. Otherwise convergence is obtained.

7. If convergence is not yet obtained, a corresponding $T_h$ based on the $T_{ci}$ incremented in step 6. is calculated using Eq. (A.7.7).

8. Calculate a corresponding $\frac{dq}{dz}$ from Eq. (A.3.2).

9. Calculate $T_{ins}$ from Eq. (A.7.1)

10. Starting with step 3. the procedure is repeated until convergence is obtained.

## A.8 Determination of f(t)

The time conduction function f(t) introduced in the equation of unsteady state heat flow to the earth and needed to obtain $\frac{dQ}{dz}$ and $U_{to}$ can be estimated from solutions for radial heat conduction from an infinitely long cylinder. Such solutions are analogous to transient fluid flow solutions used in reservoir engineering. As can be seen Figure A.5 all five solutions converge to the same line. the convergence time is of the order of one week for many reservoir problems. Thus, the line source solution will often provide useful results if times are greater than a week. From Ramey[42] an approximate equation for $\mathbf{f(t)}$ satisfying the line source solution for long times is:

$$f(t) = -ln\left(\frac{r_h}{2\sqrt{\alpha t}}\right) \tag{A.8.1}$$

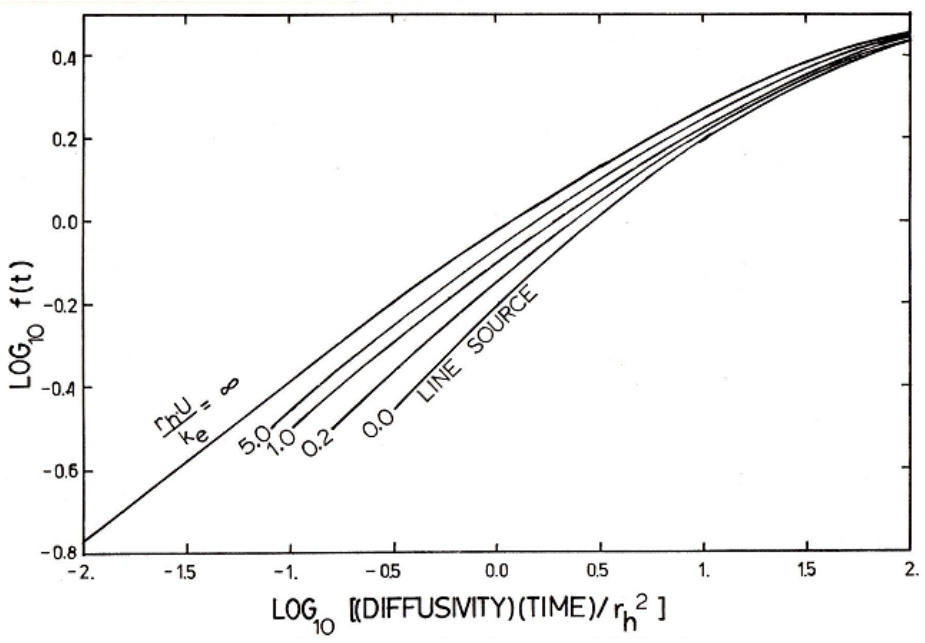


Figure A.2: Time conduction function (retrieved from[19]).

In this model, regression was used to obtain a third order polynomial approximation for each of the five curves in Figure A.5.

Lets say $K = \frac{r_h U}{k_e}$ the calculation procedure is as follows:

**Algorithm 1** $f(t)$ calculation based on the regression analysis

**Require:** $x = log_{10}\left(\frac{\alpha t}{r_h^2}\right)$ and $Y = log_{10} f(t)$
**Ensure:** $f(t) = 10^Y$
**if** $K == 0$ **then**
  $Y \leftarrow .19865 + .48034x - .08619x^2 + .00148x^3$
**else**
  **if** $K \leq .2$ **then**
    $Y \leftarrow -.12557 + .38757x - .07525x^2 + .01065x^3$
  **end if**
  **if** $K \leq 1.0$ **then**
    $Y \leftarrow -.08738 + .3689x - .04619x^2 - .00222x^3$
  **end if**
  **if** $K \leq 5.0$ **then**
    $Y \leftarrow -.03018 + .36166x - .06586x^2 - .00393x^3$
  **end if**
  **if** $K \geq 5.0$ **then**
    $Y \leftarrow -.02435 + .33116x - .033723x^2 - .00525x^3$
  **end if**
**end if**

## A.9 Evaluation of the Derrivatives

Farouq Ali[19] presented approximate correlations for specific volumes of saturated liquid and saturated vapor.

$$v_L = 0.01587 + 0.000086P^{0.225} + 0.0002P^{0.45} \tag{A.9.1}$$

$$v_L = 363.9P^{-0.9588} \tag{A.9.2}$$

Differentiating with respect to pressure we have,

$$\frac{\partial v_L}{\partial P} = 0.000019P^{-0.775} + 0.0009P^{-0.55} \tag{A.9.3}$$

$$\frac{\partial v_g}{\partial P} = -348.907P^{-1.9588} \tag{A.9.4}$$

Farouq Ali[19] also proposed correlations for the enthalpy of saturated liquid and the heat of vaporization $L_v$

$$h_L = 91P^{.2574} \tag{A.9.5}$$

$$L_v = h_g - h_l = 1318P^{-.08774} \tag{A.9.6}$$

for wet steam,

$$h_m = h_L + XL_v \tag{A.9.7}$$

$$h_m = 91P^{.2574} + X(1318P^{-.08774}) \tag{A.9.8}$$

Differentiating with respect to the steam quality X and pressure P, we have:

$$\frac{\partial h_m}{\partial X} = 1318P^{-0.08774} \tag{A.9.9}$$

$$\frac{\partial h_m}{\partial P} = 23.423P^{-0.7426} - 115.64XP^{-1.08774} \tag{A.9.10}$$

## A.10 Calculation of the Annulus Fluid Properties

There are several modification has been done for Fontanilla[19] solutions, one of them is getting annulus fluid properties automatically. We get viscosity and thermal conductivity of the fluid under 1 atm using figures from Prats[41].

**Viscosity of the annular fluid**, $\mu_{annulus}$

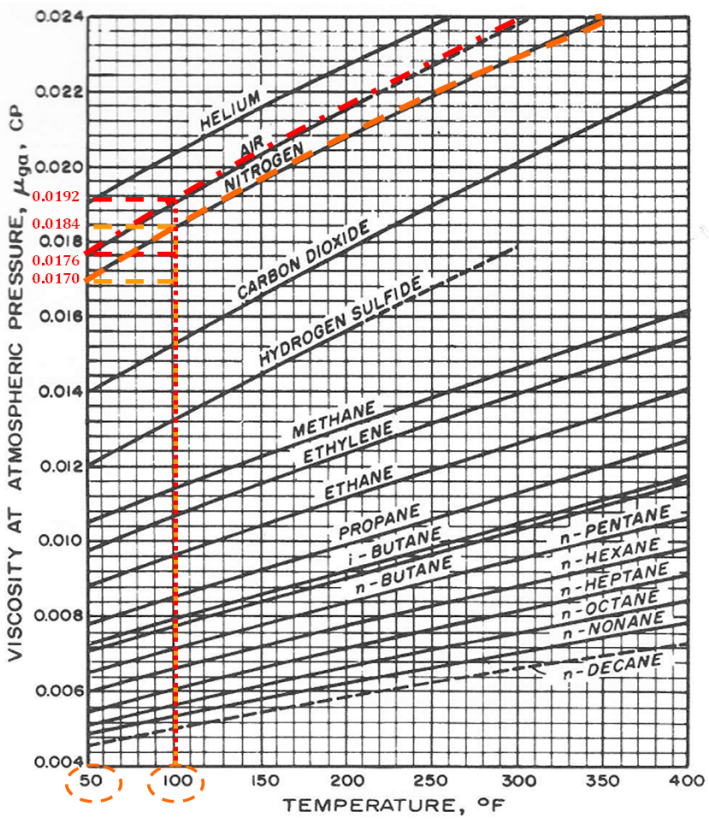


Figure A.3: Viscosity of the annular fluid with respect to Temperature.

We took two points on our curve and showed on the figure both $N_2$ and $air$ and assumed that the line is linear with increasing temperature values, because lines are only slightly different from linearity. As we know from very basic way to get slope of the line and put that value into $y = mx + n$ equation to get the correlation between temperature. Temperature values both $N_2$ and $air$ are $T_1 = 50$ and $T_2 = 100$, and viscosity values are $\mu^1_{N_2} = 0.0170$ cp and $\mu^2_{N_2}$= 0.0184 cp. For air same procedure applies $\mu^1_{air}$=0.0176 cp and $\mu^2_{air}$=0.0192 cp. Let's find $m_{N_2}$ and $m_{air}$ values as follows:

$$m_{N_2} = \left[\frac{\mu_1 - \mu_2}{T_1 - T_2}\right] = \left[\frac{0.0184 - 0.0170}{100 - 50}\right] = 2.8 * 10^{-5} \tag{A.10.1}$$

$$m_{air} = \left[\frac{\mu_1 - \mu_2}{T_1 - T_2}\right] = \left[\frac{0.0192 - 0.0176}{100 - 50}\right] = 3.2 * 10^{-5} \quad \text{(A.10.2)}$$

Thus, slope $m_{N_2}$= $2.8 * 10^{-5}$ and the correlation we got $\mu_{N_2}$=$2.8 * 10^{-5}$ T+0.0170 and for *air* $\mu_{air}$=$3.2 * 10^{-5}$ T+0.0176. We used this correaltions wrt temperature in our calculation.

**Thermal conductivity of the annular fluid**, $\lambda_{annulus}$

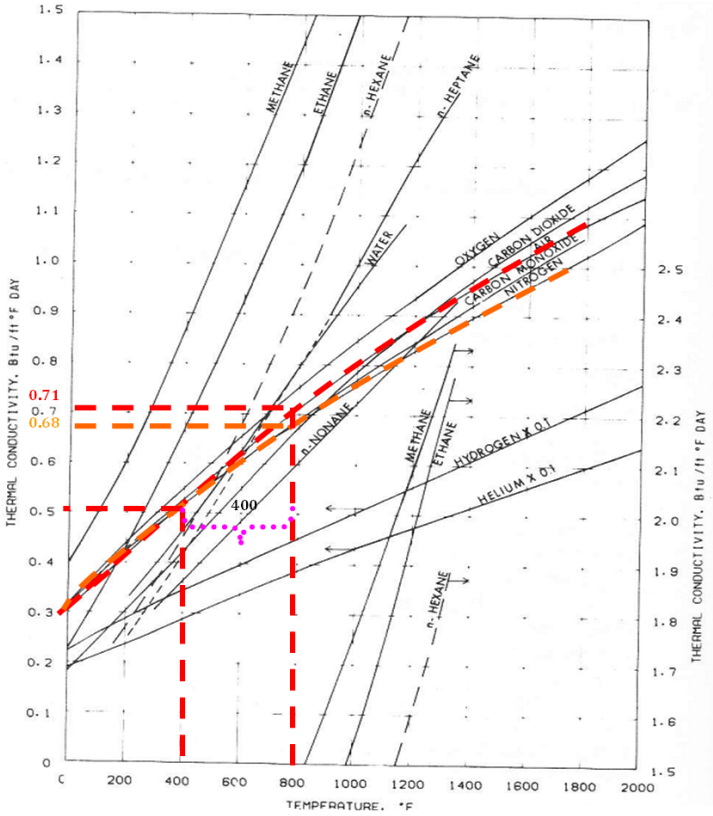


Figure A.4: Thermal conductivity of the annular fluid with respect to Temperature.

The same procedure is also applied for getting correlation both $N_2$ and *air* for thermal conductivity with respect to temperature. Temperature values both $N_2$ and *air* are $T_1$ = 400 and $T_2$ = 800, and thermal conductivity values are $\lambda^1_{N_2}$ = 0.5 BTU/ft$^oFD$ and $\lambda^2_{N_2}$= 0.68 BTU/ft$^oFD$. For air same procedure applies $\lambda^1_{air}$=0.5

BTU/ft$^oFD$ and $\lambda^2_{air}$=0.71 BTU/ft$^oFD$. Let's find $m_{N_2}$ and $m_{air}$ values as follows:

$$m_{N_2} = \left[\frac{\lambda_1 - \lambda_2}{T_1 - T_2}\right] = \left[\frac{0.68 - 0.50}{800 - 400}\right] = 4.5 * 10^{-4} \tag{A.10.3}$$

$$m_{air} = \left[\frac{\lambda_1 - \lambda_2}{T_1 - T_2}\right] = \left[\frac{0.71 - 0.5}{800 - 400}\right] = 5.25 * 10^{-4} \tag{A.10.4}$$

Thus, slope $m_{N_2}$= $4.5 * 10^{-4}$ and the correlation we got $\lambda_{N_2}$=$4.5 * 10^{-4}$ T+0.5 and for *air* $\lambda_{air}$=$5.25 * 10^{-4}$ T+0.5. We used this correaltions wrt temperature in our calculation.

# Appendix B

# Codes for Heat Loss Calculations

## B.1 Heat Losses from Surface Line

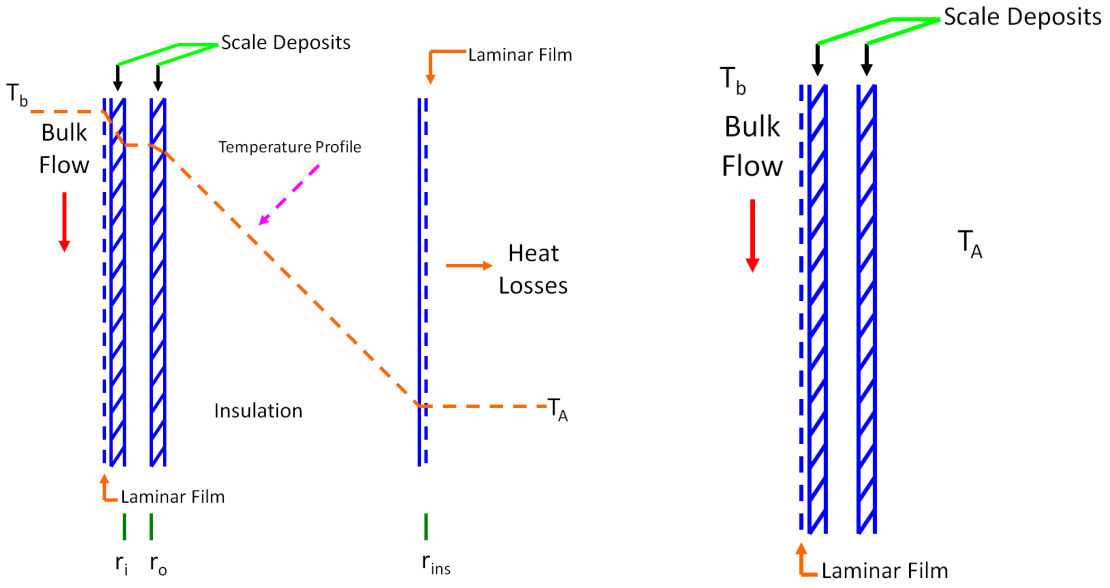


(a) Surface pipe with insulation.

(b) Surface pipe without insulation.

Figure B.1: Schematic representation of resistance to heat transfer with/without temperature profile.

The following are the *MatLab* codes for our heat loss calculation starting from surface lines with insulation and without insulation

```
%% Example 10.1 Calculations of Heat Losses from Surface Lines
% 4 inches N-80 pipe at rate of 229 B/D.
% We are looking for the solution at steady state conditions
% for pipe is insulated
% Thermal Recovery by Micheal Prats chapter 10, pgs.125-136
%%
clc;clear all; close all;
TsteamWins        = 550;          % F
TaverageWins      = 60;           % F
PipeLengthWins    = 100;          % ft
InjTimeWins       = 365*24;       % hours
AvrWindSpeedWins  = 20;           % mph
rinsideWins       = 0.1478;       % ft from Table B.15
routsideWins      = 0.1667;       % ft
rinsulatedWins    = 0.4167;       % ft
lambdaPipeWins    = 600/24;       % Btu/ft-hr-F
lambdaInsWins     = [0.166 0.194 0.388 0.499 0.569 0.96]./24;
hfWins            = 2000;         % Btu/sq ft-hr-F
hpiWins           = inf;          % Btu/sq ft-hr-F
hpoWins           = 2000;         % Btu/sq ft-hr-F

CollectDatasWithins=[];
% hfc calculation based on the Eq. 10.4
hfcWins           = (18*(AvrWindSpeedWins^0.6)*(rinsulatedWins^...
    0.6)/rinsulatedWins)/24;
colors = lines(length(lambdaInsWins));

for i=1:length(lambdaInsWins)
    % Overall specific thermal resistance
```

```
    RhWins              = 1/(2*pi)*( 1/(hfWins*rinsideWins)...
        + 1/(hpiWins*rinsideWins) + (1/lambdaPipeWins)*...
        log(routsideWins/rinsideWins) + 1/(hpoWins*routsideWins)+...
        (1/lambdaInsWins(i))*log(rinsulatedWins/routsideWins) +...
        1/(hfcWins*rinsulatedWins));
    % Heat Losses
    QlsWins             = (TsteamWins - TaverageWins)/RhWins;
    % Amount of Heat Lost from the pipe over a period of time
    QlWins              = QlsWins*InjTimeWins*PipeLengthWins;
    CollectDatasWithins=[CollectDatasWithins;[RhWins QlsWins QlWins]];
    InjTimeplotWins   =(1:InjTimeWins)';
    PlotQlWins          =(QlsWins*PipeLengthWins).*InjTimeplotWins;
    figure(1)
    plot(PlotQlWins, InjTimeplotWins./24,'color',colors(i,:),...
        'Linewidth',3)
    hold on
    grid on
    set(gca,'XAxisLocation','top','YDir','rev')
    xlabel(['Cumulative Heat Losses (in BTU) for '...
     num2str(PipeLengthWins) ' ft'],'Fontname', 'Calibri',...
     'FontSize', 16)
    ylabel(['Time (in Days) ' num2str(InjTimeWins/24)]...
        ,'Fontname', 'Calibri', 'FontSize', 16)
    LambdaValStr = sprintf('%0.3G' , lambdaInsWins(i));
    labels {i} = ['\lambda = ' num2str(LambdaValStr)];
    legend(labels,2,'Location', 'NE')
    set(gcf,'Units','normalized');
    set(gcf,'OuterPosition',[0 0 1 1]);
end
```

***Code block: SLwithoutIns.m***:

```
%% Example 10.1 Calculations of Heat Losses from Surface Lines
% 4 inches N-80 pipe at rate of 229 B/D.
% We are looking for the solution at steady state conditions
% for pipe is not-insulated
% written 2009, modified date 2011, May 9th
% Fidan, S.,
%%
clc;clear all;close all;

TsteamWOutIns        = 550;          % F
TaverageWOutIns      = 60;           % F
PipeLengthWOutIns    = 100;          % ft
InjTimeWOutIns       = 365;          % days
AvrWindSpeedWOutIns = 20;            % mph
rinsideWOutIns       = 0.1478;       % ft from Table B.15
routsideWOutIns      = 0.1667;       % ft
rinsulatedWOutIns    = 0.4167;       % ft
lambdaPipeWOutIns    = 600;          % Btu/ft-D-F
lambdaInsWOutIns     = 0.96;         % Btu/ft-D-F
hfWOutIns            = 48000;        % Btu/sq ft-D-F
hpiWOutIns           = inf;          % Btu/sq ft-D-F
hpoWOutIns           = 48000;        % Btu/sq ft-D-F

% hfc calculation based on the Eq. 10.4
hfcWOutIns           = 18*(AvrWindSpeedWOutIns^0.6)...
    *(routsideWOutIns^0.6)/routsideWOutIns;

% Overall specific thermal resistance
RhWOutIns            = 1/(2*pi)*( 1/(hfWOutIns*rinsideWOutIns)...
    + 1/(hpiWOutIns*rinsideWOutIns) + (1/lambdaPipeWOutIns)...
    *log(routsideWOutIns/rinsideWOutIns) + 1/((hfcWOutIns+...
    htTable14(TsteamWOutIns,routsideWOutIns))*...
```

```
    routsideWOutIns));
display(['The overall specific thermal...
    resistance is calculated from Eq. 10.2 is =...
    ' num2str(RhWOutIns) ' (BTU/ft-D-^F)^-1' ])

% Heat Losses
QlsWOutIns          = (TsteamWOutIns - TaverageWOutIns)...
    /RhWOutIns;
display(['Heat Losses Qls = ' num2str(QlsWOutIns)...
    ' Btu/ft-D'])

% Amount of Heat Lost from the pipe over a period of time
QlWOutIns           = QlsWOutIns*InjTimeWOutIns...
    *PipeLengthWOutIns;
display(['Cumulative Heat Losses over the period...
    of time woth given pipelength Ql =...
    ' num2str(QlWOutIns) ' Btu'])

h = figure('Color',[0 0 0]);
InjTimeplotWOutIns  =(1:InjTimeWOutIns)';
PlotQlWOutIns       =(QlsWOutIns*PipeLengthWOutIns)...
    .*InjTimeplotWOutIns;

plotHeatLoss(PlotQlWOutIns, InjTimeplotWOutIns,...
    h, QlWOutIns, PipeLengthWOutIns, lambdaInsWOutIns, 'r');
set(gcf,'Units','normalized');
set(gcf,'OuterPosition',[0 0 1 1]);
```

## B.2 Heat Losses from Sea Part

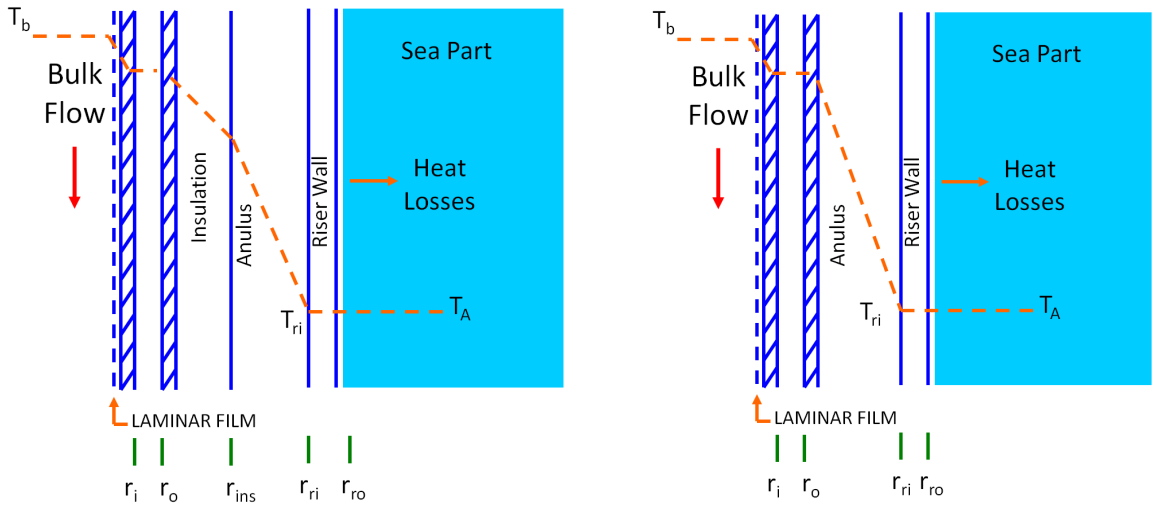


(a) Sea Part with insulation.

(b) Sea Part without insulation.

Figure B.2: Schematic representation of resistance to heat transfer with temperature profile.

The following are the *MatLab* codes for our heat loss calculation starting from sea surface to sea floor with insulation and without insulation

```
%% Solution for Offshore part with insulation materilas
% We are looking for the solution at steady state conditions
% written 2009, modified date 2011, May 9th
% Fidan, S.,
%%
clc;clear all;close all;
r_risero=18/12/2;
r_riseri=0.60;
rto = 0.1458;
rci= r_riseri;
```

```
rco = r_risero;
rh= 1;
roWithIns= rto;
rinsWithIns = 0.2292;
rciWithIns= r_riseri;
rcoWithIns= r_risero;
rwWithIns = rh;
rEaWithIns = 0;
TAWithIns = 70;
rins=rinsWithIns;

T=(TAWithIns-32)/1.8;
S=35;
alpha1 = SW_Diffusivity(T,S);% in [m^2/s]
% 1 [m^2/s] =38750.077500155 [ft^2/hr] from
q1=alpha1*38750.077500155; %[ft^2/hr]

epsci = 0.9;epsto= 0.9;epsriser = 0.9;
% thermal conductivity of water
%in [W/m K] ==1 Btu/(hr ft?F) = 1.730735 W/(mK).
k1 = SW_Conductivity(T,S);
%[Perry's Chemical Engineers' Handbook, 7th Edition, Table 1-4]
ke=k1/1.730735; % conversion factor

LamdaTub=600/24;
aEWithIns= q1;einsWithIns= 0.9;eciWithIns= 0.9;
lamda_EWithIns = ke;          % Btu/ft-hr-F
lamda_insWithIns            = [0.166 0.194 0.388 0.499 0.569 0.96]./24;
InjTimeWithIns              = 21*24;  % hrs
TbWithIns                   = 600;    % F
PipeLengthWithIns           = 164;    % ft
kins=lamda_insWithIns;
```

```
t=InjTimeWithIns;
lamdaPipe = 600/24;
Boltzman = (0.1714e-8);g=32.2*3600*3600;Tgeo=TAWithIns;Tf = TbWithIns;
% Tto = TbWithIns;

Th=TAWithIns;
colors = lines(length(lamda_insWithIns));
CollectDatasInjIns=[];

for i=1:length(lamda_insWithIns)



    % Step 1 assign random value for dqdz
    dqdz=5;
    % calculate the old T_ins from eq. 16
    Tins_old=TAWithIns;

    % h_r from eq. 15
    h_r=hr(Tins_old,TAWithIns,epsto,epsci,rci,rins,Boltzman);
    % hc from eq. 9
    Tanulus=Tan(Tins_old,TAWithIns);%F
    Beta_Gr=BetaGr(Tanulus);%R

    visAn=viscosityAn(Tanulus);%cp
    % 1 cp = 1488 lb/ft-second = 1488*3600 lb/ft-hr
    visAn = visAn*1488*3600;
    den=densityAn(Tanulus);%lbm/ft^3
    Gr1=Gr(Tins_old,TAWithIns,visAn,Beta_Gr,den,rci,rins,g);

    kha=kha1(Tanulus);
    Pr1=Pr(kha,visAn);
    khc=khc1(Gr1,Pr1,kha);
```

```
h_c=hc(khc,rci,rins);
% from eq. 8
Uto=UtoCal(h_c,h_r,rins,rto,kins(i));
% f(t) from Ramey and Willhite
ftD = FTIME(Uto,q1,t,rh,ke);

Tto=TAWithIns+dqdz/(2*pi*rto*(h_c+h_r))+dqdz/(2*pi*kins(i))*...
    log(rins/rto);
Tins_new=Tto-((dqdz*log(rins/rto))/(2*pi*kins(i)));

iter=0;
if abs(Tins_new-Tins_old)<=1
    Tins_new1=Tins_new;
    Tins_new=Tins_new1;
else

    while abs(Tins_new-Tins_old)>1
        iter=iter+1;
        Tins_old=Tins_old+0.7*(abs(Tins_new-Tins_old));

        Th=Tins_old-dqdz/(2*pi*rto*(h_c+h_r))+dqdz*log(r_risero/...
            r_riseri)/(2*pi*LamdaTub);



        dqdz=2*pi*rto*Uto*(Tf-Th);
        h_r=hr(Tins_old,TAWithIns,epsto,epsci,rci,rins,Boltzman);
        % hc from eq. 9
        Tanulus=Tan(Tins_old,TAWithIns);%F
        Beta_Gr=BetaGr(Tanulus);%R

        visAn=viscosityAn(Tanulus);%cp
        % 1 cp = 1488 lb/ft-second = 1488*3600
```

```
        visAn = visAn*1488*3600;
        den=densityAn(Tanulus);%lbm/ft^3
        Gr1=Gr(Tins_old,TAWithIns,visAn,Beta_Gr,den,rci,rins,g);

        kha=kha1(Tanulus);
        Pr1=Pr(kha,visAn);
        khc=khc1(Gr1,Pr1,kha);
        h_c=hc(khc,rci,rins);
        % from eq. 8
        Uto=UtoCal(h_c,h_r,rins,rto,kins(i));
        % f(t) from Ramey and Willhite
        ftD = FTIME(Uto,q1,t,rh,ke);

        Part1=TAWithIns*ke;
        Part2=rto*Uto*ftD*Tto;
        Part3=ke;
        Part4=rto*Uto*ftD;
        Th_old=(Part1+Part2)/(Part3+Part4);
        Tto=Tins_old+dqdz*log(rins/rto)/(2*pi*kins(i));
        Tins_new=Tto-(rto*Uto)*(Tf-Th_old)*log(rins/rto)/(kins(i));

    end

    Qls=2*pi*rto*Uto*(TbWithIns-TAWithIns);
    % TOTAL HEAT LOSS
    Ql=Qls*PipeLengthWithIns; %BTU


    InjLengthplot          =(1:PipeLengthWithIns)';
    PlotQl                 =(Qls).*InjLengthplot;

    figure(1)
```

```
        plot(PlotQl, InjLengthplot,'color',colors(i,:),'Linewidth',3)
        hold on
        grid on
        set(gca,'XAxisLocation','top','YDir','rev')
        xlabel(['Cumulative Heat Losses (in BTU) for '...
            num2str(PipeLengthWithIns) ' ft']...
            ,'Fontname', 'Calibri', 'FontSize', 16)
        ylabel('Depth (ft)')
        LambdaValStr = sprintf('%0.3G' , lamda_insWithIns(i)./24);
        labels {i} = ['\lambda = ' num2str(LambdaValStr)];
        legend(labels,2,'Location', 'NE')


        set(gcf,'Units','normalized');
        set(gcf,'OuterPosition',[0 0 1 1]);

    end
end
```

***Code block: SeaPartwithoutIns.m***:

```
%% Solution for Offshore part with insulation materilas
% We are looking for the solution at steady state conditions
% written 2009, modified date 2011, May 9th,Fidan, S.,
%%
% Heat loss calculation for without insulation case is done
clc;clear all;close all;
r_risero=18/12/2;% ft
r_riseri=0.60;
rto                 = 0.1458;               % ft
rci                 = r_riseri;             % ft
rco                 = r_risero;             % ft
rh                  = 1;                    % ft
```

```
rEaWithoutIns        = 0;                    % ft
TAWithoutIns                 = 70;           % F
T=(TAWithoutIns-32)/1.8;
S=35;
alpha1 = SW_Diffusivity(T,S);% in [m^2/s]
% 1 [m^2/s] =38750.077500155 [ft^2/hr] from
q1=alpha1*38750.077500155; %[ft^2/hr]
epsci                        = 0.9;
epsto                        = 0.9;
epsriser                     = 0.9;
% thermal conductivity of water
%in [W/m K] ==1 Btu/(hr ft ?F) = 1.730735 W/(mK)
k1 = SW_Conductivity(T,S);
%[Perry's Chemical Engineers' Handbook, 7th Edition, Table 1-4]
ke=k1/1.730735; % conversion factor
t                  = 21*24;                          % hrs
TbWithoutIns                 = 600;                  % F
PipeLengthWithoutIns         = 164;  % 50 meters     % ft
lamdaPipe                    = 600/24;
Boltzman                     = (0.1714e-8);
g=32.2*3600*3600;
Tgeo=TAWithoutIns;
Tf = TbWithoutIns;
% calculate the old T_ins from eq. 16
Tto = TbWithoutIns;%F
% h_r from eq. 15
h_r=hr(Tto,TAWithoutIns,epsto,epsci,rci,rto,Boltzman);%btu/hr-ft2-F
% hc from eq. 9
Tanulus=Tan(Tto,TAWithoutIns);%F
Beta_Gr=BetaGr(Tanulus);%R
visAn=viscosityAn(Tanulus);%cp
% 1 cp = 1488 lb/ft-second = 1488*3600 lb/ft-hr
```

```
visAn = visAn*1488*3600;
den=densityAn(Tanulus);%lbm/ft^3
Gr1=Gr(Tto,TAWithoutIns,visAn,Beta_Gr,den,rci,rto,g);
kha=kha1(Tanulus);
Pr1=Pr(kha,visAn);
khc=khc1(Gr1,Pr1,kha);
h_c=hc(khc,rci,rto);
% from eq. 8
Uto=UtoCal(h_c,h_r,rh,rco,rto,ke);
% f(t) from Ramey and Willhite
ftD = FTIME(Uto,q1,t,rh,ke);
Qls=2*pi*rto*Uto*(TbWithoutIns-TAWithoutIns);
% TOTAL HEAT LOSS
Ql=Qls*PipeLengthWithoutIns; %BTU
InjLengthplot          =(1:PipeLengthWithoutIns)';
PlotQl                 =(Qls).*InjLengthplot;
figure(1)
plot(PlotQl, InjLengthplot,'b','Linewidth',3)
% Create title
titleValStr = sprintf('%0.3G' , Ql);
title(['Heat Losses within along the' num2str(PipeLengthWithoutIns)...
    'ft is =' titleValStr  ' in Btu'],...
    'FontSize',14, 'Color', 'k');
hold on
grid on
set(gca,'XAxisLocation','top','YDir','rev')
xlabel('Cumulative Heat Losses in BTU','Fontname',...
    'Calibri', 'FontSize',16)
ylabel('Depth (ft)')
set(gcf,'Units','normalized');
set(gcf,'OuterPosition',[0 0 1 1]);
```

## B.3 Heat Losses from Sea Floor to Reservoir

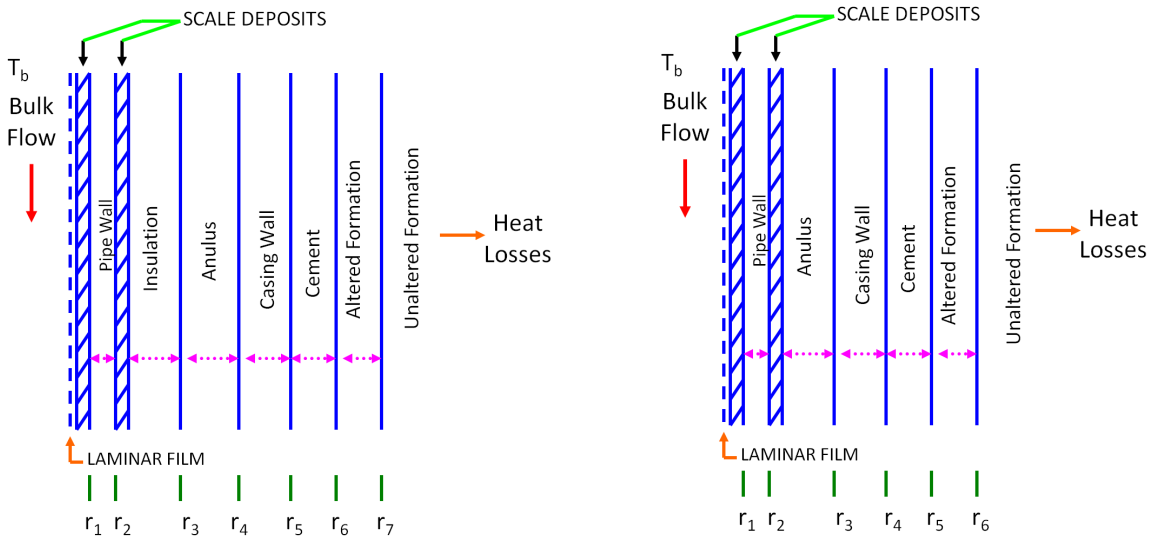


(a) Sea Floor to Reservoir with insulation.

(b) Sea Floor to Reservoir without insulation.

Figure B.3: Schematic representation of resistance to heat transfer sea floor to reservoir.

The following are the *MatLab* codes for our heat loss calculation starting from sea floor to reservoir with insulation and without insulation

```
%% Example 10.2 Calculations of Heat Losses from Surface Lines
% 3.5 in. tubing set on a packer in 9 5/8 in, 53.5 lbm/ft N-80 casing
% The annulus contatins a stagnant gas at zero gauge pressure at wellhead
% and casing is cemented to surface in a 12-in hole.
% We are looking for the solution at steady state conditions
% written 2009, modified date 2011, May 9th
% Fidan, S.,
%%
clc;clear all;close all;
```

```
roWithIns                = 0.1458;              % ft
rinsWithIns              = 0.2292;              % ft
rciWithIns               = 0.3556;              % ft
rcoWithIns               = 0.4010;              % ft
rwWithIns                = 0.5000;              % ft
rEaWithIns               = 0;                   % ft
aEWithIns                = 0.96;
einsWithIns              = 0.9;
eciWithIns               = 0.9;
lamda_EWithIns           = 24;                  % Btu/ft-hr-F
lamda_cemWithIns         = 12;                  % Btu/ft-hr-F
lamda_insWithIns         = [0.166 0.194 0.388 0.499 0.569 0.96];
InjTimeWithIns           = 21;                  % days
TAWithIns                = 100;                 % F
TbWithIns                = 600;                 % F
PipeLengthWithIns        = 1000;                % ft

colors = lines(length(lamda_insWithIns));
CollectDatasInjIns=[];

for i=1:length(lamda_insWithIns)
    % STEP1: Initial Assumption of the Total Thermal Resistance
    Rh=(log(rinsWithIns/roWithIns)/lamda_insWithIns(i))/pi;
    % STEP2: Calculate f(tD) at t
    tD=aEWithIns*InjTimeWithIns/(rwWithIns^2);
    Rh2=Rh;
    c=2*pi*Rh2*lamda_EWithIns;
    f=ft(c,tD);
    ftD=f;

    % STEP3: Calculate Tci from Eq.B68
    Up=0;
```

```
    Ucem=log(rwWithIns/rcoWithIns)/lamda_cemWithIns;
    if rEaWithIns>0
        Uea=log(rEaWithIns/rwWithIns)/lamda_EWithIns;
    else
        Uea=0;
    end
    Uf=ftD/lamda_EWithIns;
    Tci=TAWithIns+((TbWithIns-TAWithIns)/(2*pi*Rh))...
        *(Up+Ucem+Uea+Uf);
    % STEP4: Calculate Tins from Eq. B.70
    Ui=0;Upi=0;Upw=0;Upo=0;
    Uins=log(rinsWithIns/roWithIns)/lamda_insWithIns(i);
    Tins=TbWithIns-((TbWithIns-TAWithIns)/(2*pi*Rh))...
        *(Ui+Upi+Upw+Upo+Uins);
    %STEP5: Calculate hcan from Eq. B.63 through B.66
    Tan=(Tins+Tci)/2;
    den=0.076*((460+60)/(460+Tan));
    % From FigB.41 vis=2.54*10^(-5)*T+0.0164
    vis=2.54*10^(-5)*Tan+0.0164;
    % lamda_a=0.45;
    lamda_a = (2.8e-004)*Tan+0.312;
    Ban=1/(460+Tan);
    g=1;gc=1;
    Ngr=(gc/g)*7.12*10^7*(rciWithIns-rinsWithIns)^3*g*...
    den^2*Ban*(Tins-Tci)/(gc*vis^2);
    % Npr^0.4=0.92
    lamda_aa=(0.049*lamda_a*Ngr^0.333*0.92);
    F=((460+Tins)^2+(460+Tci)^2)*(920+Tins+Tci);
    hcan=4.11*10^(-8)*((1/einsWithIns)+(rinsWithIns/rciWithIns)*...
    (1/eciWithIns-1))^(-1)*F+lamda_aa/(rinsWithIns*...
log(rciWithIns/rinsWithIns));
    % STEP6: Calculate Rh using Eq. 10.6
```

```
Ucan=1/(hcan*rinsWithIns);
Rhc=1/(2*pi)*(Ui+Upi+Upw+Upo+Uins+Ucan+Up+Ucem+Uea+Uf);
counter=0;
while abs(Rhc-Rh) > 1e-4
    counter=counter+1;
    Rh=Rhc;
    % STEP2: Calculate f(tD) at t
    tD=aEWithIns*InjTimeWithIns/(rwWithIns^2);
    Rh2=Rh;
    c=2*pi*Rh2*lamda_EWithIns;
    f=ft(c,tD);
    ftD=f;
    % STEP3: Calculate Tci from Eq.B68
    Up=0;
    Ucem=log(rwWithIns/rcoWithIns)/lamda_cemWithIns;
    if rEaWithIns>0
        Uea=log(rEaWithIns/rwWithIns)/lamda_EWithIns;
    else
        Uea=0;
    end
    Uf=ftD/lamda_EWithIns;
    Tci=TAWithIns+((TbWithIns-TAWithIns)/(2*pi*Rh))...
        *(Up+Ucem+Uea+Uf);
    % STEP4: Calculate Tins from Eq. B.70
    Ui=0; Upi=0; Upw=0; Upo=0;
    Uins=log(rinsWithIns/roWithIns)/lamda_insWithIns(i);
    Tins=TbWithIns-((TbWithIns-TAWithIns)/(2*pi*Rh))*...
        (Ui+Upi+Upw+Upo+Uins);
    %STEP5: Calculate hcan from Eq. B.63 through B.66
    Tan=(Tins+Tci)/2;
    den=0.076*((460+60)/(460+Tan));
    % From FigB.41 vis=2.54*10^(-5)*T+0.0164
```

```
        vis=2.54*10^(-5)*Tan+0.0164;
        lamda_a = (2.8e-004)*Tan+0.312;
        Ban=1/(460+Tan);
        g=1; gc=1;
        Ngr=(gc/g)*7.12*10^7*(rciWithIns-rinsWithIns)^3*...
            g*den^2*Ban*(Tins-Tci)/(gc*vis^2);
        lamda_aa=(0.049*lamda_a*Ngr^0.333*0.92);
        F=((460+Tins)^2+(460+Tci)^2)*(920+Tins+Tci);
        hcan=4.11*10^(-8)*((1/einsWithIns)+...
            (rinsWithIns/rciWithIns)*...
            (1/eciWithIns-1))^(-1)*F+lamda_aa/(rinsWithIns*...
            log(rciWithIns/rinsWithIns));
        % STEP6: Calculate Rh using Eq. 10.6
        Ucan=1/(hcan*rinsWithIns);
        Rhc=1/(2*pi)*(Ui+Upi+Upw+Upo+Uins+Ucan+Up+Ucem+Uea+Uf);
    end
    Rh=Rhc;
    % HEAT LOSS PER UNIT LENGTH
    Qls=(TbWithIns-TAWithIns)/Rh;
    % TOTAL HEAT LOSS
    Ql=Qls*PipeLengthWithIns;
    CollectDatasInjIns=[CollectDatasInjIns;[Rh Qls Ql]];
    InjLengthplot          =(1:PipeLengthWithIns)';
    PlotQl                 =(Qls).*InjLengthplot;
    figure(1)
    plot(PlotQl, InjLengthplot,'color',colors(i,:),'Linewidth',3)
    hold on
    grid on
    set(gca,'XAxisLocation','top','YDir','rev')
    xlabel(['Cumulative Heat Losses (in BTU) for ' ...
num2str(PipeLengthWithIns) ' ft'],'Fontname', 'Calibri',...
'FontSize', 16)
```

```
    ylabel('Depth (ft)')
    LambdaValStr = sprintf('%0.3G' , lamda_insWithIns(i)./24);
    labels {i} = ['\lambda = ' num2str(LambdaValStr)];
    legend(labels,2,'Location', 'NE')
    set(gcf,'Units','normalized');
    set(gcf,'OuterPosition',[0 0 1 1]);
end
```

***Code block: InjWellwithoutIns.m***:

```
%% Example 10.2 Calculations of Heat Losses from Wellbore
% 3.5 in. tubing set on a packer in 9 5/8 in, 53.5 lbm/ft N-80 casing
% The annulus contatins a stagnant gas at zero gauge pressure at wellhead
% and casing is cemented to surface in a 12-in hole.
% We are looking for the solution at steady state conditions
% written 2009, modified date 2011, May 9th
% Fidan, S.,
%%
clc;clear all;close all;
roWithoutIns                = 0.1458;          % ft
rciWithoutIns               = 0.3556;          % ft
rcoWithoutIns               = 0.4010;          % ft
rwWithoutIns                = 0.5000;          % ft
rEaWithoutIns               = 0;               % ft
aEWithoutIns                = 0.96;
einsWithoutIns              = 0.9;
eciWithoutIns               = 0.9;
lamda_EWithoutIns           = 24;              % Btu/ft-hr-F
lamda_cemWithoutIns         = 12;              % Btu/ft-hr-F
InjTimeWithoutIns           = 21;              % days
TAWithoutIns                = 100;             % F
TbWithoutIns                = 600;             % F
PipeLengthWithoutIns        = 1000;            % ft
```

```
lamdaPipe=600;

% Step 1 assign random value for dqdz
dqdz=randperm(100);
dqdz=dqdz(1);
% calculate the old T_ins from eq. 16
% Step 2: Tci = Geothermal Temperature
Tci_old=TAWithoutIns;
% Step 3:h_r from eq.15, hc from eq.9 and
% Uto from eq.8 and f(t) from Ramey

% h_r from eq. 15
h_r=hr(Tins_old,Tci_old,epsins,epsci,rci,rins,Boltzman);
% hc from eq. 9
Tanulus=Tan(Tins_old,Tci_old);
Beta_Gr=BetaGr(Tanulus);

visAn=viscosityAn(Tanulus);
den=densityAn(Tanulus);
Gr1=Gr(Tins_old,Tci_old,visAn,Beta_Gr,den,rci,rins,g);

kha=kha1(Tanulus);
Pr1=Pr();%kha,visAn
khc=khc1(Gr1,Pr1,kha);
h_c=hc(khc,rci,rins);
% from eq. 8
Uto=UtoCal(h_c,h_r,rh,rins,rco,rto,kins,kcement);
% f(t) from Ramey and Willhite
ftD = FTIME(Uto,q1,t,rh,ke);
% step 4: calculate the old Th
Th_old=(rto*Uto*ftD*Tf+kcement*Tgeo)/(rto*Uto*ftD+kcement);
% step 5: calculate the new Tci
```

```
Tci_new=Th_old+((rto*Uto*log(rh/rco))/(kcement))*(Tto-Th_old);
iter=0;
if abs(Tci_new-Tci_old)<=1
    Tci_new1=Tci_new;
    Tci_new=Tci_new1;
else
    while abs(Tci_new-Tci_old)>=1e-4
        iter=iter+1;
        Tci_old=Tci_old+0.7*(abs(Tci_new-Tci_old));

        Part1=Tci_old*kcement;
        Part2=rto*Uto*log(rh/rco)*Tto;
        Part3=kcement;
        Part4=rto*Uto*log(rh/rco);
        Th=(Part1-Part2)/(Part3-Part4);

        dqdz=2*pi*rto*Uto*(Tf-Th);
        Tins_old=Tto-((dqdz*log(rins/rto))/(2*pi*kins));
        % Step 3:h_r from eq.15, hc from eq.9 and Uto
        %from eq.8 and f(t) from Ramey
        % h_r from eq. 15
        h_r=hr(Tins_old,Tci_old,epsins,epsci,rci,rins,Boltzman);
        % hc from eq. 9
        Tanulus=Tan(Tins_old,Tci_old);
        Beta_Gr=BetaGr(Tanulus);
        visAn=viscosityAn(Tanulus);
        den=densityAn(Tanulus);
        Gr1=Gr(Tins_old,Tci_old,visAn,Beta_Gr,den,rci,rins,g);
        kha=kha1(Tanulus);
        khc=khc1(Gr1,Pr1,kha);
        h_c=hc(khc,rci,rins);
        % from eq. 8
```

```
        Uto=UtoCal(h_c,h_r,rh,rins,rco,rto,kins,kcement);
        % f(t) from Ramey and Willhite
        ftD = FTIME(Uto,q1,t,rh,ke);
        % step 4: calculate the old Th
        Th_old=(rto*Uto*ftD*Tf+kcement*Tgeo)/(rto*Uto*ftD+kcement);
        % step 5: calculate the new Tci
        Tci_new=Th_old+((rto*Uto*log(rh/rco))/(kcement))*(Tto-Th_old);
    end
end
```

## B.4 Table 14 from Prats [41]

The following are the *MatLab* codes for our heat loss calculation for surface lines without insulation radiation and free convection number interpolated values using Table B.14 from Prats[41].

```
function ht=htTable14(Temp,Diameter)
% Fidan, S.
% Interpolation for the htc
% Prats pg234 table B.14

Table14=[50.9 59.5 66.2 74.4 81.8 90 107 127 149 174 202 234 269 307 352
   48.7 57.1 63.6 71.5 79 86.9 104 124 146 171 198 230 265 304 348
   46.3 54.5 60.5 68.4 75.4 83.3 100 120 141 166 194 225 260 299 343
   44.2 51.8 57.8 65.3 72.2 79.9 96.5 116 137 162 189 221 256 294 338
   42.2 49.4 70.1 62.4 69.4 76.8 93.1 112 134 158 186 217 252 290 334
   41.0 48.2 53.8 61.0 67.7 75.1 91.9 111 132 156 184 215 250 289 332
   39.4 46.3 51.6 58.8 65.3 72.7 88.8 108 129 153 180 212 247 286 329];

DimPipeIns=[0.5 1 2 4 8 12 24];

SurfTemp=[130 180 230 280 330 380 480 580 680 780 880 980 1080 1180 1280];

ht=interp2(SurfTemp,DimPipeIns,Table14,Temp,Diameter);

return
```

## B.5 f(tD) calculation also known as Ramey[42]

The following are the *MatLab* codes for our heat loss calculation for sea floor to reservoir with/without insulation interpolated values using Table 10.1 from Prats[41].

```
function f=ft(r,tD)
% Fidan, S.,
% Interpolation of the value of f(t) in unsteady conduction

A=[.311 .312 .313 .313 .314 .316 .318 .323 .330 .345 .373 .396 .417 .433 .438 .445
   .421 .422 .423 .423 .424 .427 .430 .439 .452 .473 .511 .538 .568 .572 .578 .588
   .614 .615 .616 .617 .619 .623 .629 .644 .666 .698 .745 .772 .790 .802 .806 .811
   .800 .801 .802 .803 .806 .811 .820 .842 .872 .910 .958 .984 1.00 1.01 1.01 1.02
   1.00 1.01 1.02 1.02 1.03 1.04 1.05 1.08 1.11 1.15 1.20 1.22 1.24 1.24 1.24 1.25
   1.34 1.35 1.36 1.37 1.37 1.38 1.40 1.44 1.48 1.52 1.56 1.57 1.58 1.59 1.59 1.59
   1.63 1.64 1.65 1.66 1.66 1.67 1.69 1.73 1.77 1.81 1.84 1.86 1.86 1.87 1.87 1.88
   1.94 1.95 1.96 1.97 1.97 1.99 2.00 2.05 2.09 2.12 2.15 2.16 2.16 2.17 2.17 2.17
   2.37 2.38 2.39 2.39 2.40 2.42 2.44 2.48 2.51 2.54 2.56 2.57 2.57 2.57 2.58 2.58
   2.71 2.72 2.73 2.73 2.74 2.75 2.77 2.81 2.84 2.86 2.88 2.89 2.89 2.89 2.89 2.90];

t=[.1 .2 .5 1 2 5 10 20 50 100];
R=[1000 500 100 50 20 10 5 2 1 .5 .2 .1 .05 .02 .01 0];

if tD>100
    f=0.5*log(tD)+0.403;
else
    f=interp2(R,t,A,r,tD);
end

return
```

# Appendix C

# Results for Different Insulation Materials

$Using White Aerogel \lambda_{WA} = 0.0081 BTU/(ft - hr - ^o F)$

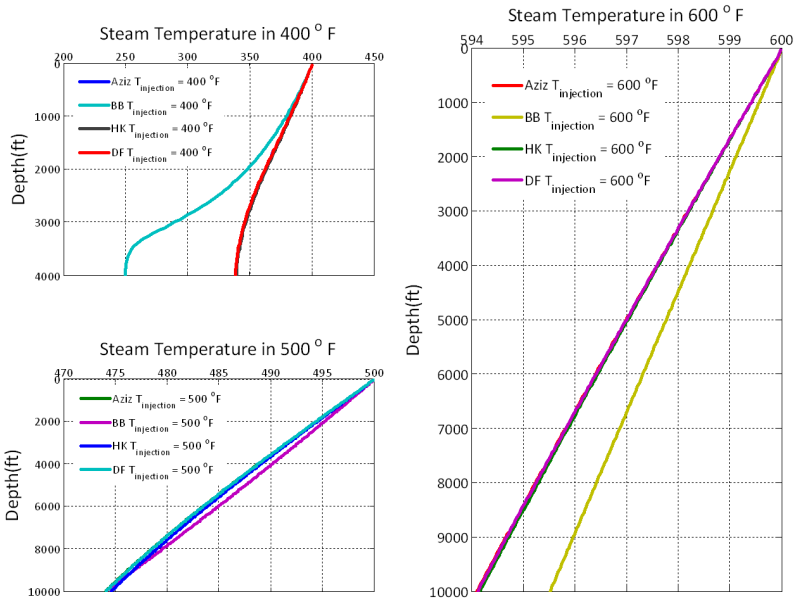


Figure C.1: Steam temperature distribution for different injection temperature vs depth (ft) , 1 year, $T_m = 122\ ^oF$ and injection rate 4850 lbm/hr with white aerogel.

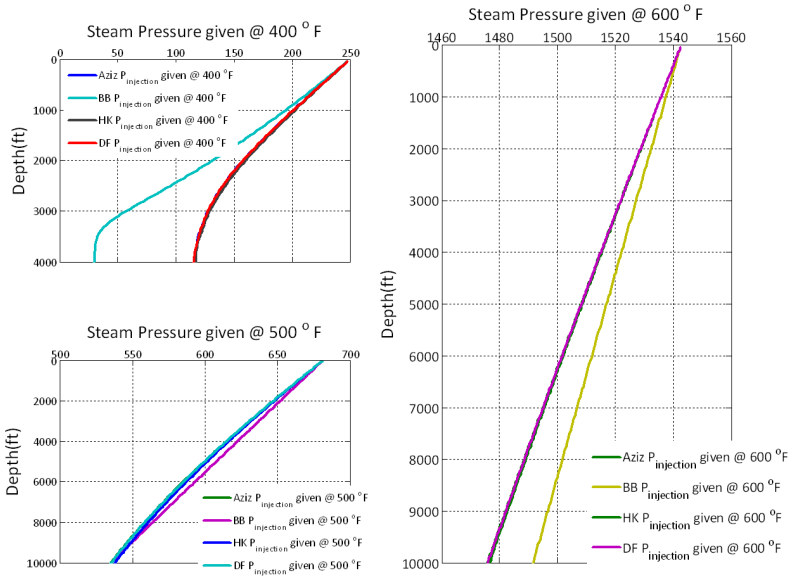


Figure C.2: Steam pressure distribution for different injection temperature vs depth (ft), 1 year, $T_m = 122\ ^oF$ and injection rate 4850 lbm/hr with white aerogel.

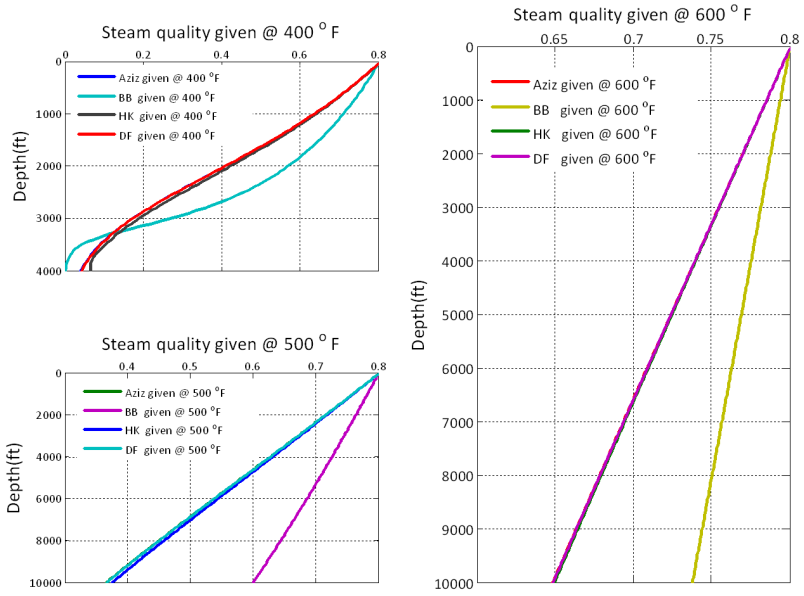


Figure C.3: Steam quality distribution for different injection temperature vs depth (ft), 1 year, $T_m = 122\ ^oF$ and injection rate 4850 lbm/hr with white aerogel.

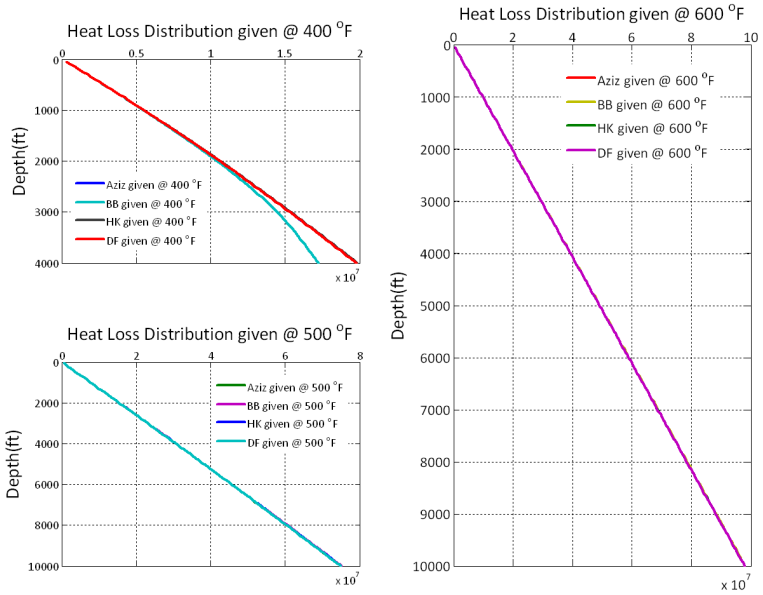


Figure C.4: Heat loss distribution for different injection temperature vs depth (ft), 1 year, $T_m = 122\ ^oF$ and injection rate 4850 lbm/hr with white aerogel.

$$Using Fiberglass \lambda_{FG} = 0.0162 BTU/(ft - hr - ^o F)$$

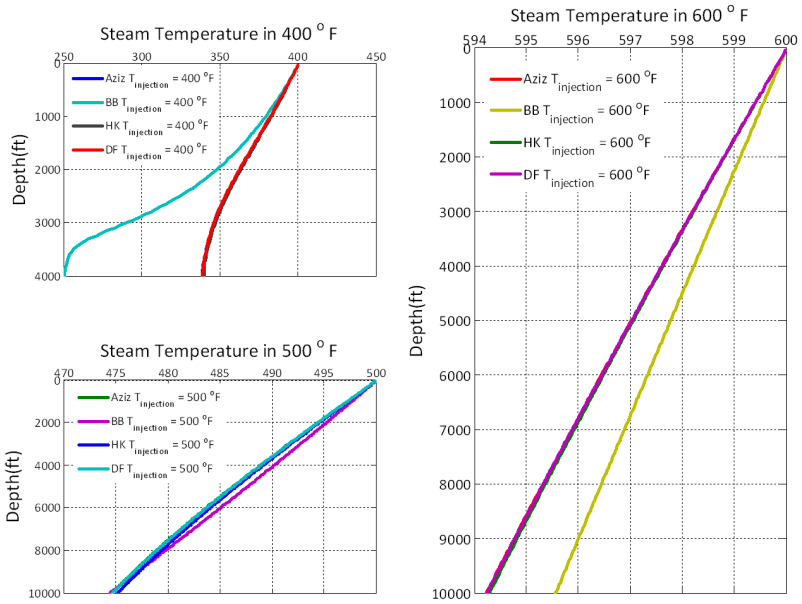


Figure C.5: Steam temperature distribution for different injection temperature vs depth (ft), 1 year, $T_m = 122\ ^oF$ and injection rate 4850 lbm/hr with fiber glass.

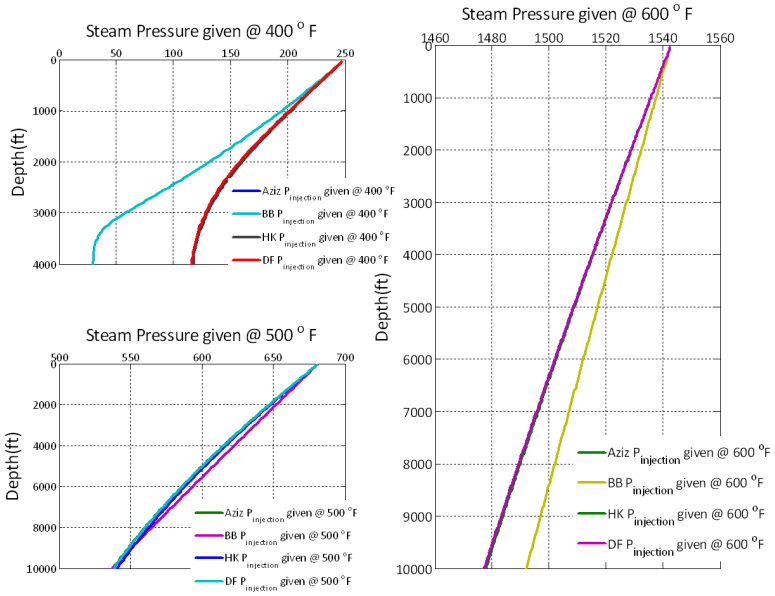


Figure C.6: Steam pressure distribution for different injection temperature vs depth (ft), 1 year, $T_m = 122\ ^oF$ and injection rate 4850 lbm/hr with fiber glass.

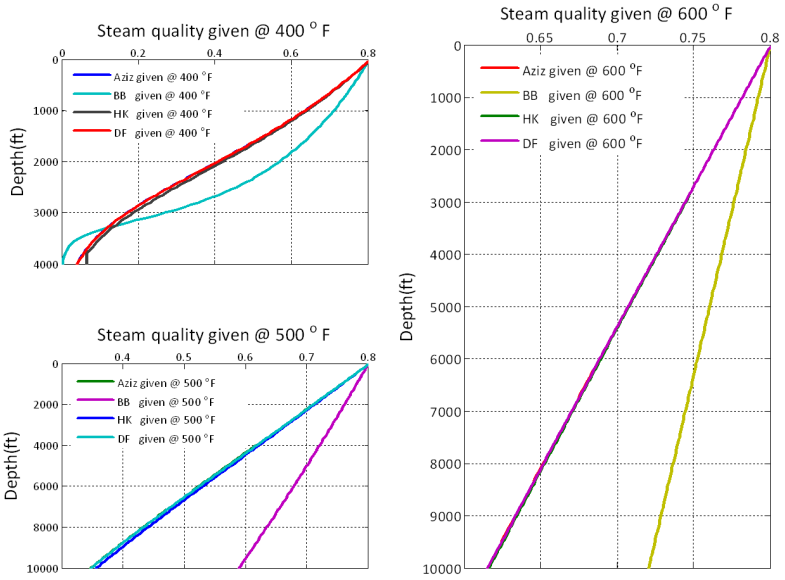


Figure C.7: Steam quality distribution for different injection temperature vs depth (ft), 1 year, $T_m = 122\ ^oF$ and injection rate 4850 lbm/hr with fiber glass.

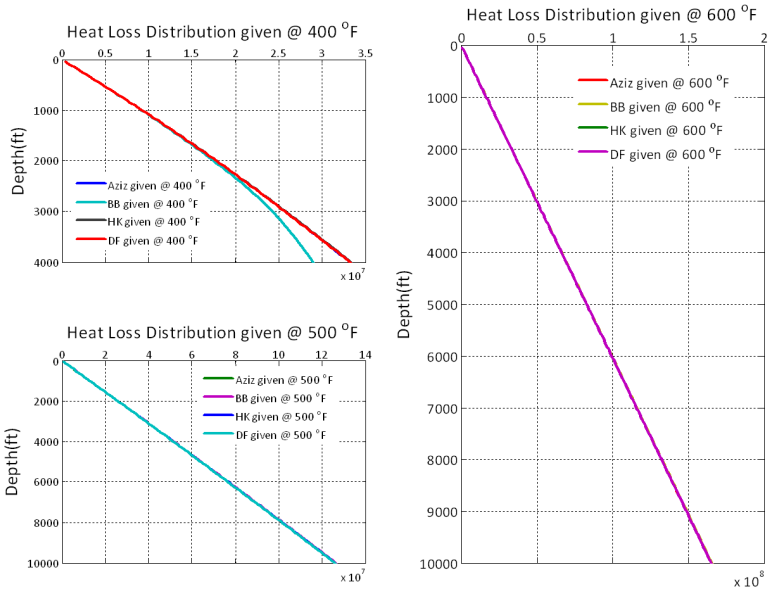


Figure C.8: Heat loss distribution for different injection temperature vs depth (ft), 1 year, $T_m = 122\ ^oF$ and injection rate 4850 lbm/hr with fiber glass.

$$UsingCarbonFiber \lambda_{CF} = 0.0208 BTU/(ft - hr -^o F)$$

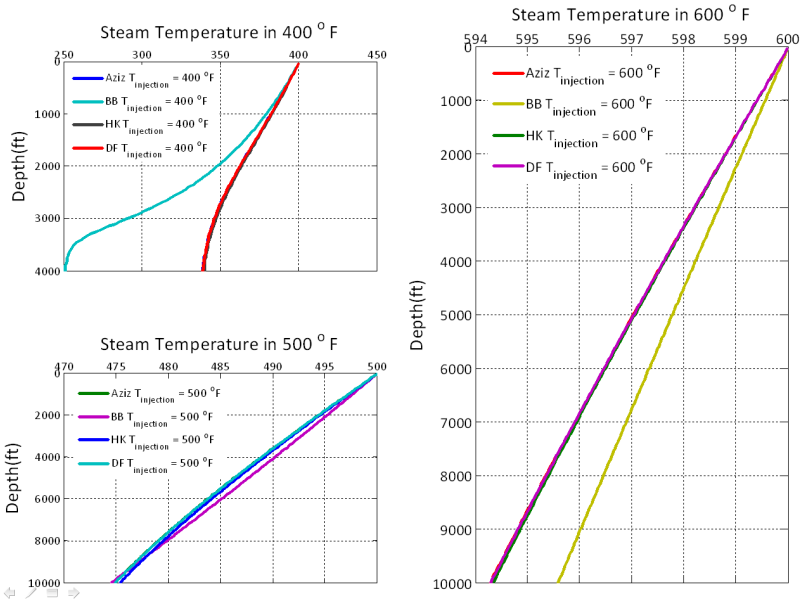


Figure C.9: Steam temperature distribution for different injection temperature vs depth (ft), 1 year, $T_m = 122\ ^oF$ and injection rate 4850 lbm/hr with carbon fiber.

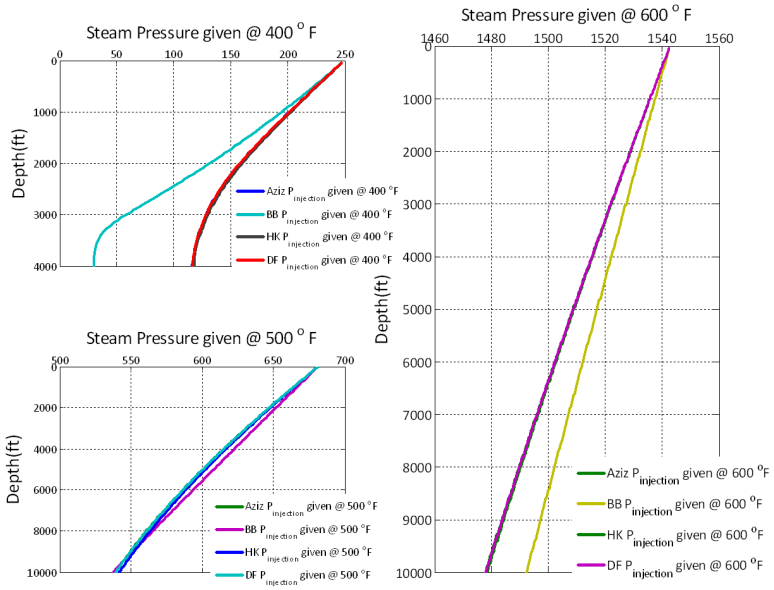


Figure C.10: Steam pressure distribution for different injection temperature vs depth (ft), 1 year, $T_m = 122\ ^oF$ and injection rate 4850 lbm/hr with carbon fiber.

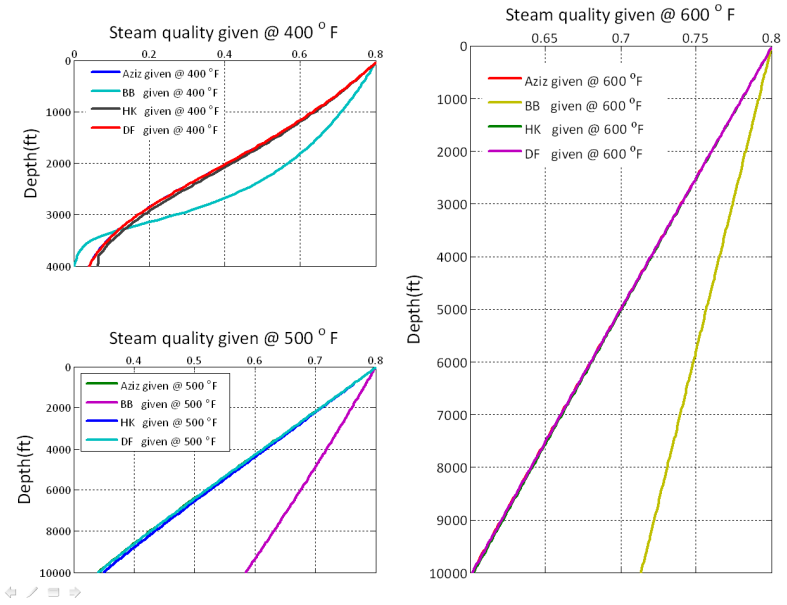


Figure C.11: Steam quality distribution for different injection temperature vs depth (ft), 1 year, $T_m = 122\ ^oF$ and injection rate 4850 lbm/hr with carbon fiber.

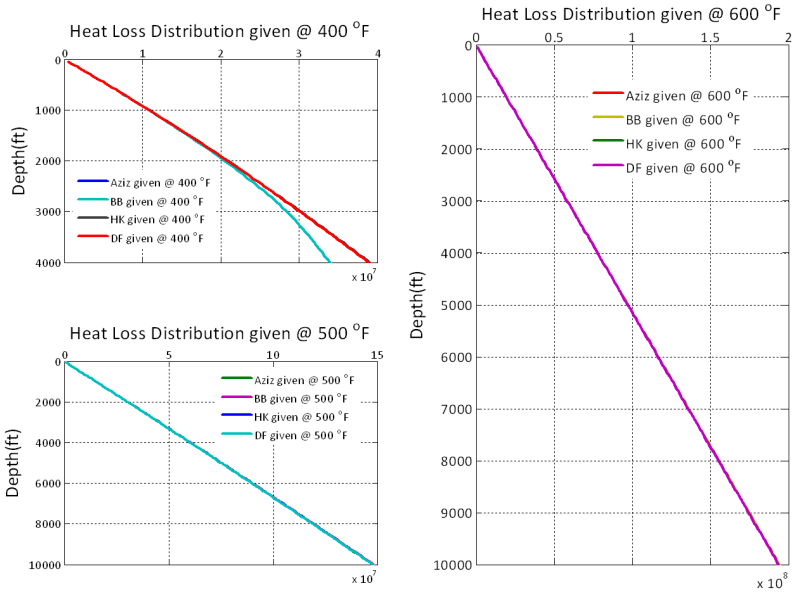


Figure C.12: Heat loss distribution for different injection temperature vs depth (ft), 1 year, $T_m = 122\ ^oF$ and injection rate 4850 lbm/hr with carbon fiber.

$$Using Thermolastic Insulation \lambda_{TI} = 0.0237 BTU/(ft - hr -^o F)$$

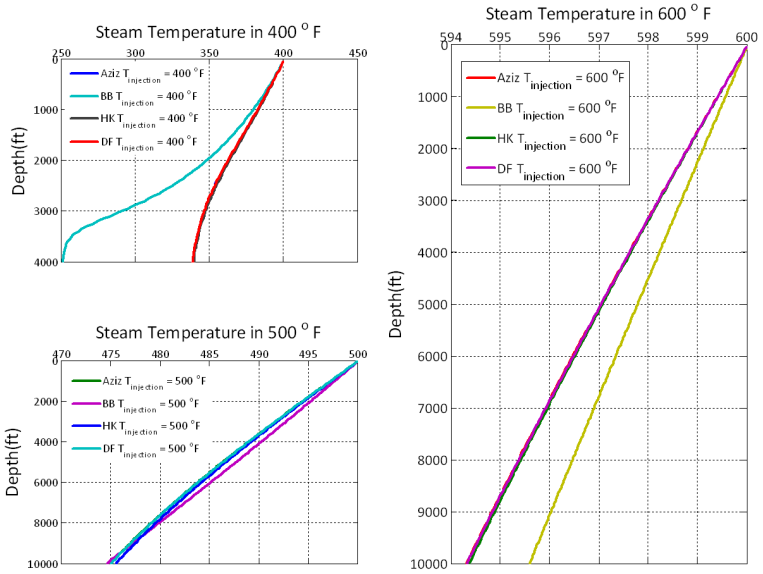


Figure C.13: Steam temperature distribution for different injection temperature vs depth (ft), 1 year, $T_m = 122\ ^oF$ and injection rate 4850 lbm/hr with thermolastic insulation.

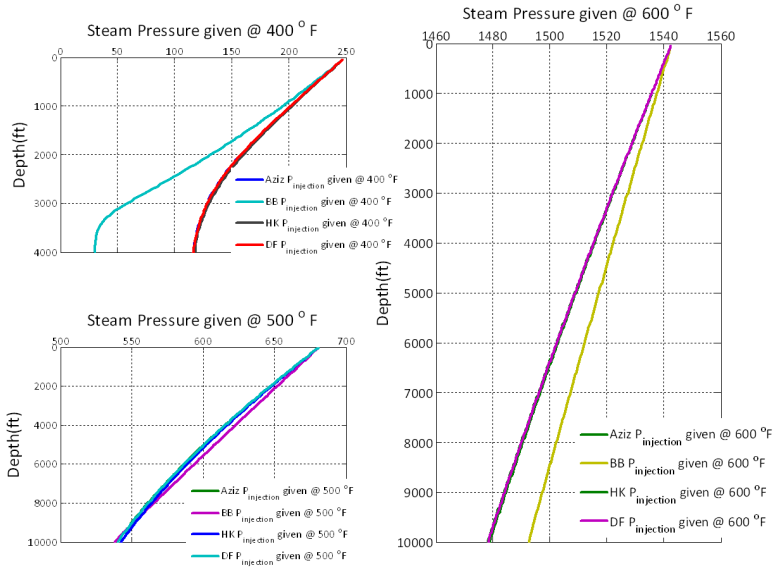


Figure C.14: Steam pressure distribution for different injection temperature vs depth (ft), 1 year, $T_m = 122\ ^oF$ and injection rate 4850 lbm/hr with thermolastic insulation.

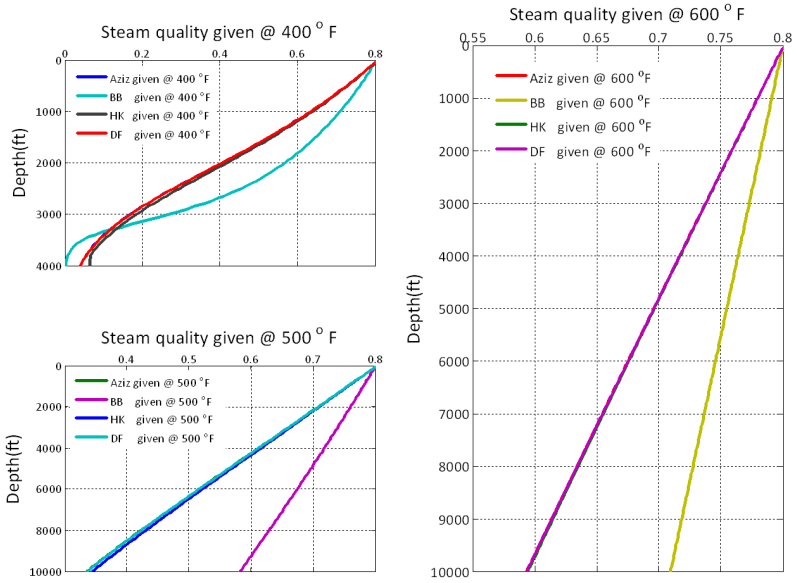


Figure C.15: Steam quality distribution for different injection temperature vs depth (ft), 1 year, $T_m = 122\ ^oF$ and injection rate 4850 lbm/hr with thermolastic insulation.

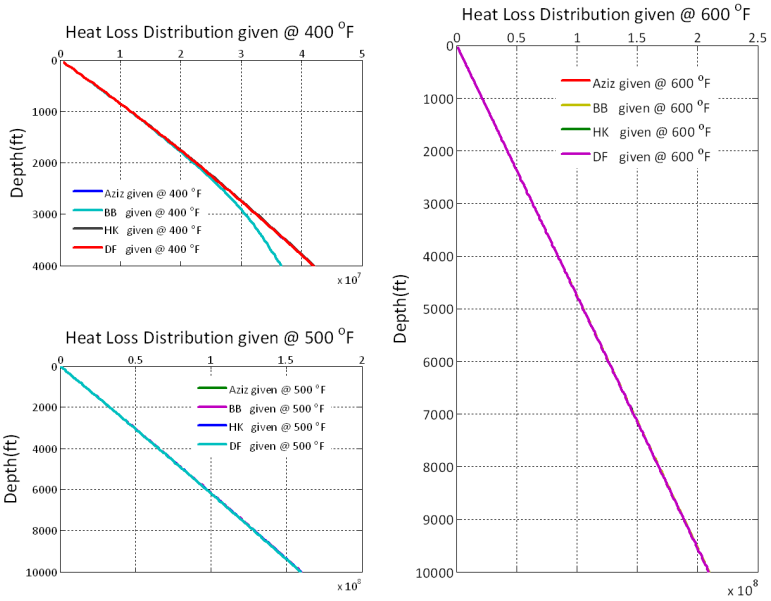


Figure C.16: Heat loss distribution for different injection temperature vs depth (ft), 1 year, $T_m = 122\ ^oF$ and injection rate 4850 lbm/hr with thermolastic insulation.

$$UsingCalciumSilicateInsulation\lambda_{CaSil} = 0.04BTU/(ft - hr - ^o\ F)$$

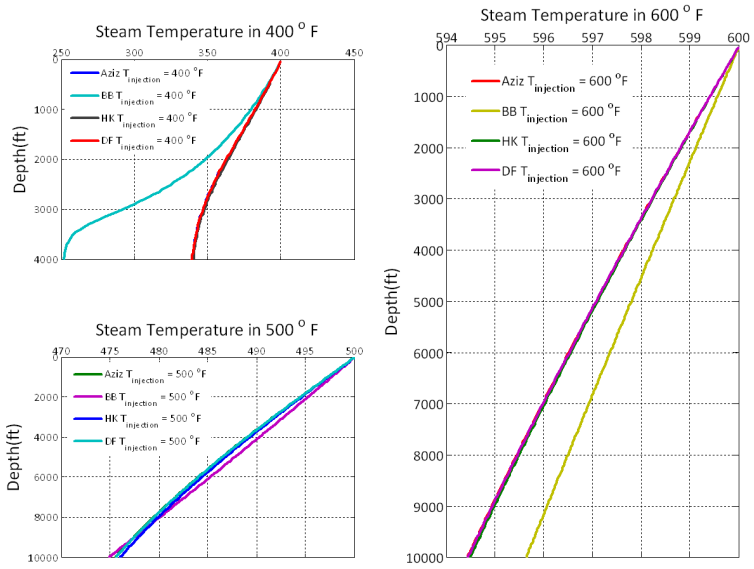


Figure C.17: Steam temperature distribution for different injection temperature vs depth (ft), 1 year, $T_m = 122\ ^oF$ and injection rate 4850 lbm/hr with calcium silicate.

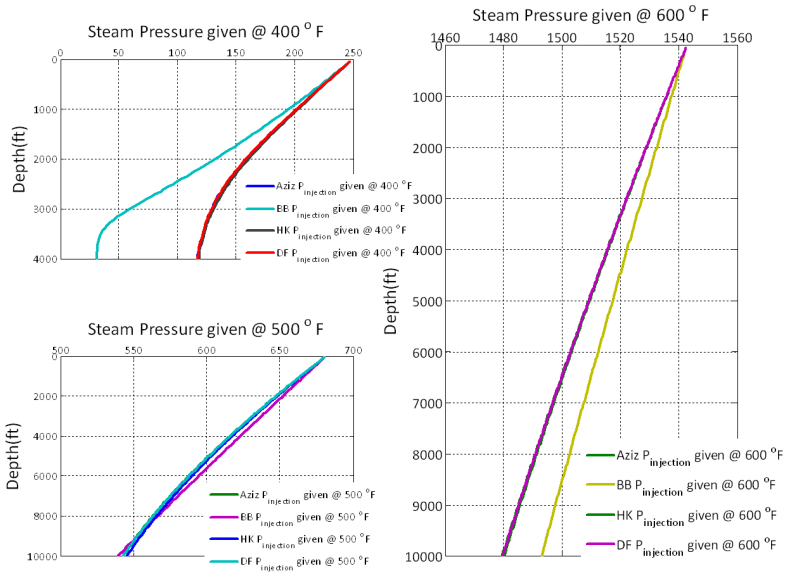


Figure C.18: Steam pressure distribution for different injection temperature vs depth (ft), 1 year, $T_m = 122\ ^oF$ and injection rate 4850 lbm/hr with calcium silicate.

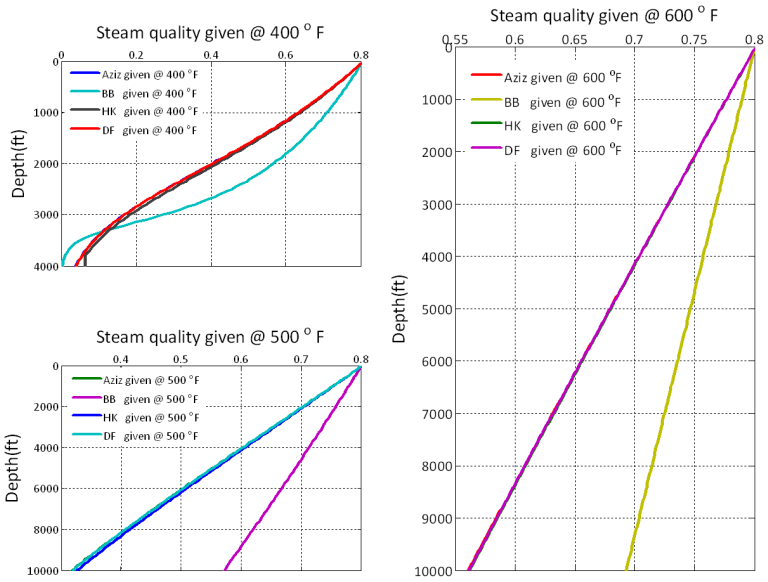


Figure C.19: Steam quality distribution for different injection temperature vs depth (ft), 1 year, $T_m = 122\ ^oF$ and injection rate 4850 lbm/hr with calcium silicate.

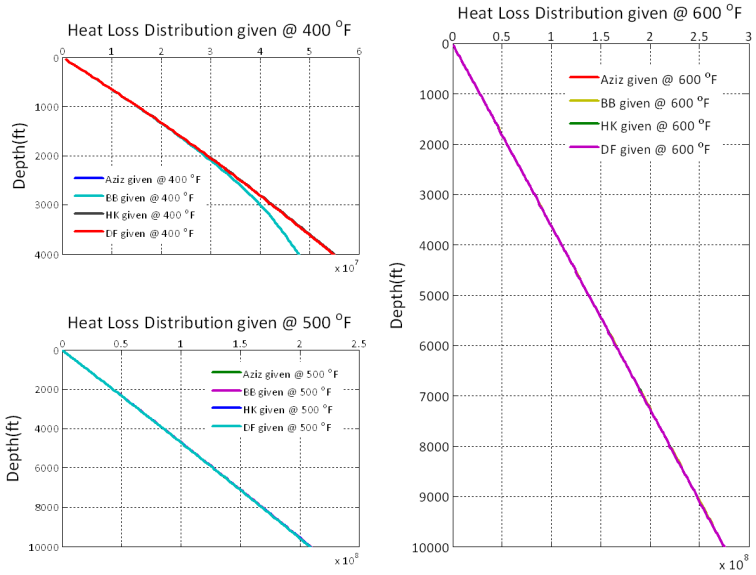


Figure C.20: Heat loss distribution for different injection temperature vs depth (ft), 1 year, $T_m = 122\ ^oF$ and injection rate 4850 lbm/hr with calcium silicate.

$$UsingWhiteAerogel\lambda_{WA} = 0.0081BTU/(ft - hr - ^o F)$$

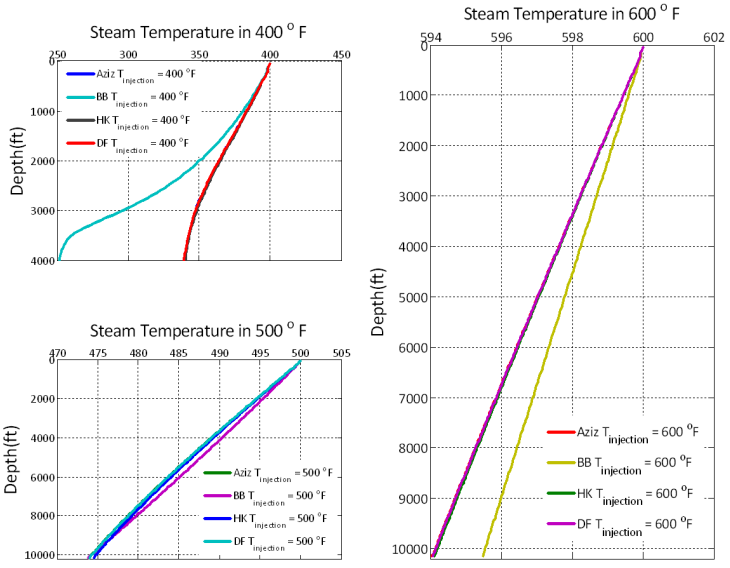


Figure C.21: Steam temperature distribution for different injection temperature vs depth (ft), 1 year, $T_m = 122\ ^oF$ and injection rate 4850 lbm/hr with white aerogel.

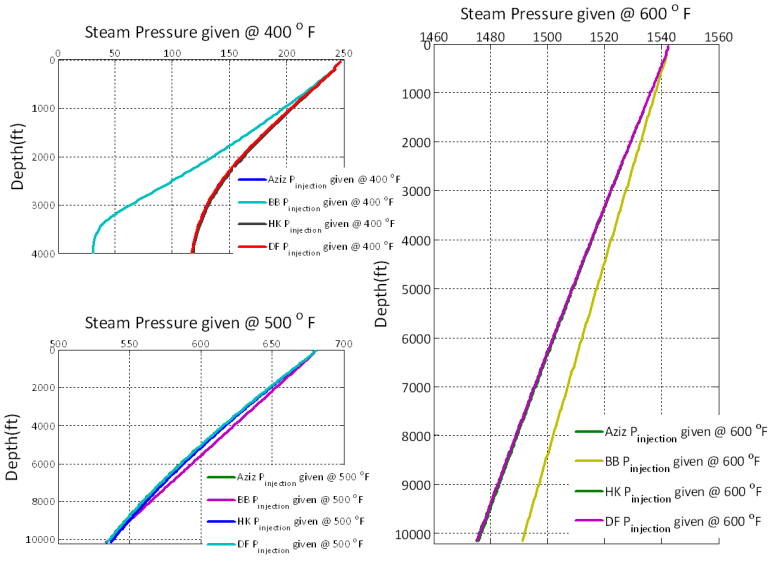


Figure C.22: Steam pressure distribution for different injection temperature vs depth (ft), 1 year, $T_m = 122\ ^oF$ and injection rate 4850 lbm/hr with white aerogel.

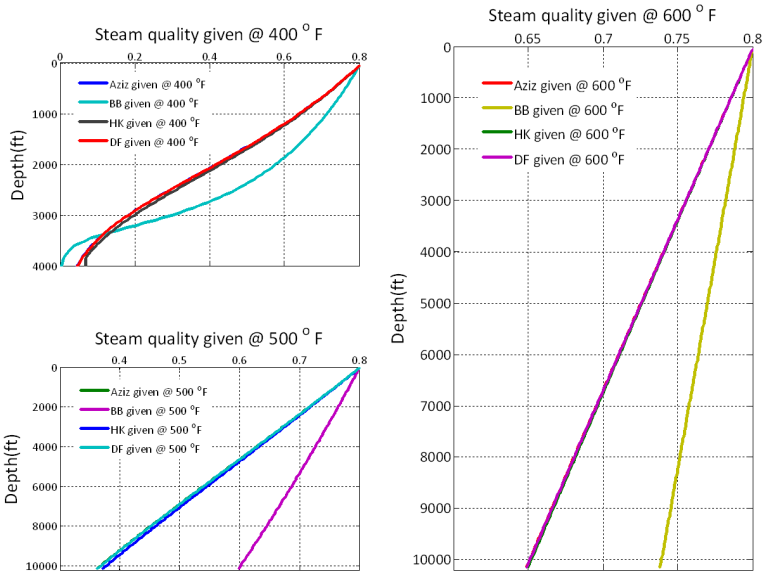


Figure C.23: Steam quality distribution for different injection temperature vs depth (ft), 1 year, $T_m = 122\ ^oF$ and injection rate 4850 lbm/hr with white aerogel.

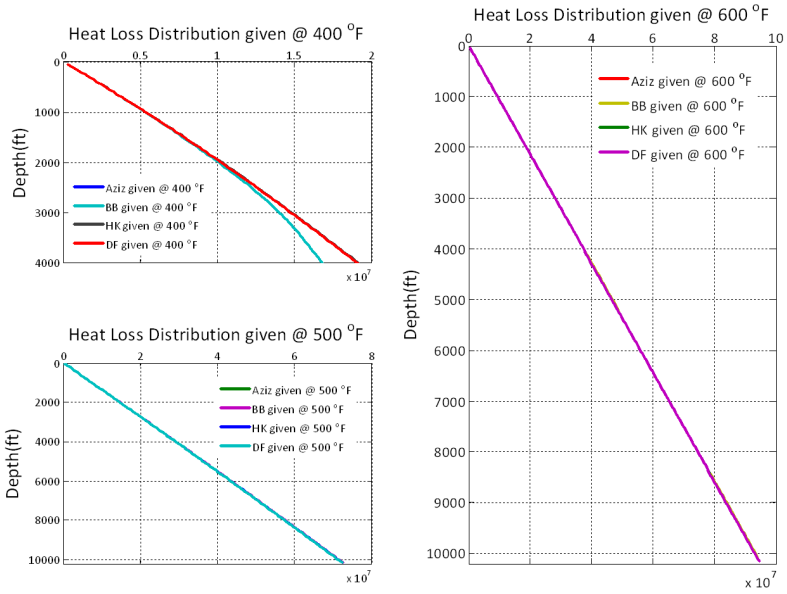


Figure C.24: Heat loss distribution for different injection temperature vs depth (ft), 1 year, $T_m = 122\ ^oF$ and injection rate 4850 lbm/hr with white aerogel.

$$Using Fiberglass \lambda_{FG} = 0.0162 BTU/(ft - hr - ^o F)$$

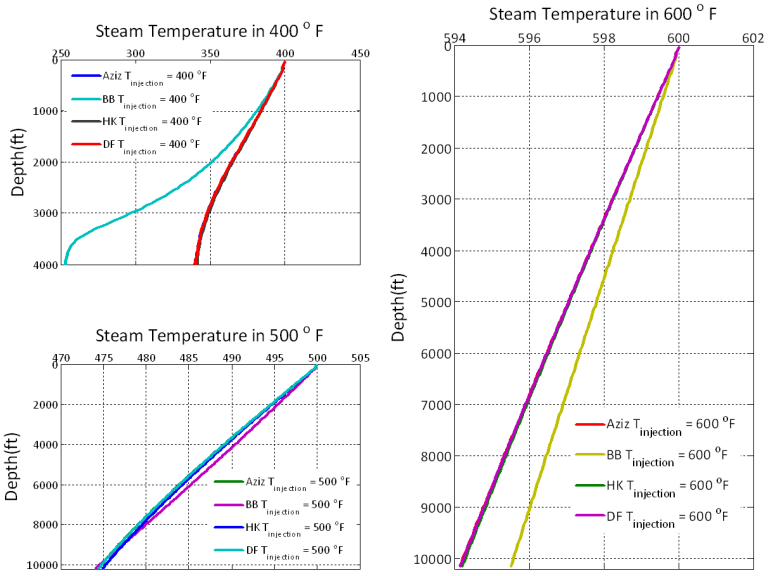


Figure C.25: Steam temperature distribution for different injection temperature vs depth (ft), 1 year, $T_m = 122\ ^oF$ and injection rate 4850 lbm/hr with fiber glass.

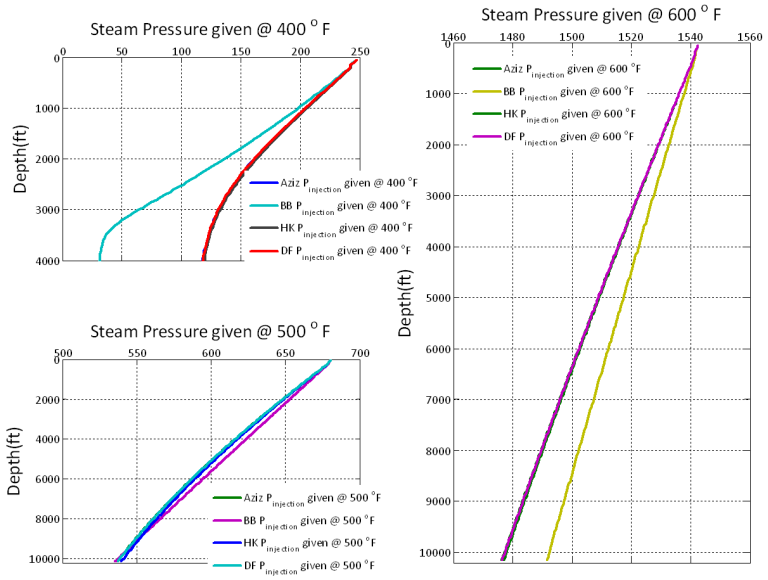


Figure C.26: Steam pressure distribution for different injection temperature vs depth (ft), 1 year, $T_m = 122\ ^oF$ and injection rate 4850 lbm/hr with fiber glass.

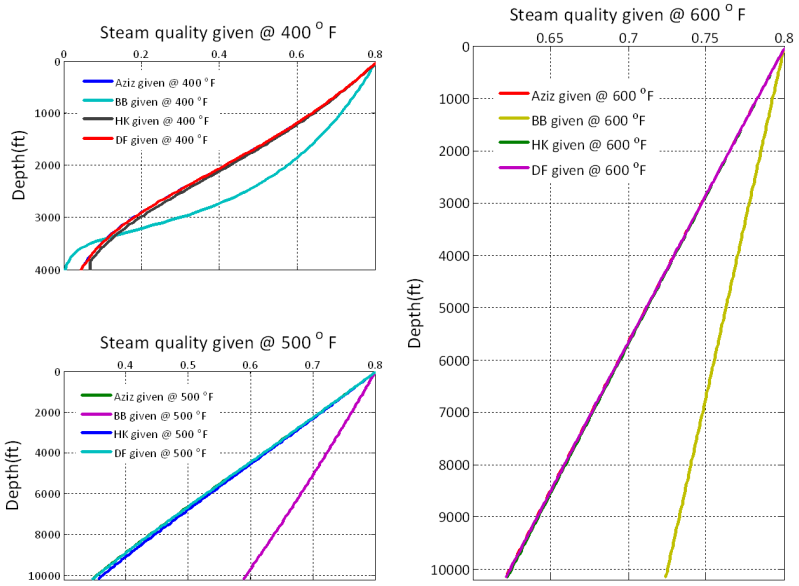


Figure C.27: Steam quality distribution for different injection temperature vs depth (ft), 1 year, $T_m = 122\ ^oF$ and injection rate 4850 lbm/hr with fiber glass.

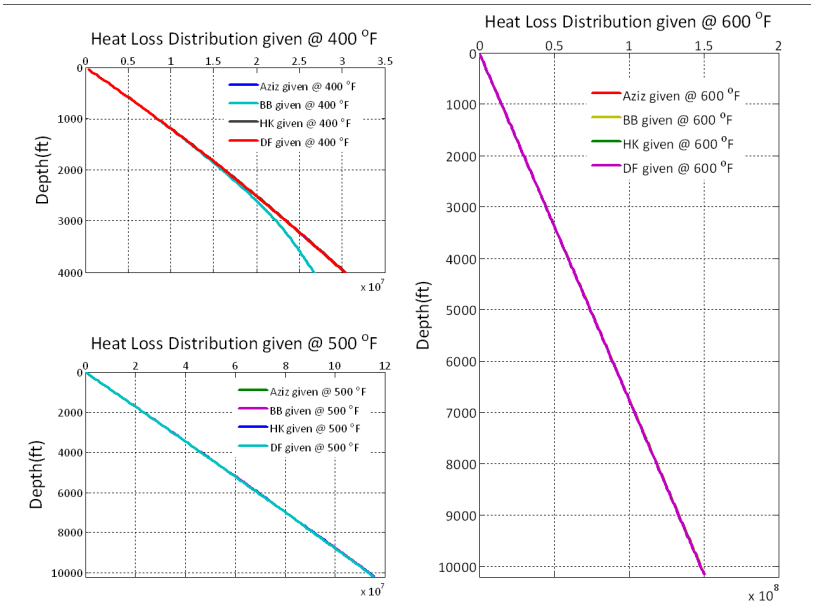


Figure C.28: Heat loss distribution for different injection temperature vs depth (ft), 1 year, $T_m = 122\ ^oF$ and injection rate 4850 lbm/hr with fiber glass.

$$UsingCarbonFiber\lambda_{CF} = 0.0208BTU/(ft - hr - ^o F)$$

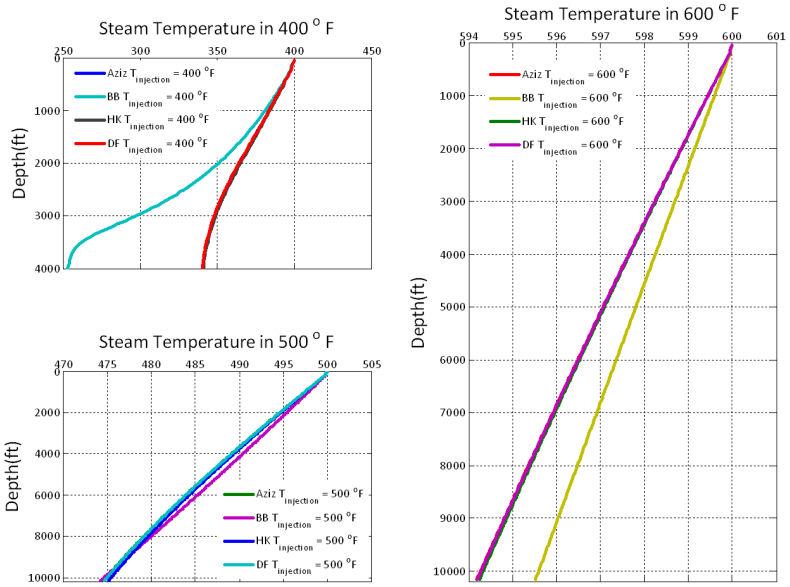


Figure C.29: Steam temperature distribution for different injection temperature vs depth (ft), 1 year, $T_m = 122\ ^oF$ and injection rate 4850 lbm/hr with carbon fiber.

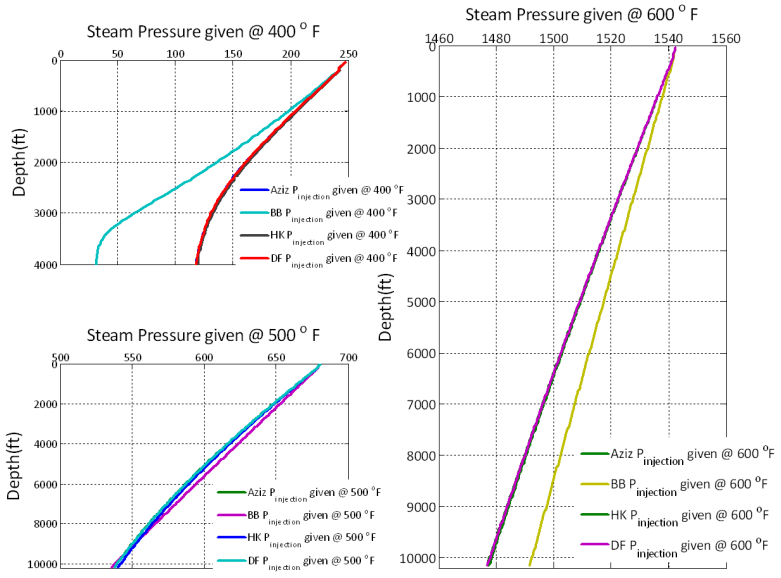


Figure C.30: Steam pressure distribution for different injection temperature vs depth (ft), 1 year, $T_m = 122\ ^oF$ and injection rate 4850 lbm/hr with carbon fiber.

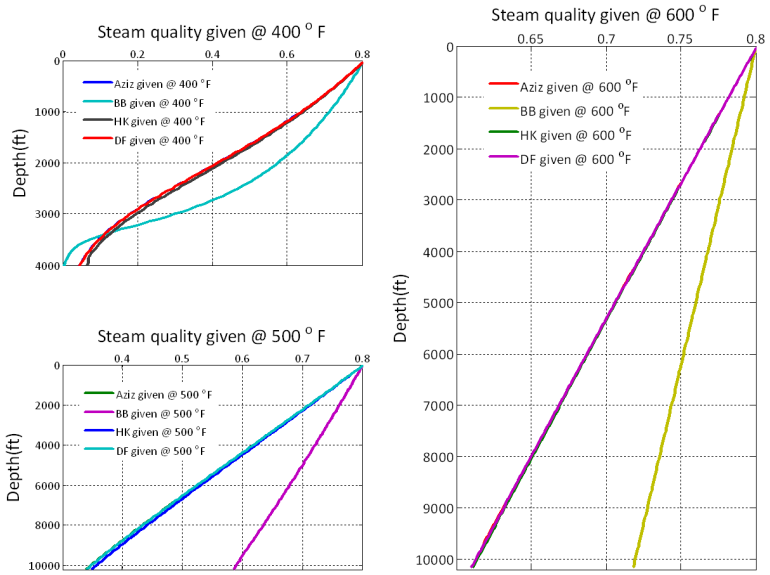


Figure C.31: Steam quality distribution for different injection temperature vs depth (ft), 1 year, $T_m = 122\ ^oF$ and injection rate 4850 lbm/hr with carbon fiber.

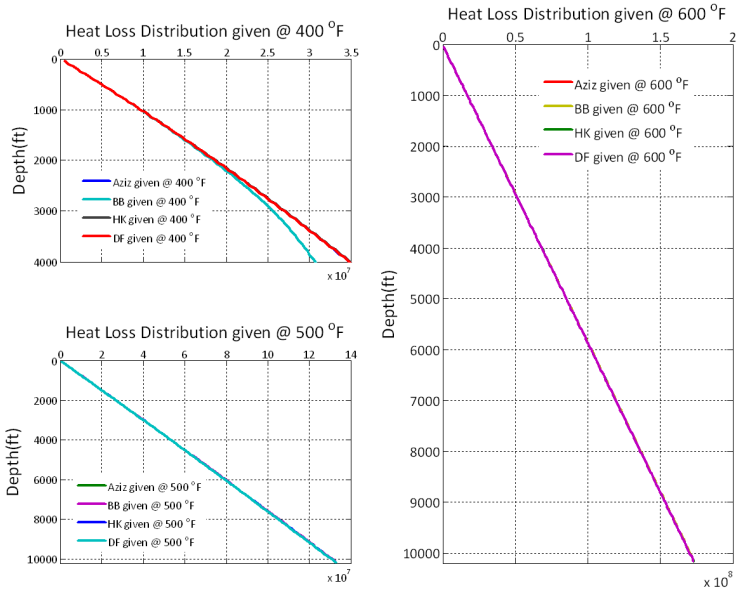


Figure C.32: Heat loss distribution for different injection temperature vs depth (ft), 1 year, $T_m = 122\ ^oF$ and injection rate 4850 lbm/hr with carbon fiber.

$$UsingThermolasticInsulation\lambda_{TI} = 0.0237BTU/(ft - hr -^o F)$$

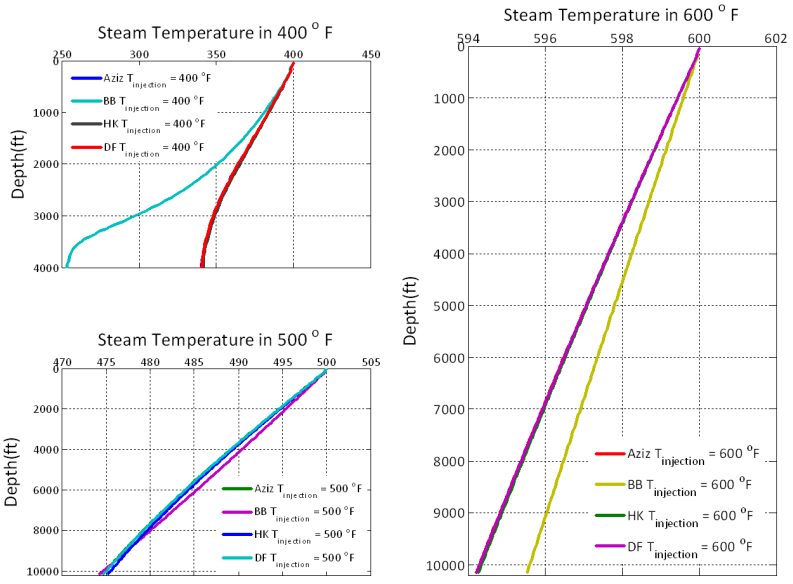


Figure C.33: Steam temperature distribution for different injection temperature vs depth (ft), 1 year, $T_m = 122\ ^oF$ and injection rate 4850 lbm/hr with thermolastic insulation.

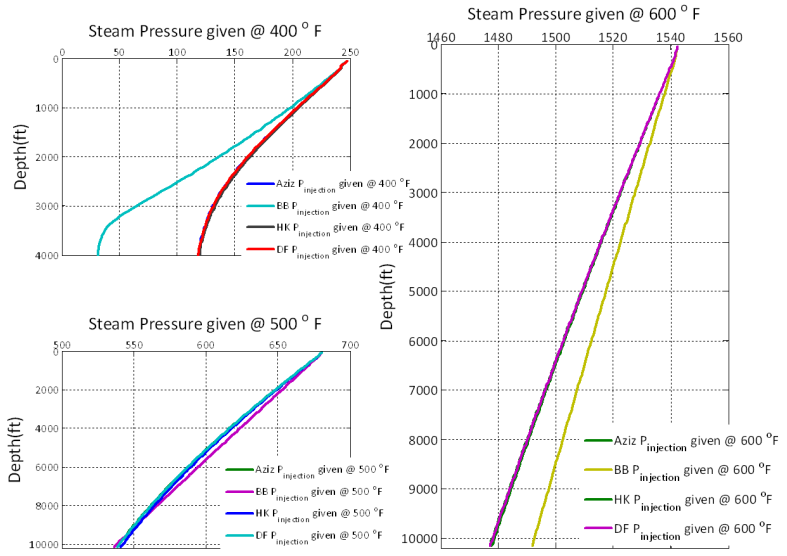


Figure C.34: Steam pressure distribution for different injection temperature vs depth (ft), 1 year, $T_m = 122\ ^oF$ and injection rate 4850 lbm/hr with thermolastic insulation.

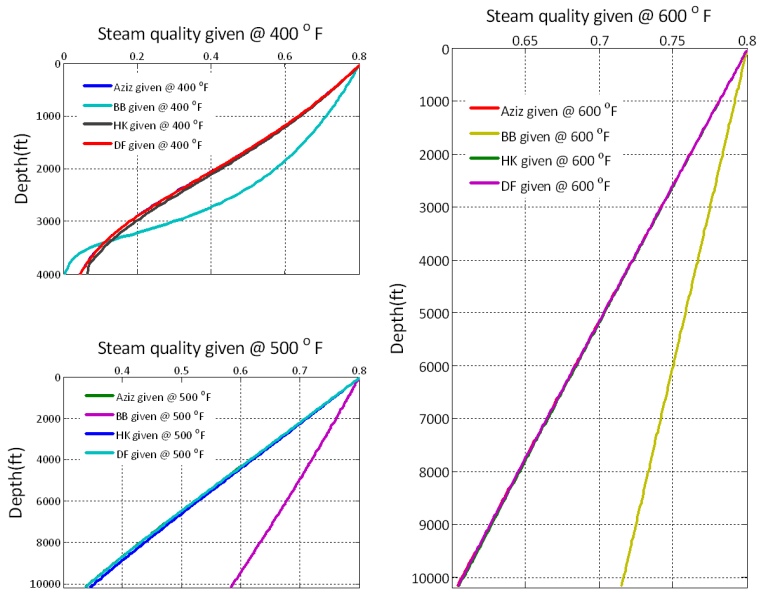


Figure C.35: Steam quality distribution for different injection temperature vs depth (ft), 1 year, $T_m = 122\ ^oF$ and injection rate 4850 lbm/hr with thermolastic insulation.

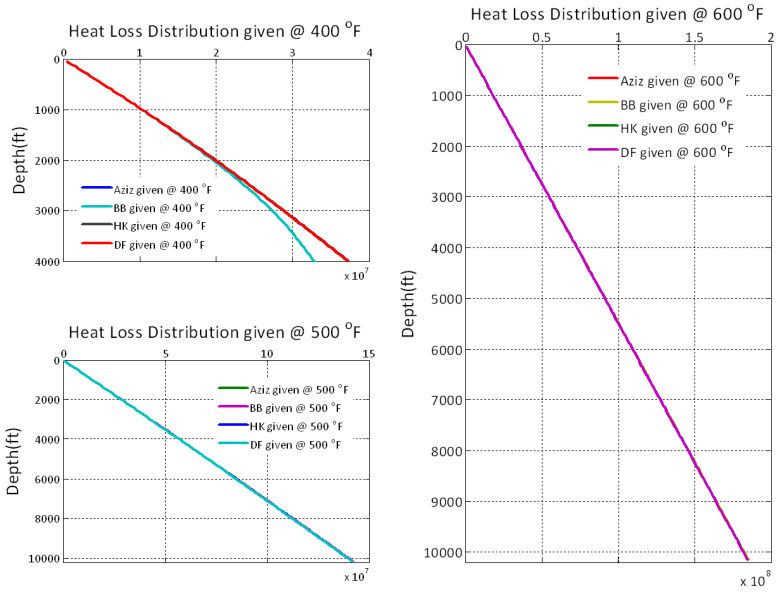


Figure C.36: Heat loss distribution for different injection temperature vs depth (ft), 1 year, $T_m = 122\ ^oF$ and injection rate 4850 lbm/hr with thermolastic insulation.

$$UsingCalciumSilicateInsulation\lambda_{CaSil} = 0.04BTU/(ft - hr - ^o F)$$

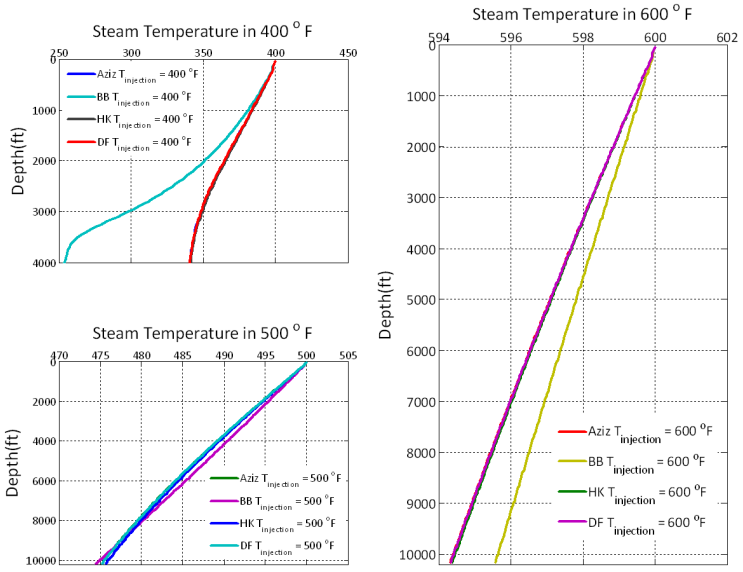


Figure C.37: Steam temperature distribution for different injection temperature vs depth (ft), 1 year, $T_m = 122\ ^oF$ and injection rate 4850 lbm/hr with calcium silicate.

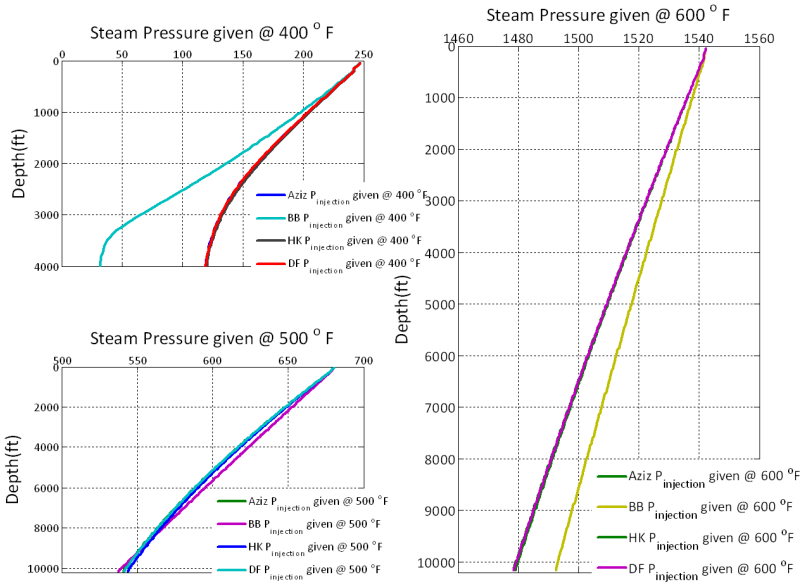


Figure C.38: Steam pressure distribution for different injection temperature vs depth (ft), 1 year, $T_m = 122\ ^oF$ and injection rate 4850 lbm/hr with calcium silicate.

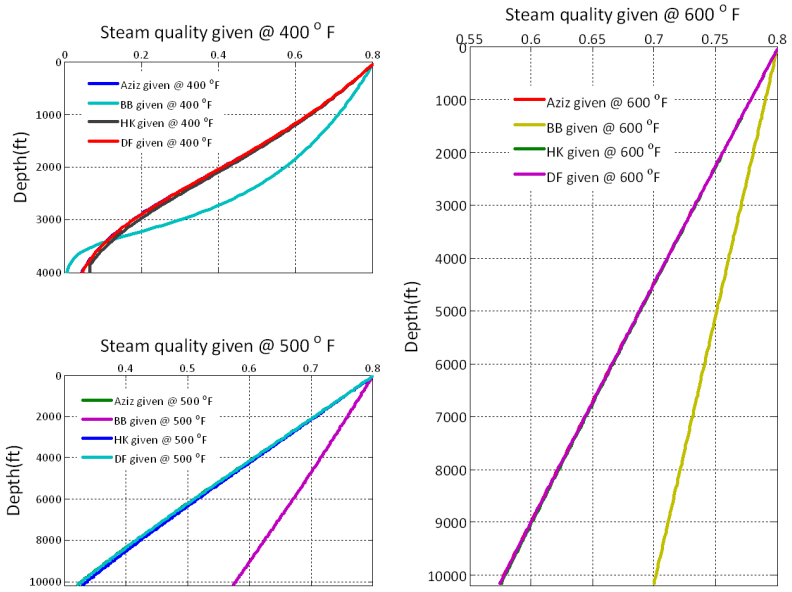


Figure C.39: Steam quality distribution for different injection temperature vs depth (ft), 1 year, $T_m = 122\ ^oF$ and injection rate 4850 lbm/hr with calcium silicate.

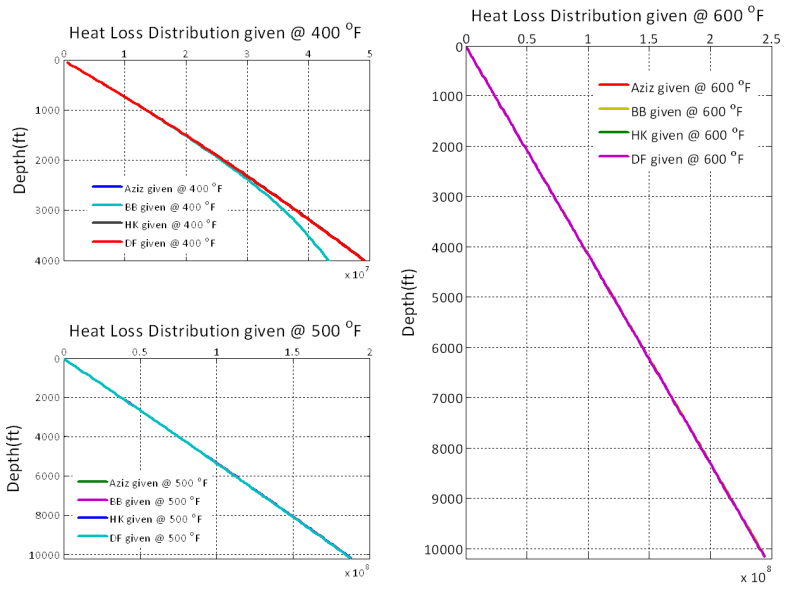


Figure C.40: Heat loss distribution for different injection temperature vs depth (ft), 1 year, $T_m = 122\ ^oF$ and injection rate 4850 lbm/hr with calcium silicate.

# Bibliography


[1] Schematic view of one of the heat transfer mechanism: Convection. http://www.ic.sunysb.edu/Class/phy141md/doku.php?id=phy141:lectures:35.

[2] Schematic view of the offshore platform. http://www.consrv.ca.gov/dog/Picture-a-well/PublishingImages /OFFSHORE-PLATFORM-2.jp.

[3] Two phase flow correlations : *Modified Beggs and Brill two phase correlations*. www.fekete.com/software/rta/media/webhelp/c-te-correlations.htm.

[4] Two phase flow correlations with pressure loss calculation : *Modified Beggs and Brill two phase correlations with Pressure Loss*. www.fekete.com/software/feketeharmony/media/webhelp/HTML-Files/Reference-Material/Calculations-and-Correlations/Pressure-Loss-Calculations.htm.

[5] Abu Al-Soof Nimat B Al-Najjar, Hazim S.H. Alternative flow-pattern maps can improve pressure-drop calculations of the aziz et al. multiphase-flow correlation. *SPE Production Engineering*, 4(3), 1989.

[6] Chen Chou-Ming Ayres, Paul S. and Burton D. Ziels. Vacuum insulated steam injection tubing, united states patent 4512721. http://www.patentgenius.com/patent/4512721.html, 1982.

[7] H.D. Beggs and J.P. Brill. A study of two-phase flow in inclined pipes. *Journal of Petroleum Technology*, 25(5):607–617, 1973.

[8] Kraus Allan D Bejan, Adrian. *Heat Transfer Handbook*. John Wiley & Sons, 2003.

[9] Dominuque Monfrin Bernard M. Couderc, J.F. Verpeaux and Lisette H. Quettier. Emeraude vapeur: A steam pilot in an offshore environment. Paper SPE 16723 presented at the SPE Annual Technical Conference and Exhibition held in Dallas, TX, 27-30 September, 1987.

[10] Malcolm Alister Grant & Paul F Bixley. *Geothermal Reservoir Engineering*. Academic Press, second edition, 2011.

[11] W.B. Bleakley. Here are case histories of two thermal projects. *The Oil and Gas Journal*, pages 123–130, 1964.

[12] Dr. Ove Bratland. The flow assurance site multi-phase flow assurance. http://www.drbratland.com/PipeFlow2/chapter1.html, 2010.

[13] J. P. Brill and H. D. Beggs. *Two-Phase Flow in Pipes*.

[14] J. P.. Brill and H. Mukherjee. *Multiphase Flow in Wells*. Society of Petroleum Engineers, 1999.

[15] G.W. Runberg A.J. Cornelius B.T. Willman, V.V. Valleroy and L.W. Powers. Laboratory studies of oil recovery by steam injection. *Journal of Petroleum Technology*, 13(7):681–690, 1961.

[16] Jr. D.H. Gibson S.W. Gosch P.D. Pattillo J.W. Sharp C.E. Taylor D.W. Bradford, D.G. Fritchie. Marlin failure analysis and redesign; part 1, description of

failure. Paper SPE 74528 presented at the IADC/SPE Drilling Conference, 26-28 February 2002, Dallas, Texas.

[17] Robert C. Earlougher Jr. Some practical considerations in the design of steam injection wells. *Journal of Petroleum Technology*, 21(1):79–86, 1969.

[18] S.M. Farouq Ali. A comprehensive wellbore stream/water flow model for steam injection and geothermal applications. *SPE Journal*, 21(5):527–534, 1981.

[19] J. P. Fontanilla. *A Mathematical Model for the Prediction of Wellbore Heat Loss and Pressure Drop in Steam Injection Wells.* Master's thesis, Department of Chemical Engineering, University of Calgary, 1980.

[20] Jerry P. Fontanilla and Khalid Aziz. Prediction of bottom-hole conditions for wet steam injection wells. *Journal of Canadian Petroleum Technology*, 21(2):82–88, 1982.

[21] L.J. Durlofsky K. Aziz L.R. Diaz B. Alkaya G. Oddie H. Shi, J.A. Holmes. Drift-flux modeling of multiphase flow in wellbores. *SPE Annual Technical Conference and Exhibition, 5-8 October 2003, Denver, Colorado*, 2003.

[22] Alton R. Hagedorn and Kermit E. Brown. Experimental study of pressure gradients occurring during continuous two-phase flow in small-diameter vertical conduits. *Journal of Petroleum Technology*, 17(4):475–484, 1965.

[23] A.R. Hasan and C. S. Kabir. *Fluid Flow and Heat Transfer in Wellbores.* Society of Petroleum Engineers, first edition, 2002.

[24] M. Holmgren. X steam for matlab. http://www.x-eng.com, 2006.

[25] P.H. Holst and D.L. Flock. Wellbore behaviour during saturated steam injection. *Journal of Canadian Petroleum Technology*, 5(4):184–193, 1966.

[26] Hans H. A. Huygen and J. L. Huitt. Wellbore heat losses and casing temperatures during steam injection. *American Petroleum Institute*, pages 25–32, 1966.

[27] Jan Dirk Jansen. Modeling and Optimization of Oil and Gas Production Systems. Advanced Production Engineering Lecture Notes, 2011.

[28] H. Duns Jr. and N. C. J. Ros. Vertical flow of gas and liquid mixtures in wells. 6th World Petroleum Congress, June 19 - 26, 1963 , Frankfurt am Main, Germany, 1963.

[29] and Maria Fogarasi Khalid Aziz, George W. Govier. Pressure drop in wells producing oil and gas. *Journal of Canadian Petroleum Technology*, 11(3), 1972.

[30] L.W. Lake. *Enhanced Oil Recovery*. Society of Petroleum Engineers, 1989.

[31] K. Leutwyler. Casing temperature studies in steam injection wells. *Journal of Petroleum Technology*, 18(9):1157–1162, 1966.

[32] Miller Mark A. Liang, Zhiyue and Kamy Sepehrnoori. New functional correlations for saturated steam properties. *Society of Petroleum Engineers*, 1992.

[33] D. R. Liles. Two-phase flow. *Los Alamos Science*, pages 26–35.

[34] Cristovao Marques. *Thaw-Front Dynamics of Super-Insulated Wells in Cold Environments*. Master's thesis, Department of Energy Resources Engineering, Stanford University, 2007.

[35] A.F. Mills. *Basic Heat and Mass Transfer*. Prentice Hall, second edition, 1999.

[36] Syed M. Zubair Mostafa H. Sharqawy, John H. Lienhard Va. Thermophysical properties of seawater: a review of existing correlations and data. *Desalination and Water Treatment*, 2009.

[37] Brill James P. Mukherjee, Hemanta. Empirical equations to predict flow patterns in two-phase inclined flow. *International Journal of Multiphase Flow*, 11(3):299–315, 1985.

[38] E.F. Pacheco and S.M. Farouq Ali. Wellbore heat losses and pressure drop in steam injection. *Journal of Petroleum Technology*, 24(2):139–144, 1972.

[39] Palmer C.M. Brill J.P. Payne, G.A. and H.D. Beggs. Evaluation of inclined-pipe, two-phase liquid holdup and pressure-loss correlation using experimental data. *Journal of Petroleum Technology*, 31(9):1198–1208, 1979.

[40] Palmer C.M. Brill J.P. Payne, G.A. and H.D. Beggs. A study of multiphase flow behavior in vertical wells. *SPE Production Engineering*, 3(2):263–272, 1988.

[41] M. Prats. *Thermal Recovery*. Society of Petroleum Engineers, 1986.

[42] H.J. Ramey JR. Wellbore heat transmission. *Journal of Petroleum Technology*, 14(4):436–440, 1962.

[43] D.H. Gibson S.W. Gosch P.D. Pattillo R.C. Ellis, D.G. Fritchie Jr. Marlin failure analysis and redesign: Part 2 - redesign. Paper SPE 74529 presented at the IADC/SPE Drilling Conference, 26-28 February 2002, Dallas, Texas.

[44] P. S. Sarathi and D. K. Olsen. *Petroleum Reservoir Simulation*. Applied Science Publishers, 1992.

[45] A. Satter. Heat losses during flow of steam down a wellbore. *Journal of Petroleum Technology*, 17(7):845–851, 1965.

[46] O. Shoham. *Mechanistic Modeling of Gas-Liquid two-phase Flow in Pipes*. Society of Petroleum Engineers, first edition, 2005.

[47] Smith D.D. Squier, D.P. and E.L. Dougherty. Calculated temperature behavior of hot-water injection wells. *Journal of Petroleum Technology*, 14(4):427–435, 1962.

[48] P.D. Pattillo J.W. Sharp S.W. Gosch, D.J. Horne and P.C. Shah. Marlin failure analysis and redesign; part 3, vit completion with real-time monitoring. Paper SPE 74530 presented at the IADC/SPE Drilling Conference, 26-28 February 2002, Dallas, Texas.

[49] G.P. Willhite. Over-all heat transfer coefficients in steam and hot water injection wells. *Journal of Petroleum Technology*, 19(5):607–615, 1967.

[50] Yu-Shu Wu and Karsten Pruess. An analytical solution for wellbore heat transmission in layered formations (includes associated papers 23410 and 23411 ). *SPE Reservoir Engineering*, 5(4):531–538, 1990.